Copy 5
RM L56I17a

NACA RM L56I17a

C.1

RESEARCH MEMORANDUM

INVESTIGATION OF DRAG AND STATIC LONGITUDINAL AND LATERAL STABILITY CHARACTERISTICS OF A MODEL OF A 40.4° SWEPT-WING AIRPLANE AT MACH NUMBERS OF 1.56 AND 2.06

By Melvin M. Carmel and Kenneth L. Turner

Langley Aeronautical Laboratory
Langley Field, Va.

CLASSIFIED DOCUMENT

This material contains information affecting the National Defense of the United States within the meaning of the espionage laws, Title 18, U.S.C., Secs. 793 and 794, the transmission or revelation of which in any manner to an unauthorized person is prohibited by law.

NATIONAL ADVISORY COMMITTEE FOR AERONAUTICS

WASHINGTON

January 18, 1957

NATIONAL ADVISORY COMMITTEE FOR AERONAUTICS

RESEARCH MEMORANDUM

INVESTIGATION OF DRAG AND STATIC LONGITUDINAL AND LATERAL STABILITY CHARACTERISTICS OF A MODEL OF A 40.4° SWEPT-WING AIRPLANE AT MACH NUMBERS OF 1.56 AND 2.06

By Melvin M. Carmel and Kenneth L. Turner

SUMMARY

An investigation has been conducted in the Langley Unitary Plan wind tunnel to determine the drag, longitudinal stability, and lateral stability characteristics of a model of a fighter-type airplane. During the program, several modifications were made to the model in an attempt to eliminate pitch-up. These data are included in this report. The tests were made at Mach numbers of 1.56 and 2.06 and at Reynolds numbers, based on the mean aerodynamic chord of the wing, of 1.225×10^6 and 1.026×10^6, respectively.

INTRODUCTION

An investigation of the aerodynamic characteristics of a model of a 40.4° swept-wing fighter-type airplane at supersonic speeds has been undertaken by the National Advisory Committee for Aeronautics. The airplane, at this time, is in the process of being flight tested, and there is urgent need for data concerning the supersonic directional stability and pitch-up problems of this airplane. The test program was therefore designed to place the greatest emphasis on these two problems. This paper contains results obtained at Mach numbers of 1.56 and 2.06 in the Langley Unitary Plan wind tunnel.

COEFFICIENTS AND SYMBOLS

A_B base axial force behind choke, lb

A_C balance-chamber axial force, lb

[redacted]

b	wing span, in.
$\bar{c}$	mean aerodynamic chord, in.
$\bar{c}_t$	mean aerodynamic chord of horizontal tail, in.
D_i'	internal duct force along X stability axis, lb
F_D'	force along X stability axis, lb
h_R	right aileron hinge moment, ft-lb
h_L	left aileron hinge moment, ft-lb
h_r	rudder hinge moment, ft-lb
h_s	stabilator hinge moment, in-lb
i_t	incidence of horizontal tail, deg
i_{t_c}	incidence of tail with negative dihedral, deg
L	lift, lb
l	rolling moment, in-lb
M	free-stream Mach number
m	pitching-moment, in-lb
M_a	moment area of aileron, cu ft
M_{a_r}	moment area of rudder, cu ft
m_E	mass flow at choke
m_1	free-stream mass flow based on inlet area
m_E/m_1	mass-flow ratio
n	yawing-moment, in-lb
p	free-stream static pressure, lb/sq ft

[redacted]

q free-stream dynamic pressure, lb/sq ft

S wing area (theoretical total), sq ft

S_H stabilator area (theoretical total), sq ft

Y side force, lb

C'_D drag coefficient, F'_D/qS

C'_{D_B} choke base drag coefficient, $-\left(\frac{A_B \cdot \cos \alpha}{qS}\right)$

C'_{D_c} balance-chamber drag coefficient, $-\left(\frac{A_C \cos \alpha}{qS}\right)$

C_{D_e} net external drag coefficient

ΔC_D difference in drag coefficient with and without fixed transition

C'_{D_i} internal duct drag coefficient, D_i/qS

C_{h_R} right aileron hinge-moment coefficient, $h_R/2M_aq$

C_{h_L} left aileron hinge-moment coefficient, $h_L/2M_aq$

C_{h_r} rudder hinge-moment coefficient, $h_r/2Ma_rq$

C_{h_s} stabilator hinge-moment coefficient, $h_s/qS_H\bar{c}_t$

C_L lift coefficient, L/qS

C_l rolling-moment coefficient, l/qSb

C_m pitching-moment coefficient, $m/qS\bar{c}$

C_n yawing-moment coefficient, n/qSb

C_Y side force coefficient, Y/qS

α angle of attack of wing, deg

β angle of sideslip of fuselage center line, deg

[redacted]

δ_a aileron angle, deg

δ_r rudder angle, deg

The results of these tests are presented as coefficients of forces and moments referred to the stability-axes system. All aerodynamic moments were taken about the center of gravity of the model, which is longitudinally located at 0.2857$\bar{c}$ and 0.525 inch above the wing root chord line. All hinge moments were taken about their respective hinge center lines.

APPARATUS AND METHODS

Tunnel

The tests were conducted in the low Mach number test section of the Langley Unitary Plan wind tunnel. This tunnel is a variable-pressure, continuous, return-flow type. The test section is 4 feet square and approximately 7 feet long. The nozzle leading to the test section is of the asymmetric sliding-block type. Mach number may be continuously varied through the range of approximately 1.56 to 2.80 without tunnel shutdown.

Model and Support System

A three-view drawing of the model is presented in figure 1. Geometric characteristics of the model are presented in table I. Photographs of the configurations tested are presented in figure 2. Sketches of the pitch-up "fixes" used in an attempt to eliminate pitch-up are presented in figure 3. The rearward end of the model fuselage was cut off to simulate the proper side contour of the airplane. (See fig. 4.) For the basic model condition this piece, called the fuselage fairing, was attached to the sting; there was a clearance gap between it and the model of approximately 3/16 inch. A few tests were also performed with the fuselage fairing attached to the model to determine its effect on aerodynamic characteristics so that comparisons might be made with other wind-tunnel data.

The model was attached to the forward end of an enclosed NACA six-component, electrical, strain-gage balance. This balance was connected to the tunnel central-support system by means of a sting. The central-support components consisted of a remotely operated, adjustable coupling; a variable offset coupling; and, for the pitch runs, a 10° bent coupling. The adjustable coupling was used to change the angle of the

model in the vertical plane. The variable offset coupling was a means of offsetting the model from the tunnel center line in order to get increased angle-of-attack range for sideslip tests. The 10° bent coupling was used for the same purpose during pitch tests.

MEASUREMENTS AND ACCURACY

Pitch tests were made through an angle-of-attack range of approximately +1° to +21°, at angles of sideslip of 0° and ±2°. At angles of attack of approximately 1°, 4°, 10°, 12°, 16°, and 19°, sideslip tests were made through an angle range of approximately -4° to 10°. The tests were performed at Mach number of 1.56 and 2.06. All tests with tails on were performed with a horizontal-tail incidence of -4°. The angles of attack and sideslip are corrected for deflection of the sting and balance under load and angles for a given run are estimated to be accurate within ±0.1°. It may be noted, in some instances, that the C_L data for a given angle of attack for a pitch run does not check exactly with that for a sideslip run. This is believed to be due to a slightly erroneous zero angle setting for the sideslip run. The exact angle of attack for the sideslip runs, however, is relatively unimportant as the aerodynamic coefficient data for a given value of C_L or β are accurate.

The maximum deviation of local Mach number in the part of the tunnel occupied by the model is ±0.015 from the average values given.

The dewpoint, measured at stagnation pressure, for all tests was maintained below -30° F. The stagnation temperature was approximately 125° F and the wind-tunnel stagnation pressure was maintained at approximately 9 pounds per square inch absolute.

The tunnel, as yet, has not been completely calibrated and any angularity of flow that might exist in the tunnel has not been determined. The pressure gradients in the region of the model have been determined and are sufficiently small so as not to induce any buoyancy effect on the model.

The accuracy of the force and moment coefficients, based on balance calibration and repeatability of data, is estimated to be within the following limits:

C_L	±0.002
C_D	±0.001
C_m	±0.001
C_l	±0.0002

C_n	±0.0005
C_Y	±0.0015
C_{h_R}	±0.015
C_{h_L}	±0.012
C_{h_r}	±0.010
C_{h_s}	±0.001

The drag data have been adjusted to correspond to zero balance-chamber drag coefficient $C_{D_c} = 0$. An example of the measured balance-chamber drag coefficients plotted against angle of attack for both test Mach numbers are presented in figure 5 in order to show the magnitude of these coefficients.

Internal duct drag and choke base pressure drag were obtained for one of the pitch runs only. The internal drag was obtained from a single-tube, total-pressure measurement ahead of the choke location within the duct. Choke base pressure drag was obtained from measurements of the static pressure just behind the solid part of the choke. The internal duct drag and choke base pressure drag coefficients plotted against angle of attack for both test Mach numbers are also presented in figure 5.

In order to assure turbulent flow over the model, a transition strip was fixed around the model nose, one inch rearward of the tip, and also on the 10 percent chord of the wing (top and bottom, full span). The transition strips were 1/4 inch wide and consisted of number 60 carborundum grains imbedded in shellac with approximately 30 grains per 0.25 square inch. The results of these tests are presented in figure 6. To obtain net external drag, the drag coefficients shown on the characteristic plots must first be increased by the incremental difference in drag coefficient shown in figure 6 at the same model attitude, and this resultant drag coefficient must then be reduced by the amount of the internal drag and the choke base pressure drag at the same model attitude $\left(C_{D_e} = C_D' + \Delta C_D - C_{D_i}' - C_{D_B}'\right)$. It is recognized that a small part of the drag due to fixing transition on the model is due to the wave drag of the transition strips; however, it is believed that this is more than offset by the differences in smoothness between the model and the full-scale aircraft.

As previously mentioned, the model was tested with the fuselage fairing attached to the sting and, for a few runs, with the fairing attached to the model. A comparison of the aerodynamic coefficient data for these two configurations is shown in figures 7 and 8. With the fairing attached to the sting, the pitching-moment coefficient was more

positive at a given lift coefficient at both test Mach numbers. However, the slope of the pitching-moment curves with respect to lift coefficient remained essentially unchanged. The other aerodynamic coefficients were relatively unaffected by this difference in the configuration with fuselage fairing.

The reference area used in computing the coefficients is shown as the shaded area in figure 9. It should be noted that the use of the smaller area makes the coefficient data appear larger in magnitude than would be expected.

Figure 10 presents curves of mass-flow ratio against angle of attack at Mach numbers of 1.56 and 2.06.

Schlieren photographs were taken of many of the model configurations and attitudes. Typical examples of the schlieren photographs are presented in figure 11.

A study of the position of the model in the tunnel reveals that for a Mach number of 1.56 any data taken at angles of attack beyond 20° are influenced by wall-reflected shock waves acting on the tail of the model.

PRESENTATION OF RESULTS

The results of the investigation are presented in the following figures:

[redacted]

SUMMARY OF RESULTS

The basic results are presented without analysis; however, some general observations relative to the data are as follows:

1. The results indicate positive static directional stability for complete-model configurations at angles of attack to 19° for both test Mach numbers. The directional stability decreases with angle of attack, and at angles of attack greater than 19° the data indicate neutral directional stability. The results also show that at low angles of attack the directional stability decreases with Mach number, but this effect diminishes with increasing angle of attack. Addition of missiles to the basic configuration decreases the static directional stability.

[redacted]

2. Positive effective dihedral is indicated at all angles of attack to 19° at both test Mach numbers for complete-model configurations.

3. The neutral point for the tail-on model configurations with and without missiles is located at approximately 75 percent of the mean aerodynamic chord for a Mach number of 1.56 and moves forward to the 71 percent chord at a Mach number of 2.06. For the model with the tails off, the neutral point is located at approximately 43 and 40 percent of the mean aerodynamic chord for Mach numbers of 1.56 and 2.06, respectively.

4. The data indicate that a 5° rudder angle is necessary to compensate for the yawing moment produced by approximately 1° of sideslip at both test Mach numbers for lift coefficients up to 0.5. At lift coefficients above 0.5, the effect of sideslip diminishes until it is zero at lift coefficients above 1.0 (neutral directional stability); however, the rudder effectiveness remains relatively constant up to the higher lift coefficients.

5. The tail with negative dihedral and the delta wing were the only fixes that had any effect on pitch-up. The fix that simulated the delta-wing configuration was found to delay the pitch-up, but it did not eliminate it. The delta wing also decreased the minimum drag and increased the maximum lift-drag ratio.

Langley Aeronautical Laboratory,
National Advisory Committee for Aeronautics,
Langley Field, Va., August 31, 1956.

TABLE I.- GEOMETRIC CHARACTERISTICS OF MODEL

Model scale, percent	5
Center-of-gravity location, percent of mean aerodynamic chord	28.57
Wing:	
Loading (take-off gross weight), lb/sq ft	122
Loading (combat gross weight), lb/sq ft	100
Exposed area, sq ft	0.790
Theoretical area (see shaded area of fig. 9), sq ft	0.922
Span, in.	23.812
Aspect ratio	4.272
Sweepback angle of zero percent chord line, deg	40.4
Dihedral, deg	0
Incidence, deg	1.0
Geometric twist, deg	0
Root section	NACA 65A007 (modified)
Tip section	NACA 65A006 (modified)
Root chord, in.	8.662
Tip chord, in.	2.464
Root-chord location, longitudinal (fuselage station), in.	18.389
Root-chord location, vertical (water line), in.	1.725
Mean aerodynamic chord, in.	6.146
Mean-aerodynamic-chord location:	
Longitudinal (fuselage station), in.	24.365
Lateral (body line), in.	4.834
Vertical (water line), in.	2.250
Leading-edge flaps	None
Ailerons:	
Type	Plain, piano-hinged, unsealed
Area, sq ft	0.037
Span, in.	4.458
Sweepback of hinge line, deg	26.28
Location:	
Longitudinal hinge center line, percent chord	72.85
Lateral, inboard edge (body line), in.	6.048
Lateral, outboard edge (body line), in.	10.506
Chord, inboard edge, in.	1.496
Chord, outboard edge, in.	0.863
Deflection, deg	±25
Aileron trim tab	None
Fuselage:	
Length, in.	40.206
Width, in.	4.60
Depth, in.	4.112
Frontal area, sq ft	0.106
Side area, sq ft	0.819
Base area, sq ft	0.02765

TABLE I.- GEOMETRIC CHARACTERISTICS OF MODEL - Concluded

Horizontal tail:	
Type	Stabilator
Area (theoretical), sq ft	0.189
Span, in.	9.45
Aspect ratio	3.301
Taper ratio	0.460
Root-chord length, in.	3.925
Mean-aerodynamic-chord length, in.	2.988
Mean-aerodynamic-chord location, 25 percent chord:	
Longitudinal (fuselage station), in.	41.855
Lateral (body line), in.	2.075
Vertical (water line), in.	8.204
Tail length, 28.57 percent $\bar{c}$ to tail 25 percent chord, in.	17.49
Sweepback, 29.34 percent chord line, deg	35
Dihedral, deg	10
Geometric twist, deg	0
Root section	NACA 65A007 (modified)
Tip section	NACA 65A006 (modified)
Tip-chord length, in.	1.80
Elevators	None
Vertical tail:	
Area (theoretical), sq ft	0.2124
Span, in.	4.50
Aspect ratio	0.662
Taper ratio	0.509
Root-chord length, in.	9.00
Mean-aerodynamic-chord length, in.	7.030
Mean-aerodynamic-chord location, 25 percent $\bar{c}$:	
Longitudinal (fuselage station), in.	38.469
Vertical (water line), in.	6.606
Tail length, in.	14.112
Root section	NACA 65A007 (modified)
Tip section	NACA 65A007 (modified)
Tip-chord length, in.	4.582
Rudder:	
Type	Plain unsealed
Area, sq ft	0.0305
Lower-edge location (water line), in.	5.016
Upper-edge location (water line), in.	8.576
Chord (lower edge), in.	1.547
Chord (upper edge), in.	0.916
Deflection, deg	±25
Duct areas:	
Inlet (one side), sq ft	0.0100
Compressor face (one side), sq ft	0.012137
Exit (one side), sq ft	0.012935

[redacted]

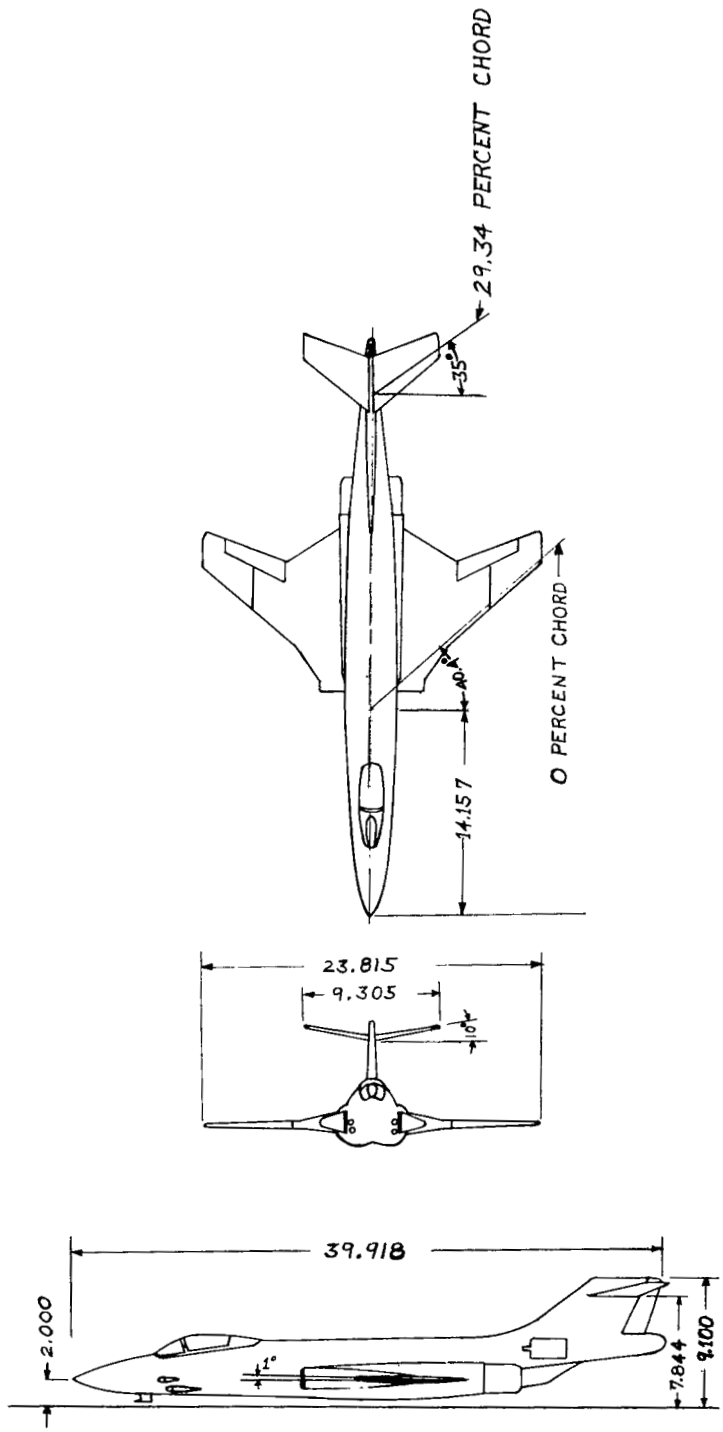

Figure 1.- Three-view drawing of model. All dimensions are in inches.

(a) Top view. L-92956

Figure 2.- Photographs of model.

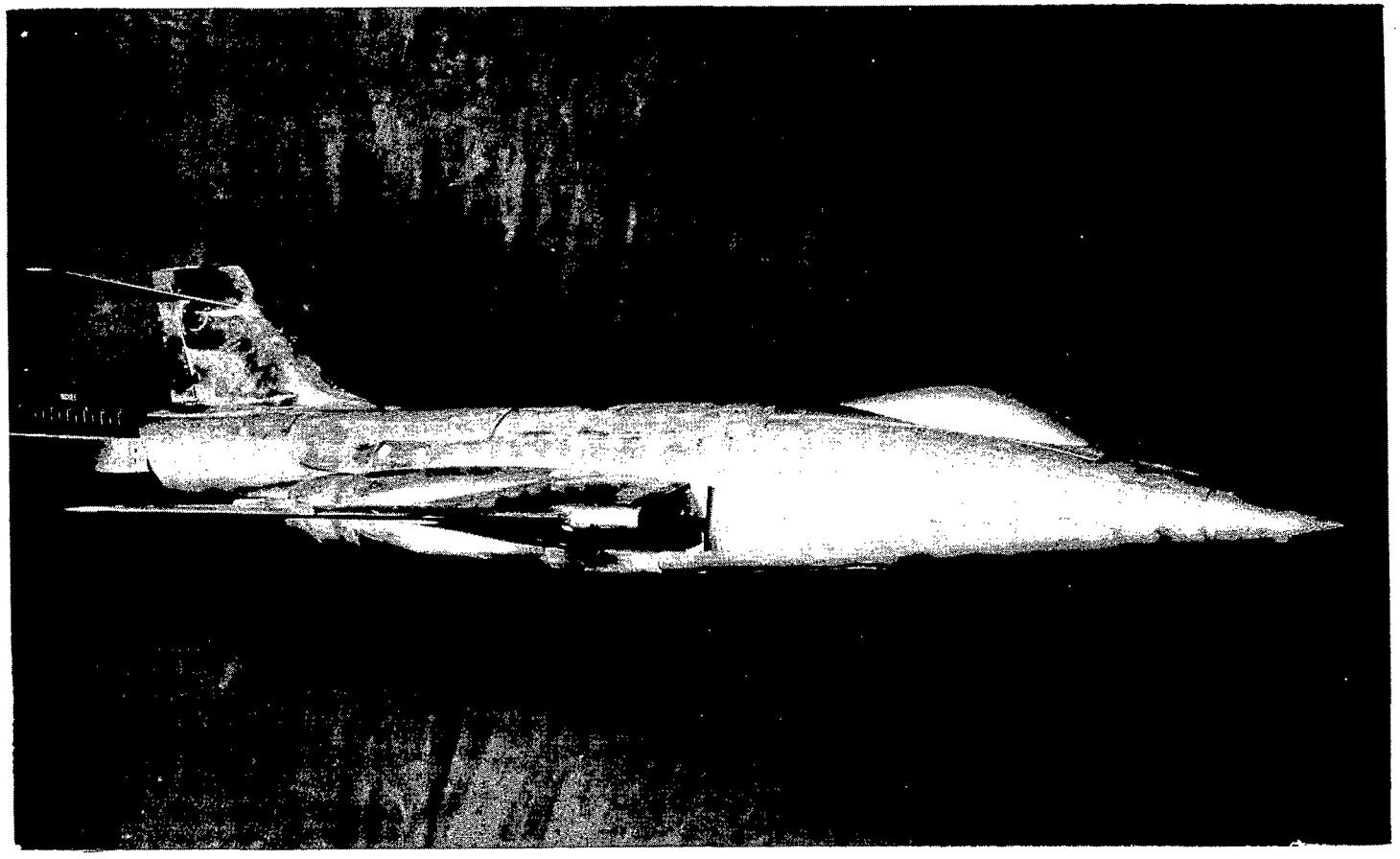

L-92952

(b) Three-quarter front view.

Figure 2.- Continued.

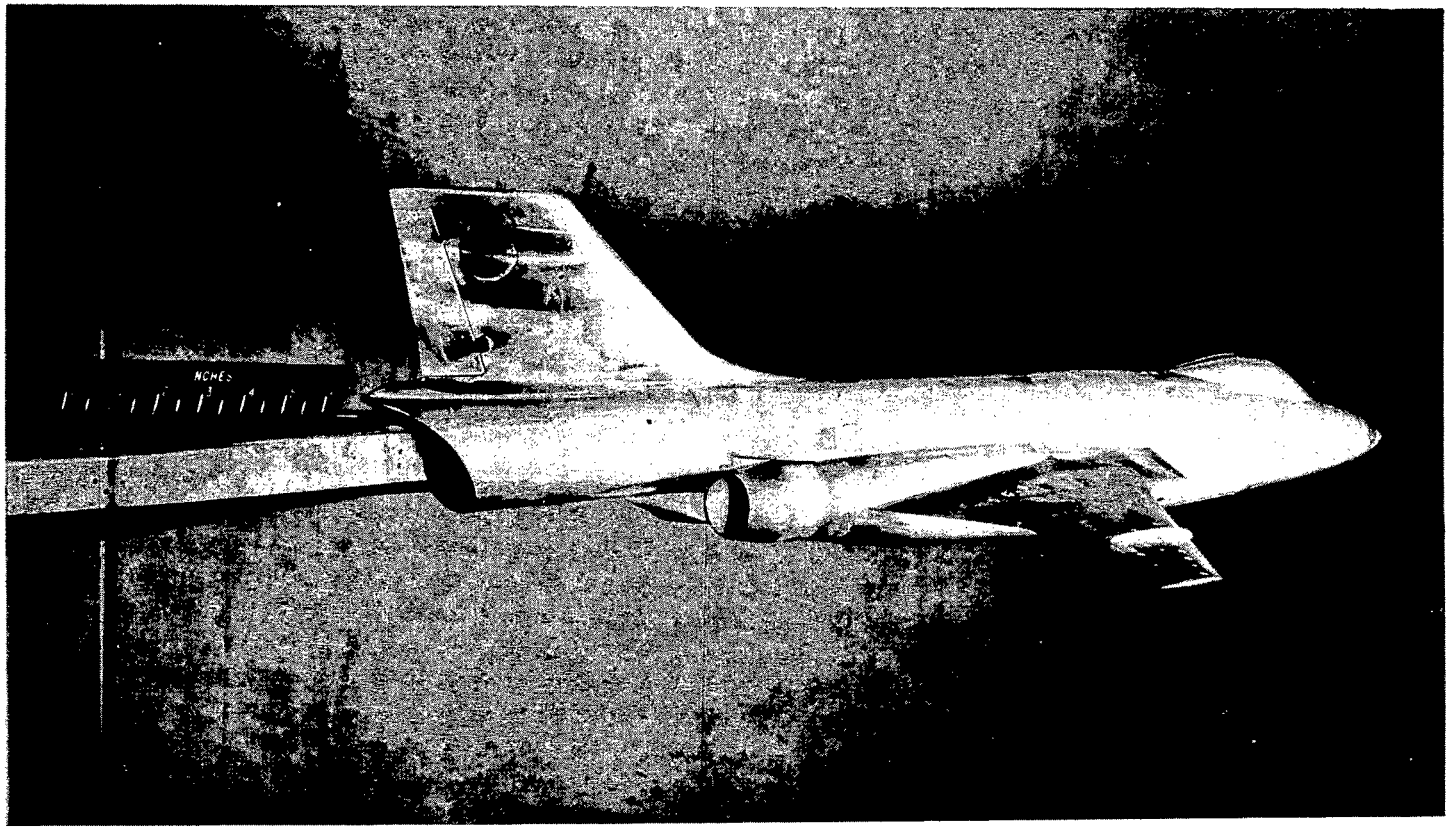

L-92953

(c) Three-quarter rear view.

Figure 2.- Continued.

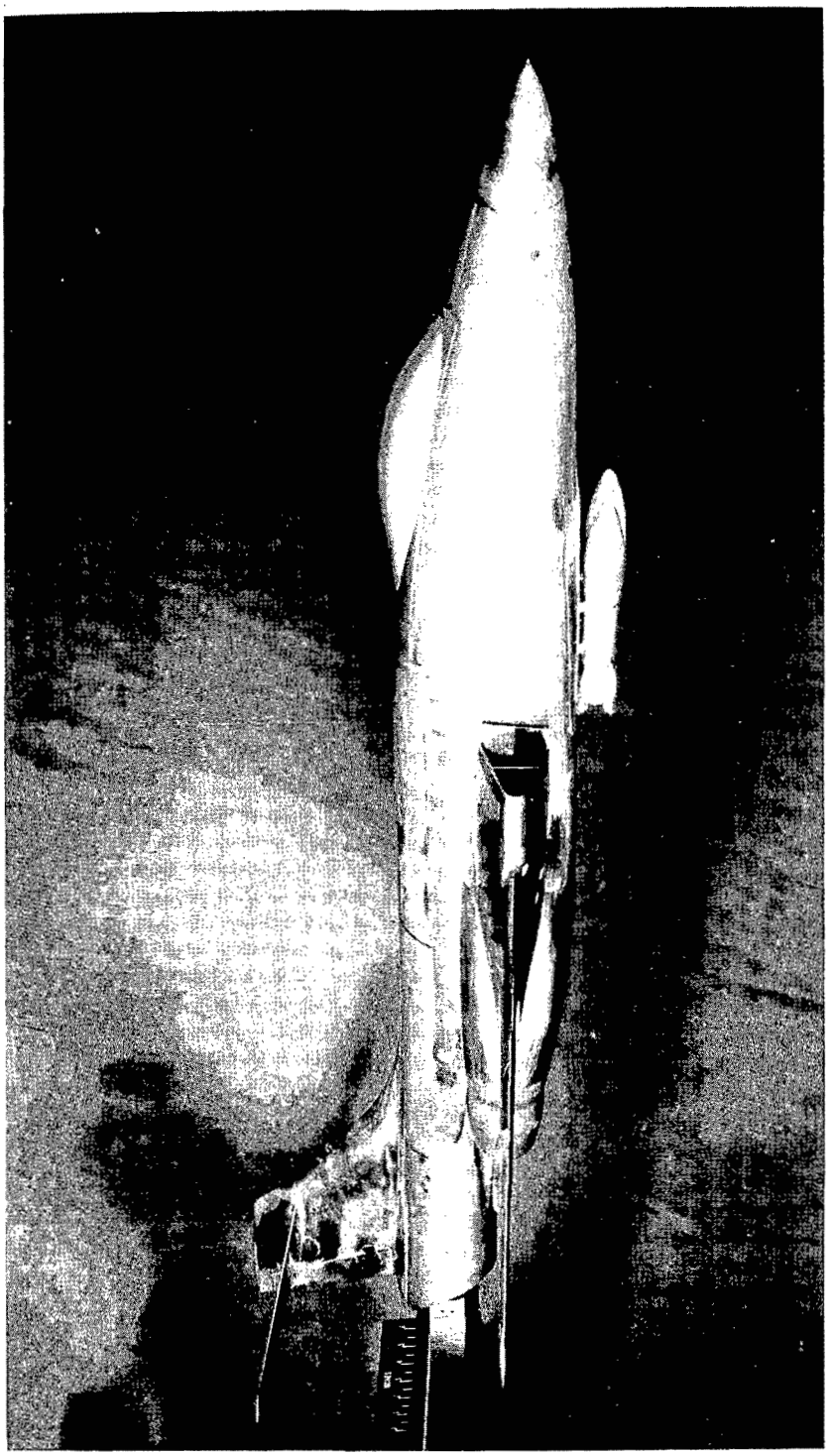

L-92950

(d) Model with missiles.

Figure 2.- Concluded.

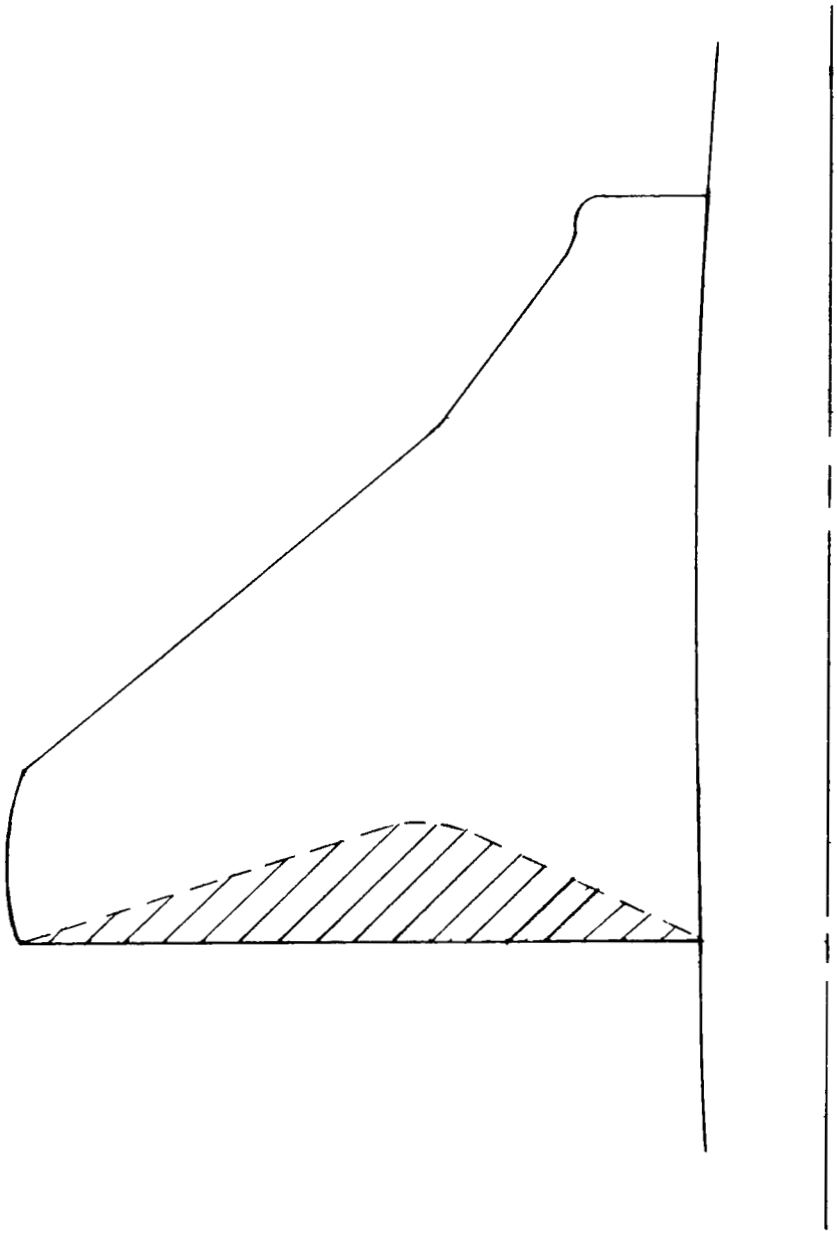

(a) Area added to simulate delta wing.

Figure 3.- "Fixes" used in an attempt to eliminate pitch-up.

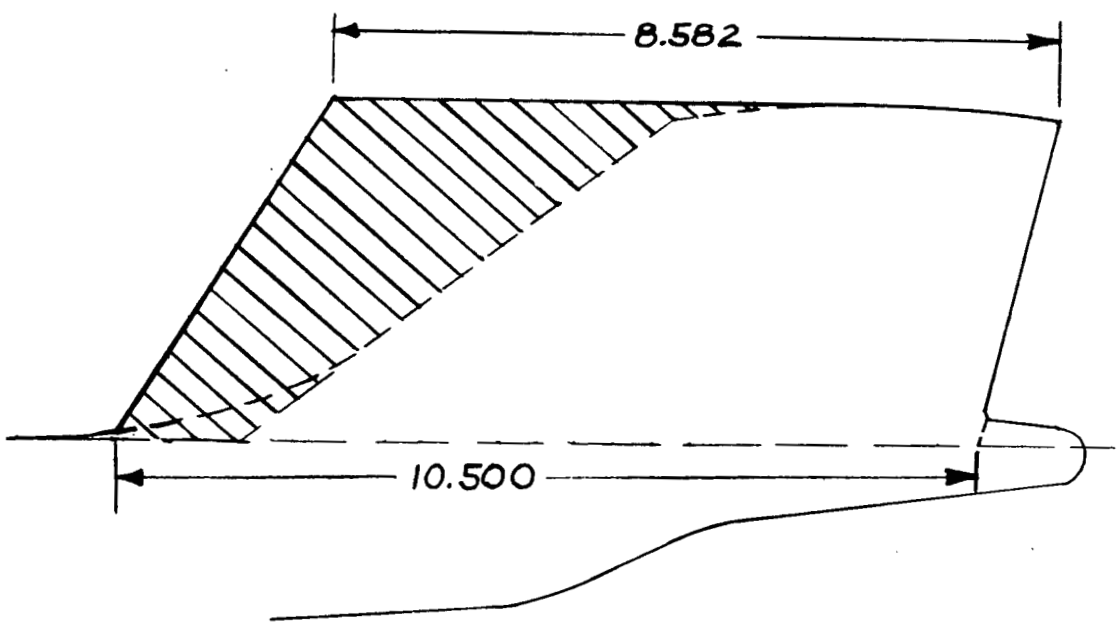

(b) Area added to fin.

Figure 3.- Continued.

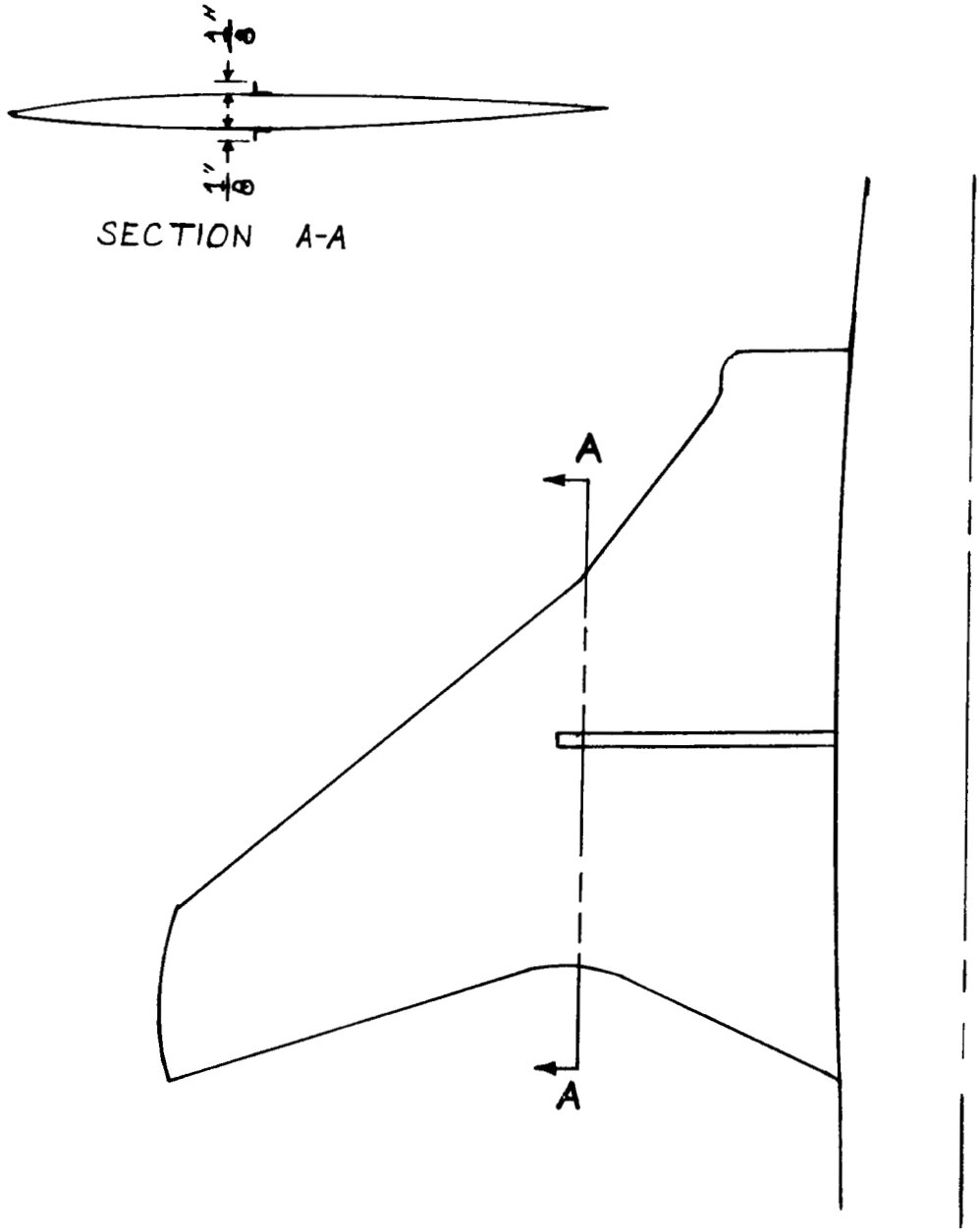

(c) Wing spoilers.

Figure 3.- Continued.

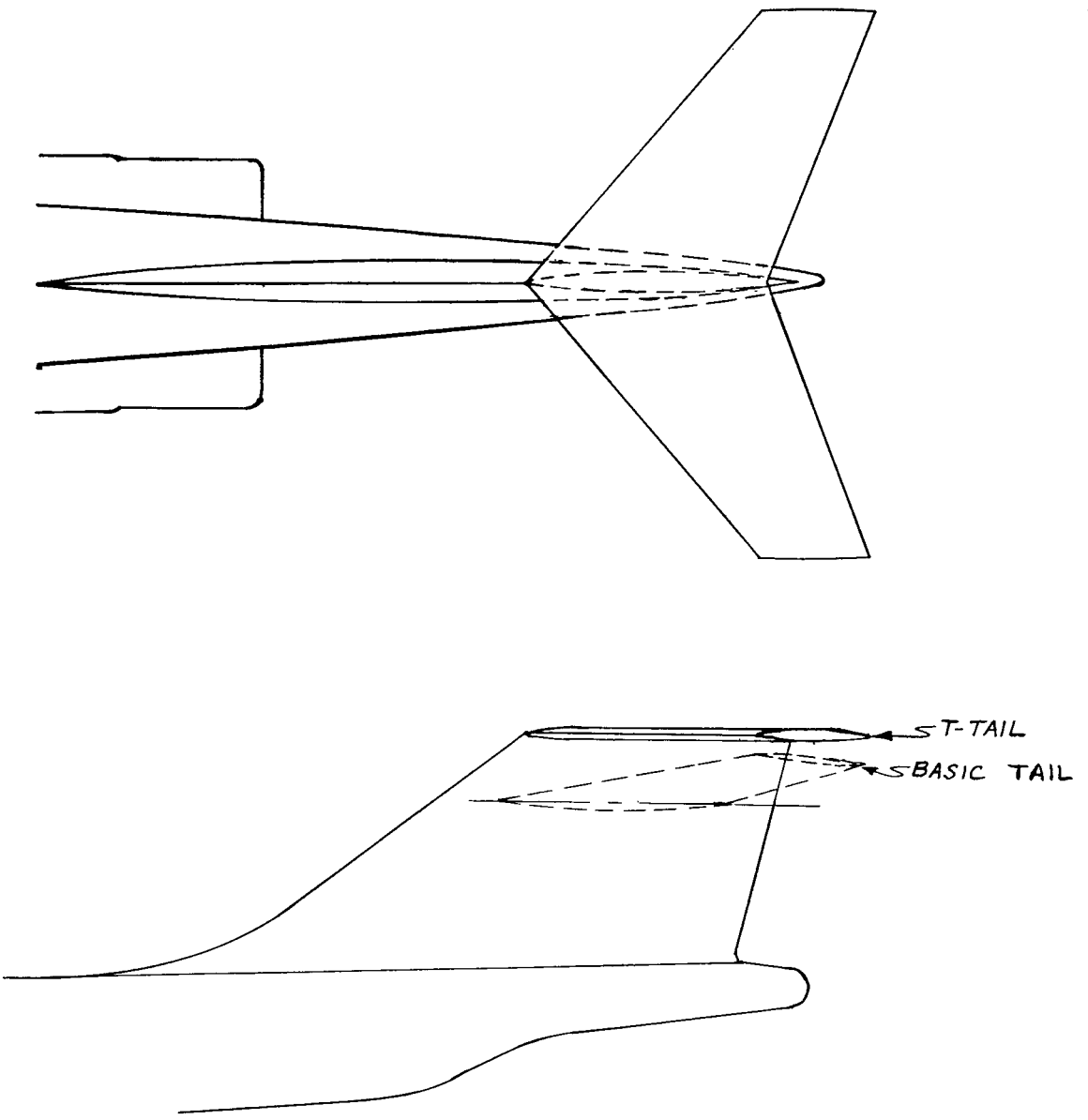

(d) T-tail.

Figure 3.- Continued.

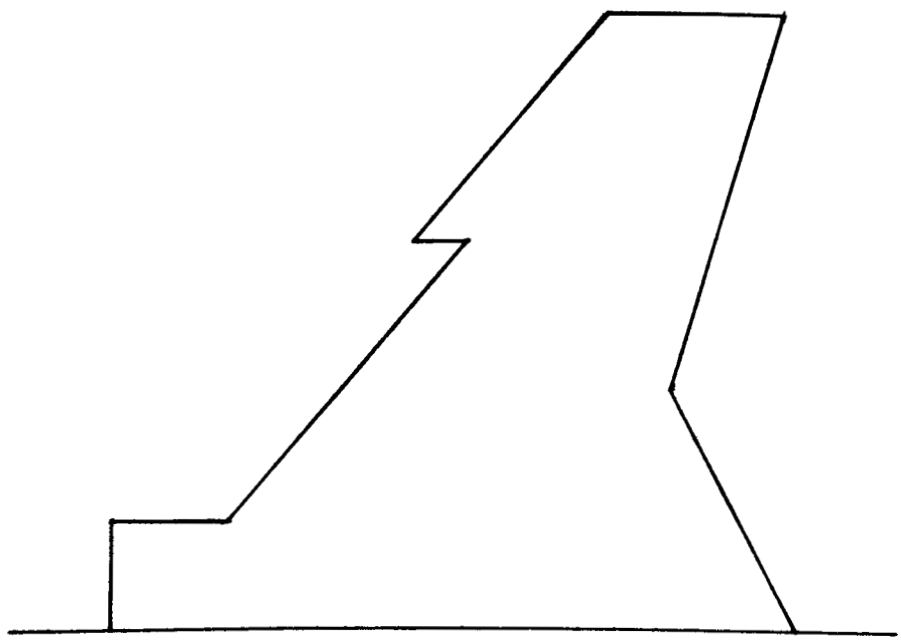

(e) Wing leading-edge extension.

Figure 3.- Continued.

Area	.1212 ft²
Aspect Ratio	3.00
Taper Ratio	.50

(f) Tail with negative dihedral.

Figure 3.- Concluded.

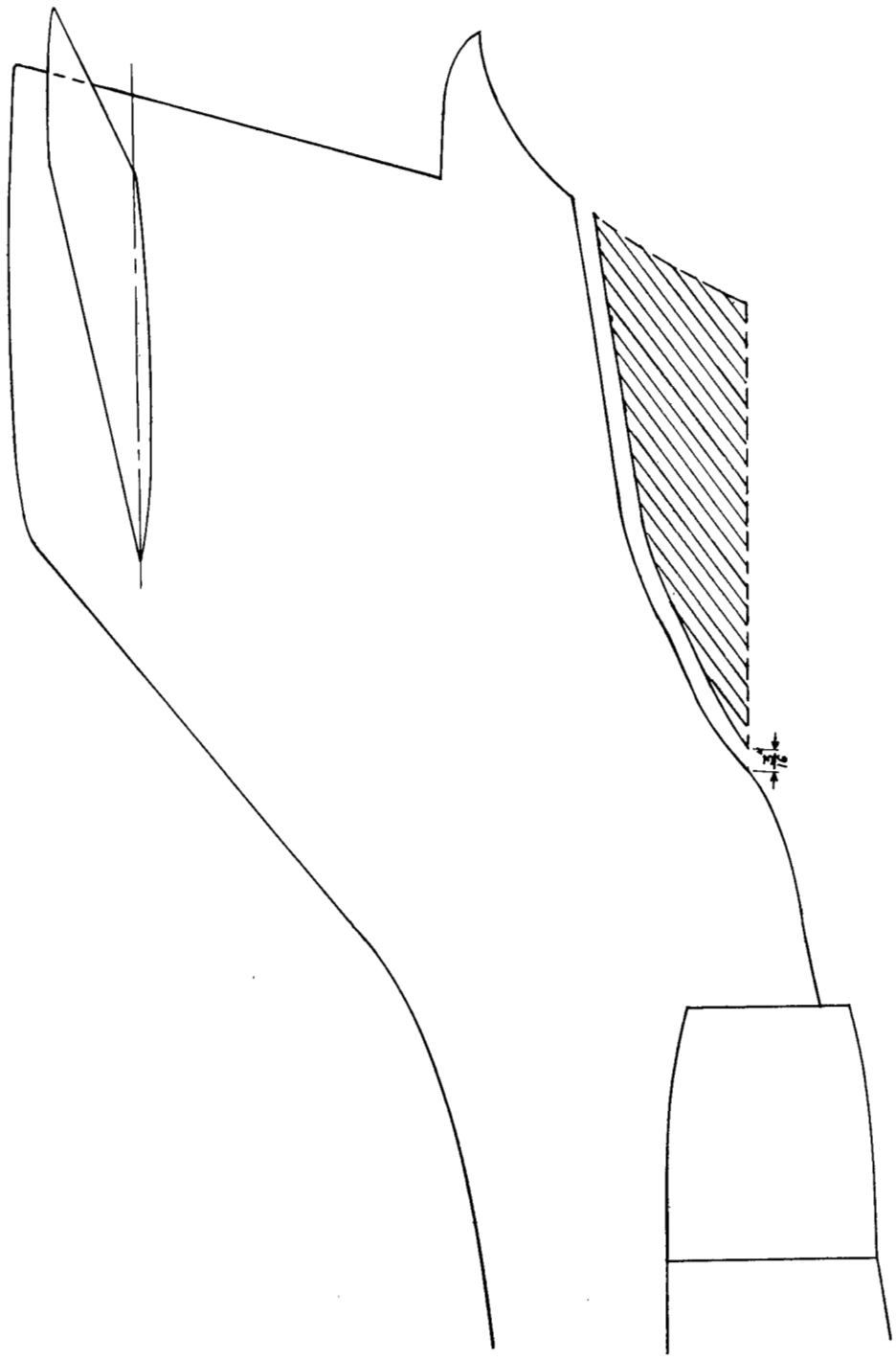

Figure 4.- Fuselage fairing.

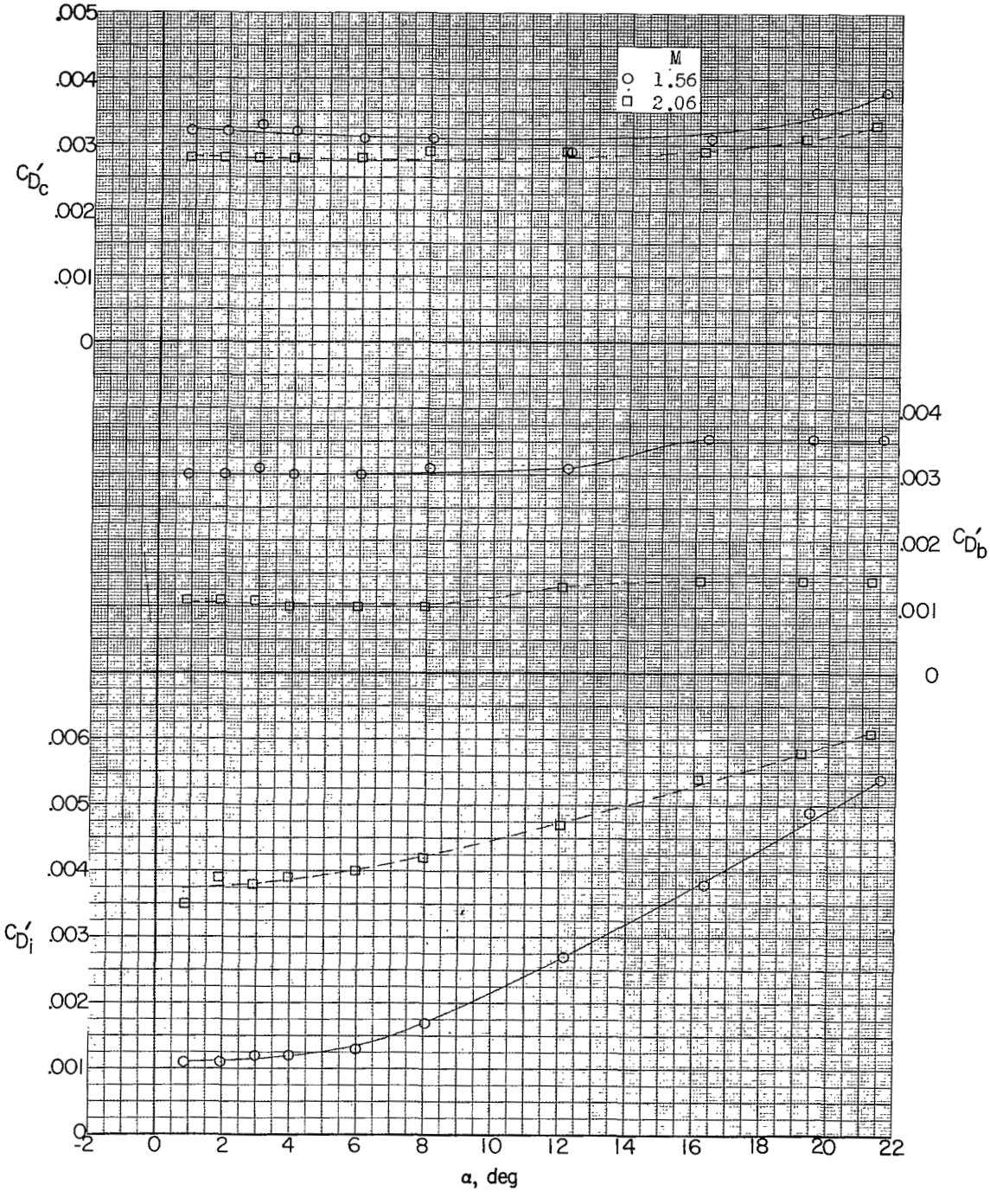

Figure 5.- Effect of angle of attack on chamber, duct base, and internal duct drag coefficients; $\beta = 0^{\circ}$.

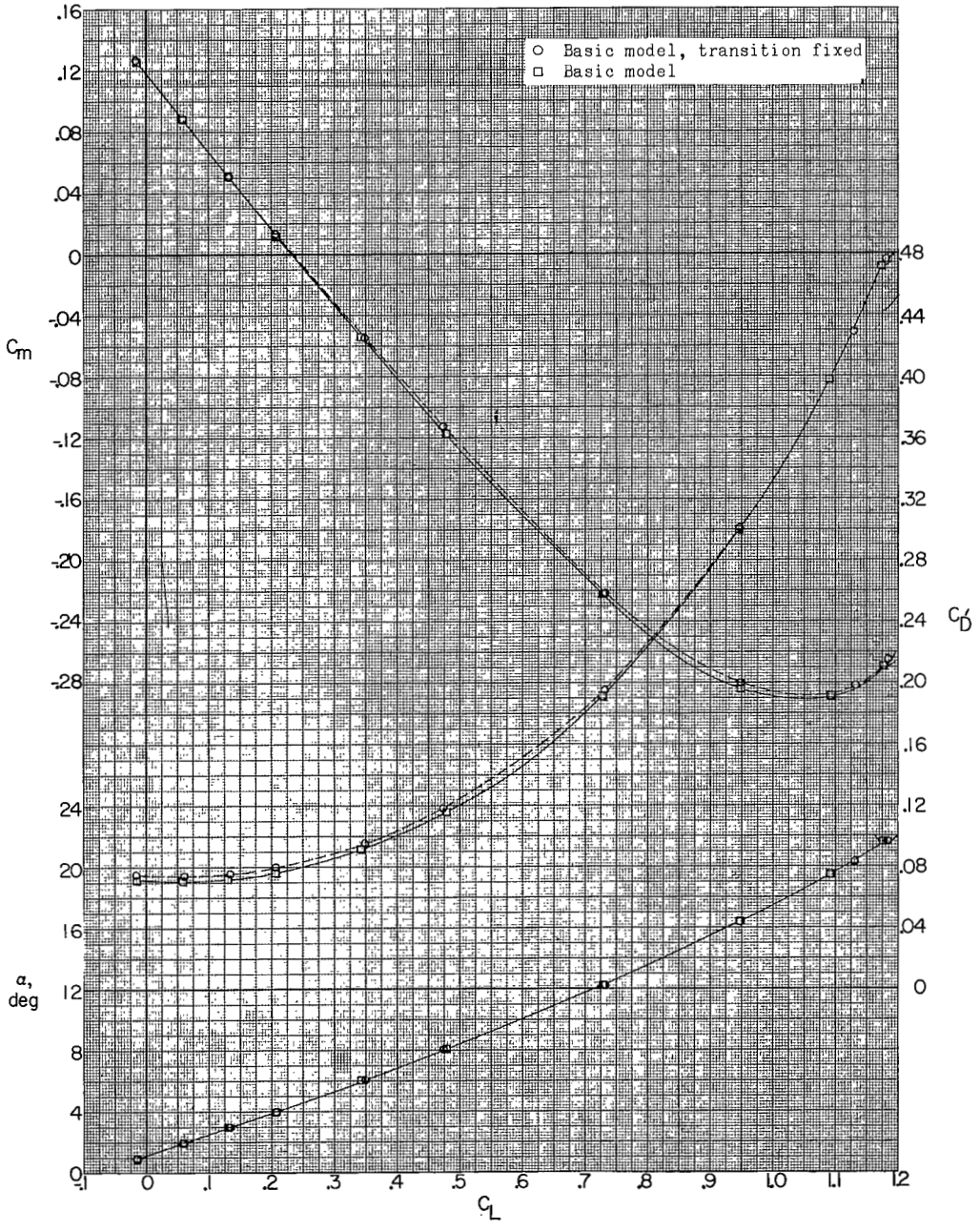

(a) M = 1.56.

Figure 6.- Effect of fixed transition on aerodynamic characteristics in pitch; $\beta = 0^{\circ}$. Data uncorrected for base and internal duct drag. (Flagged symbols denote wall reflected shock waves striking tail.)

[redacted]

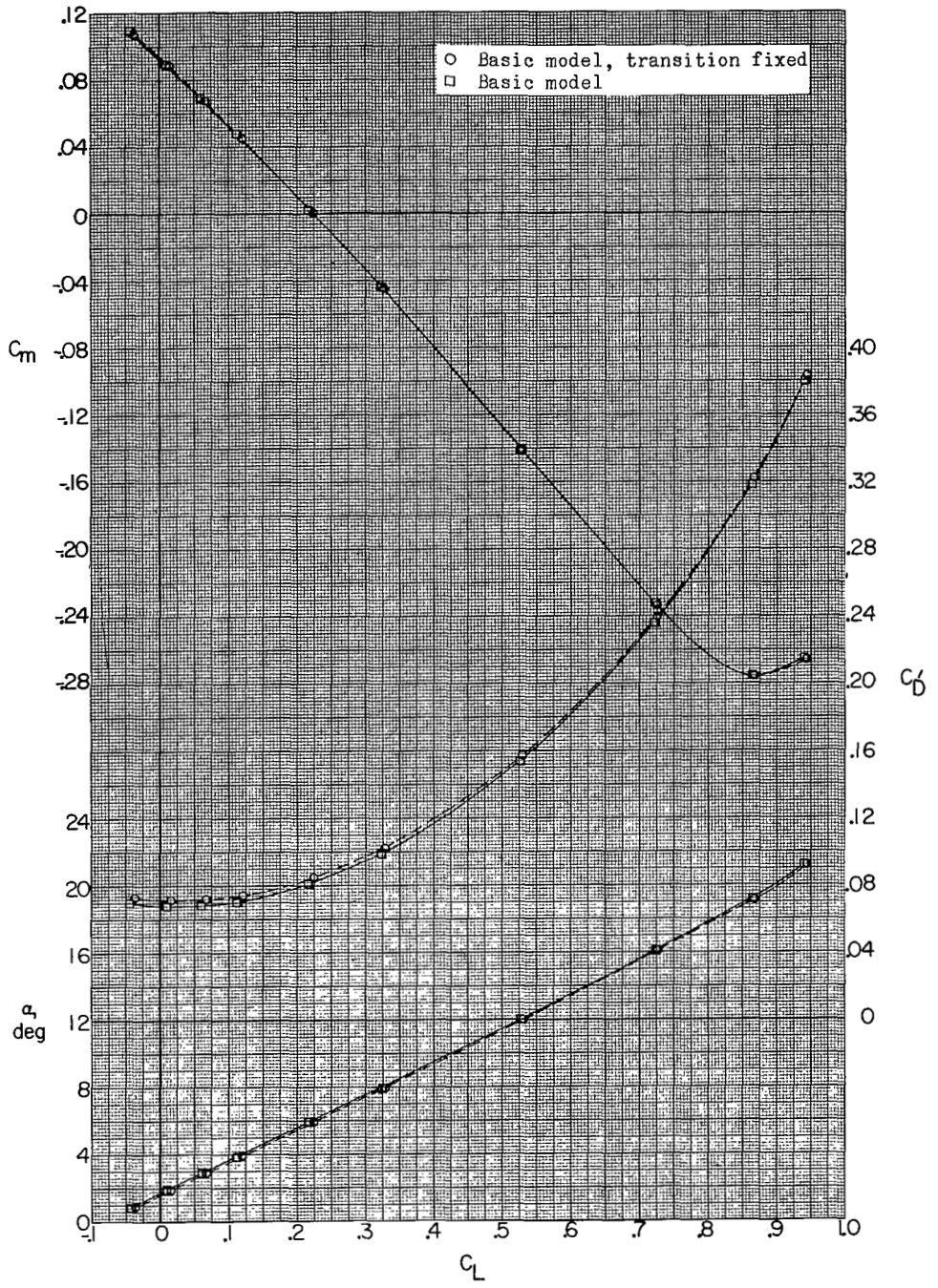

(b) M = 2.06.

Figure 6.- Concluded.

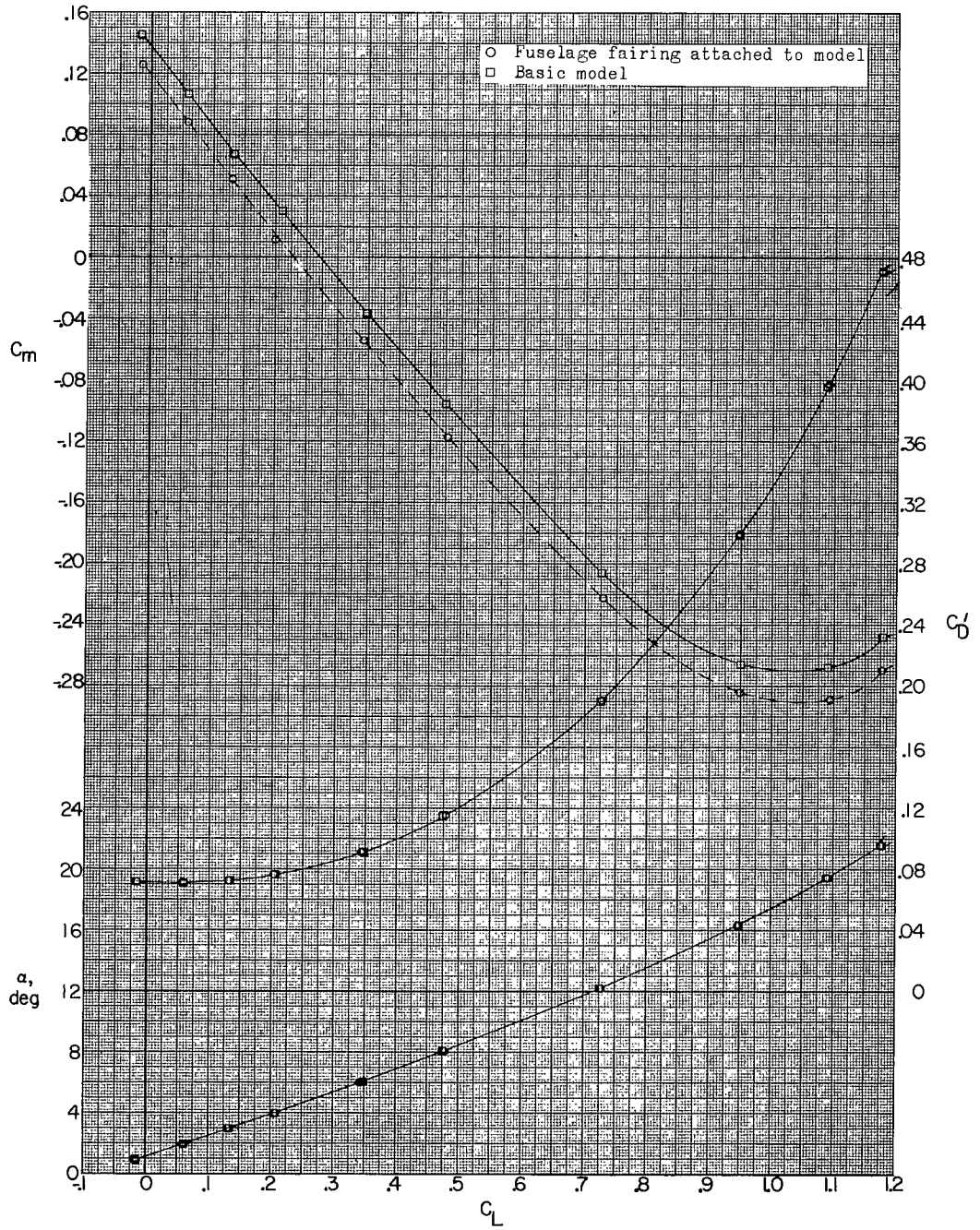

(a) M = 1.56.

Figure 7.- Effect of fuselage fairing on aerodynamic characteristics in pitch; $\beta = 0^\circ$. Data uncorrected for base and internal duct drag. (Flagged symbols denote wall reflected shock waves striking tail.)

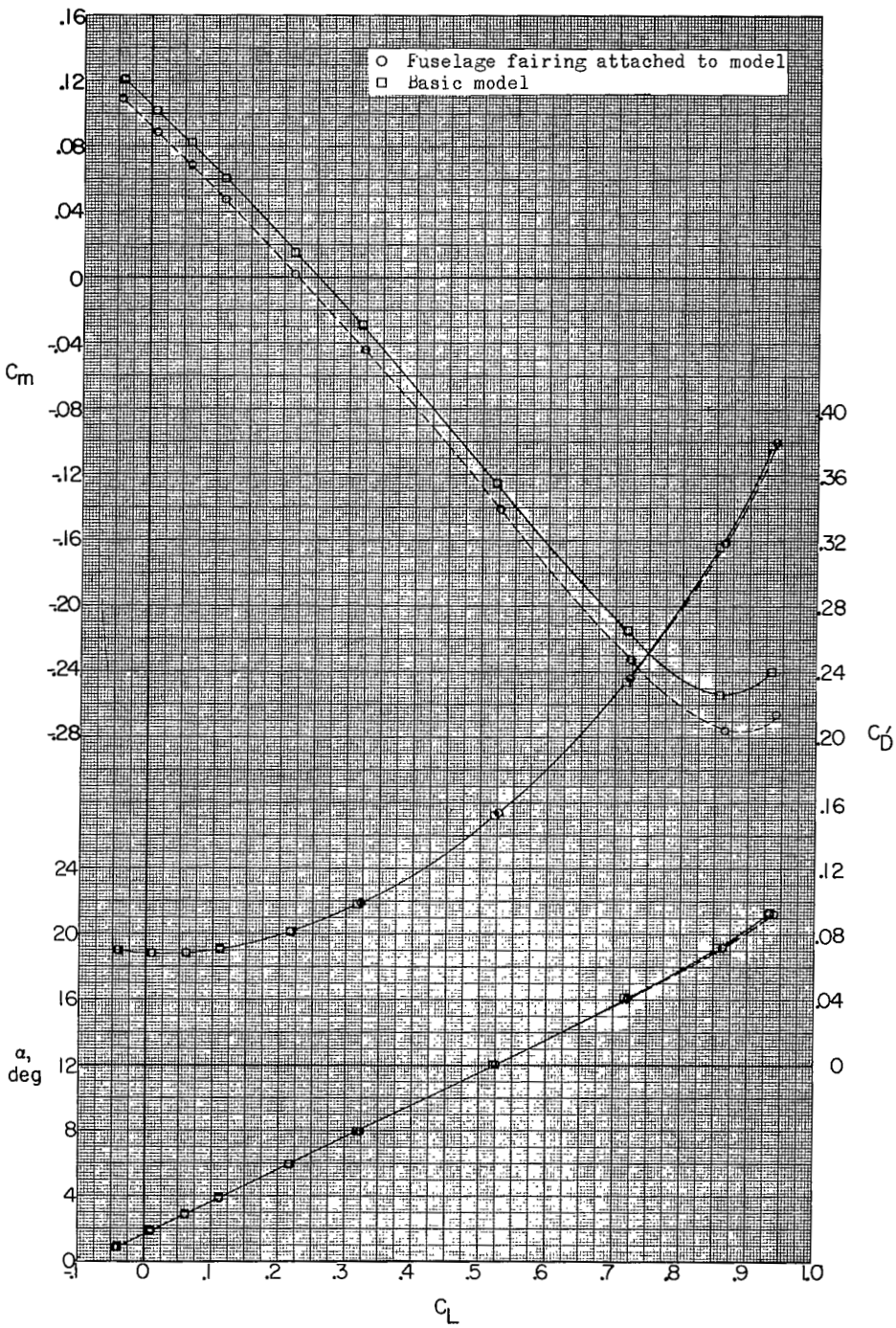

(b) M = 2.06.

Figure 7.- Concluded.

[redacted]

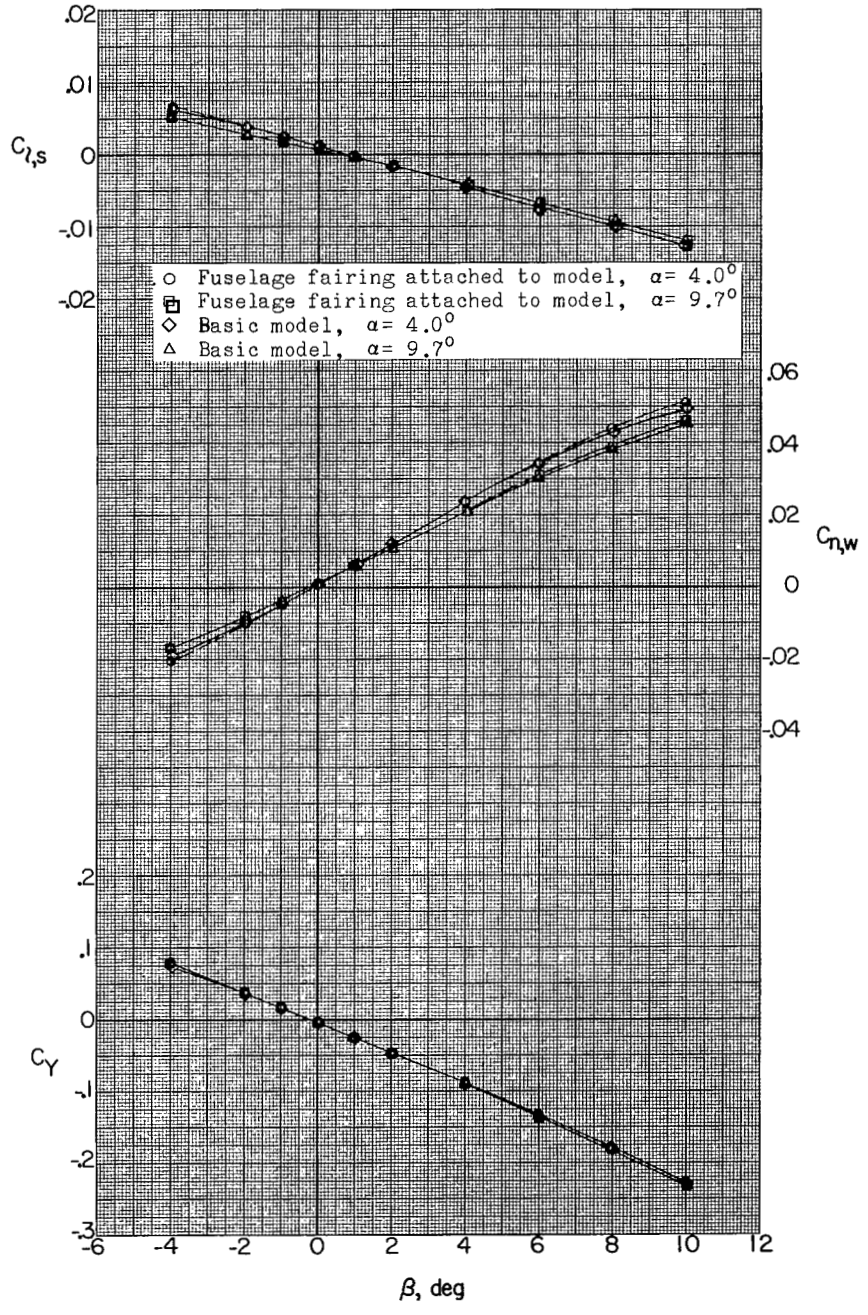

(a) M = 1.56.

Figure 8.- Effect of fuselage fairing attached to model on aerodynamic characteristics in sideslip.

[redacted]

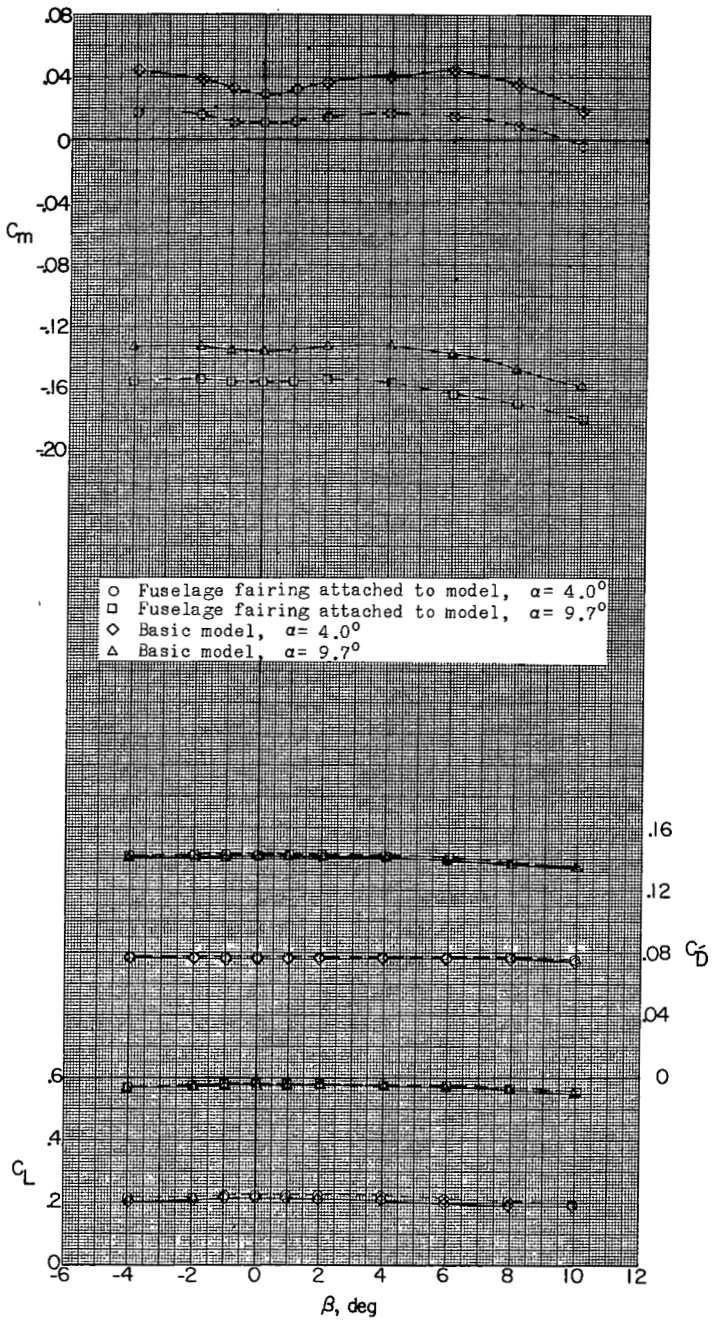

(a) Continued.

Figure 8.- Continued.

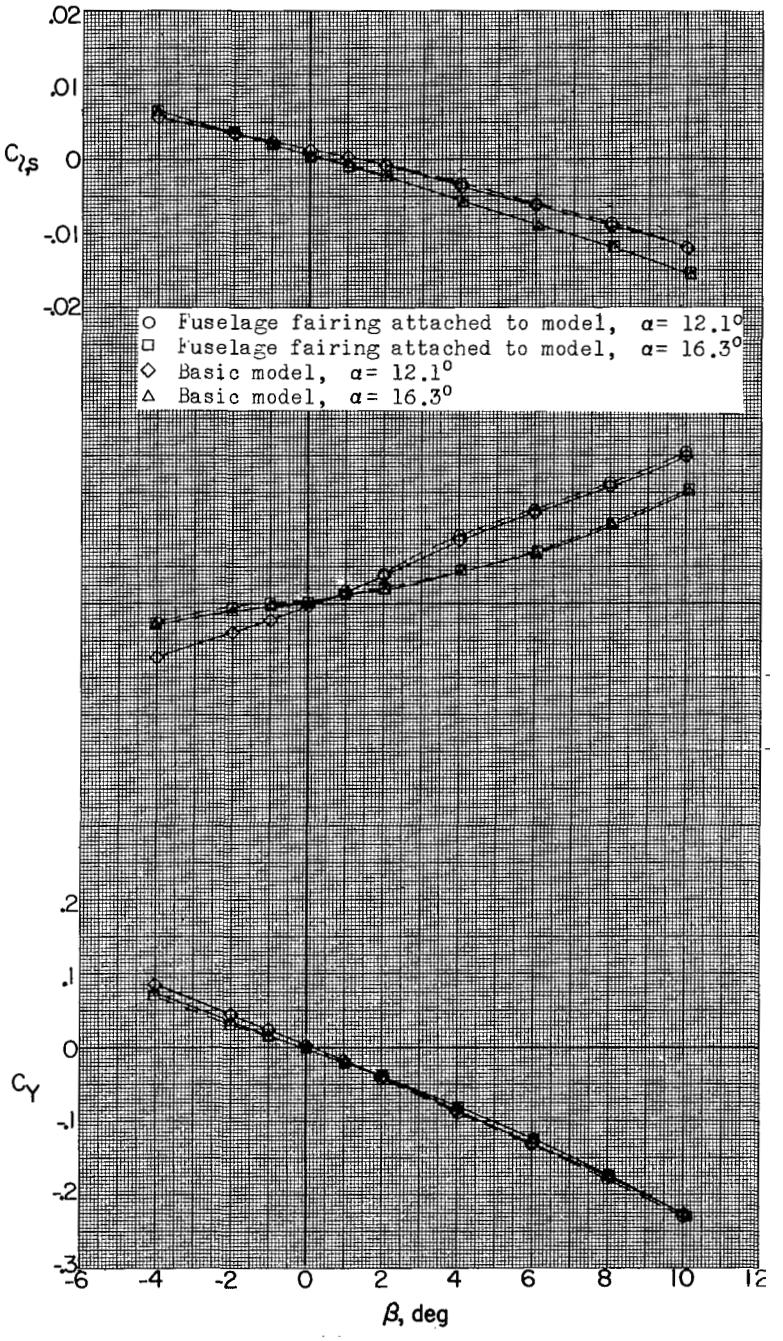

(a) Continued.

Figure 8.- Continued.

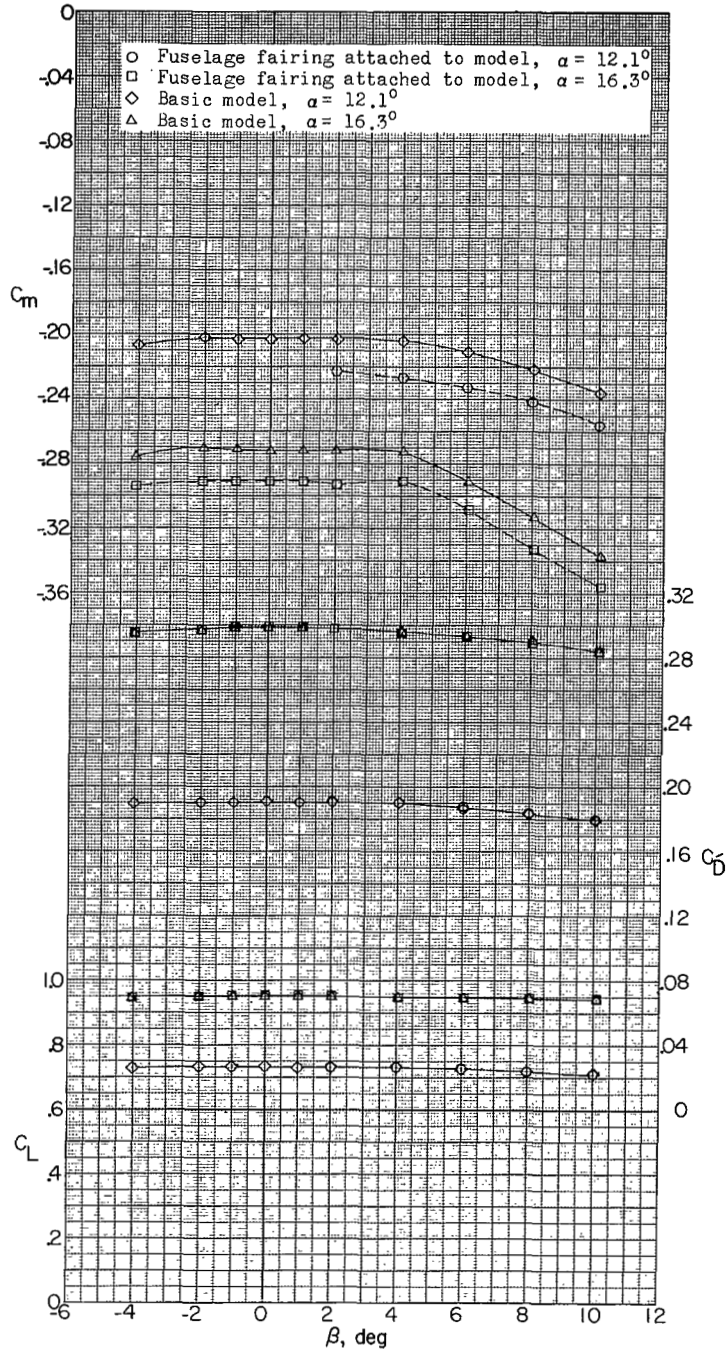

(a) Concluded.

Figure 8.- Continued.

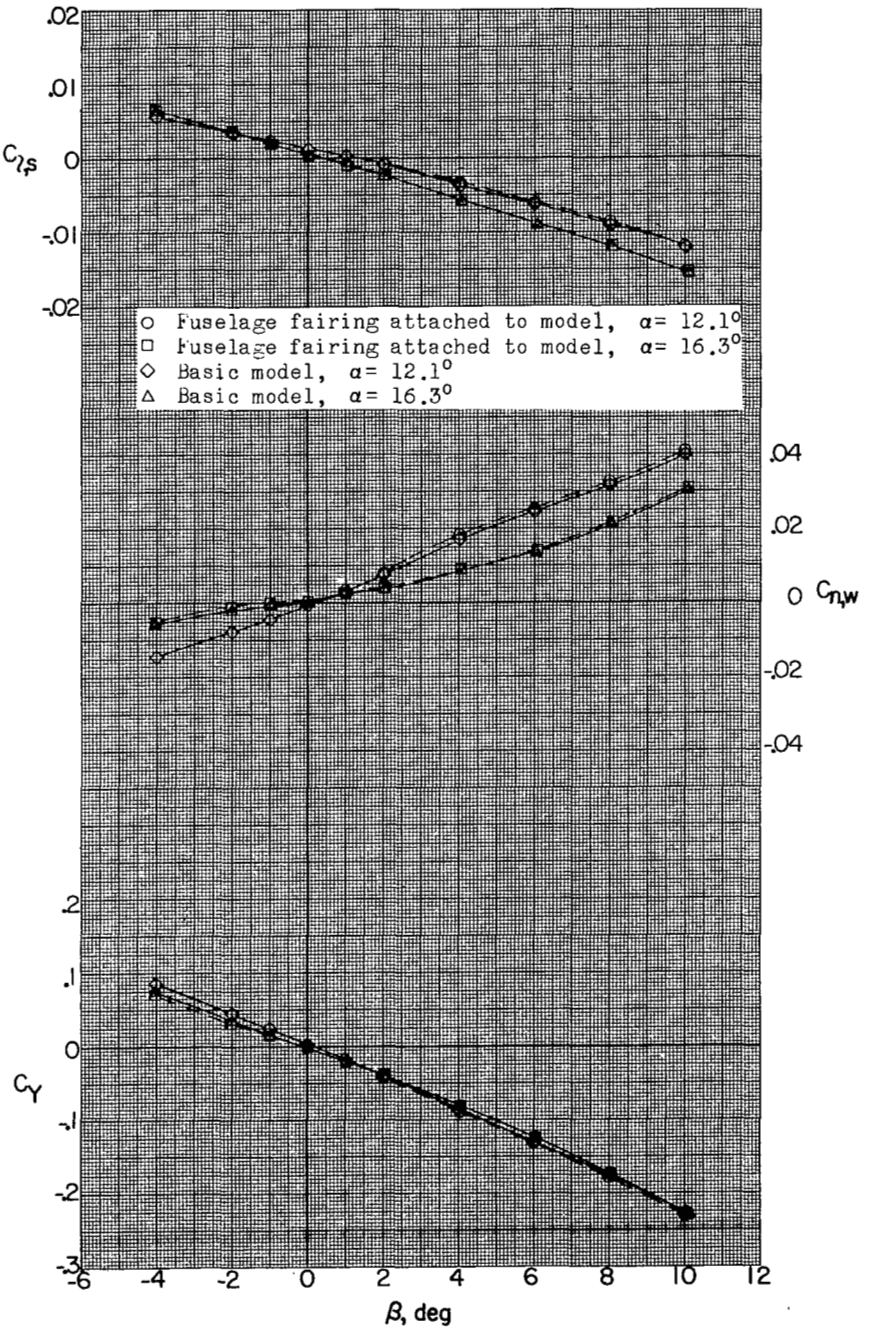

(a) Continued.

Figure 8.- Continued.

[redacted]

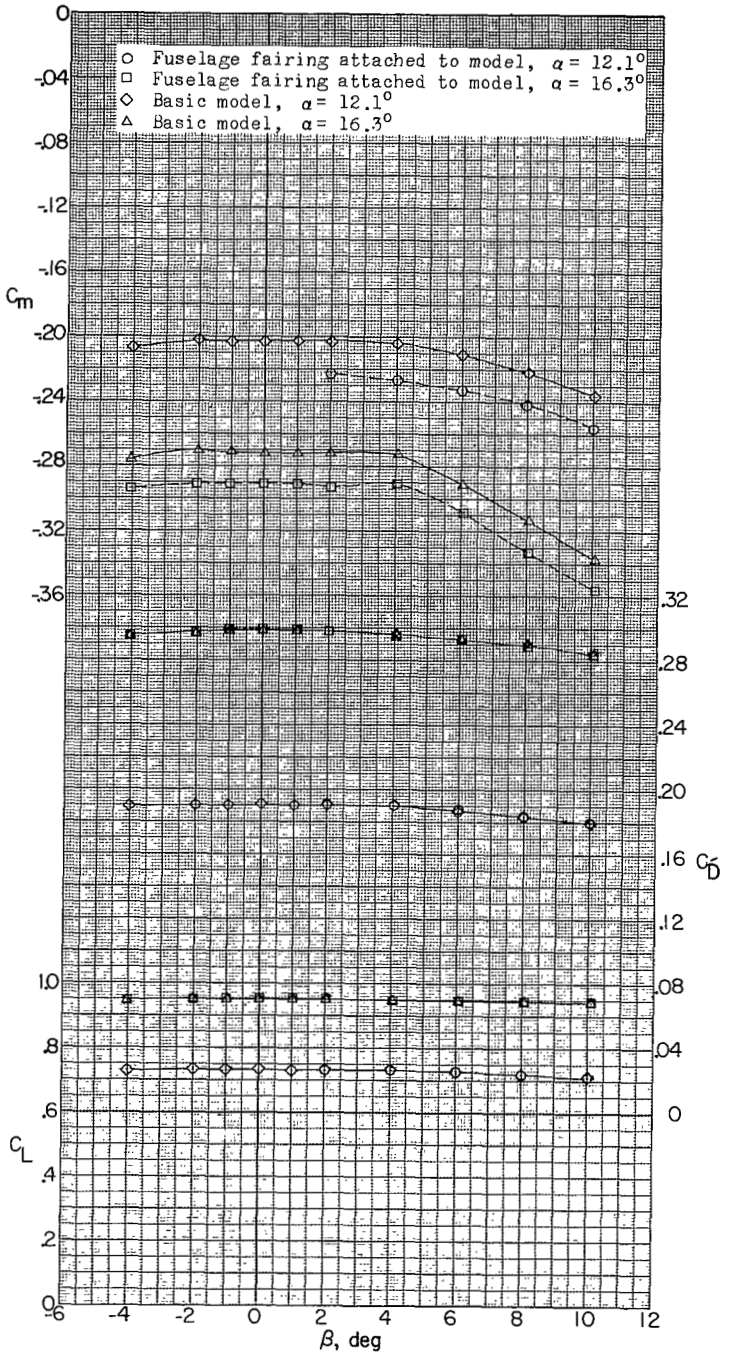

(a) Concluded.

Figure 8.- Continued.

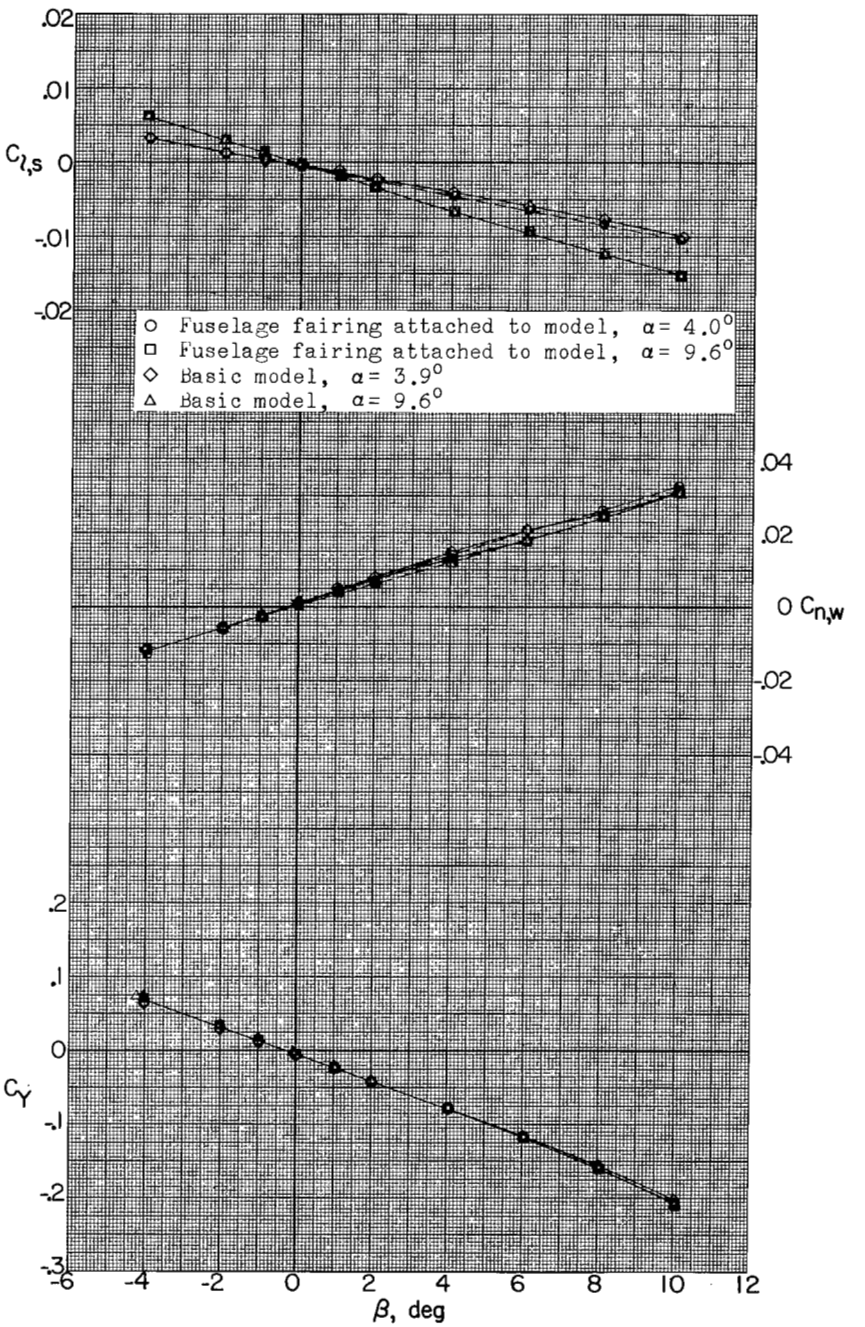

(b) M = 2.06.

Figure 8.- Continued.

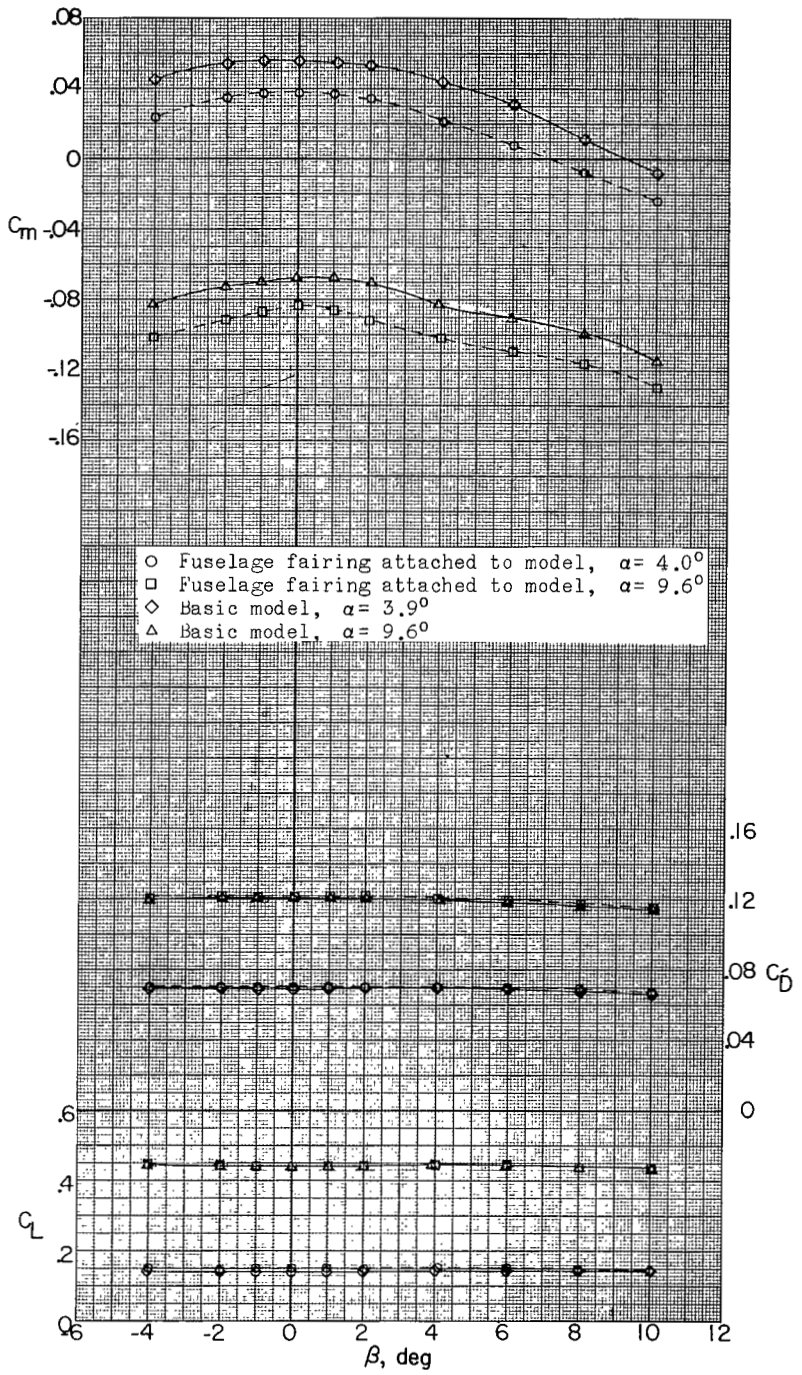

(b) Continued.

Figure 8.- Continued.

[redacted]

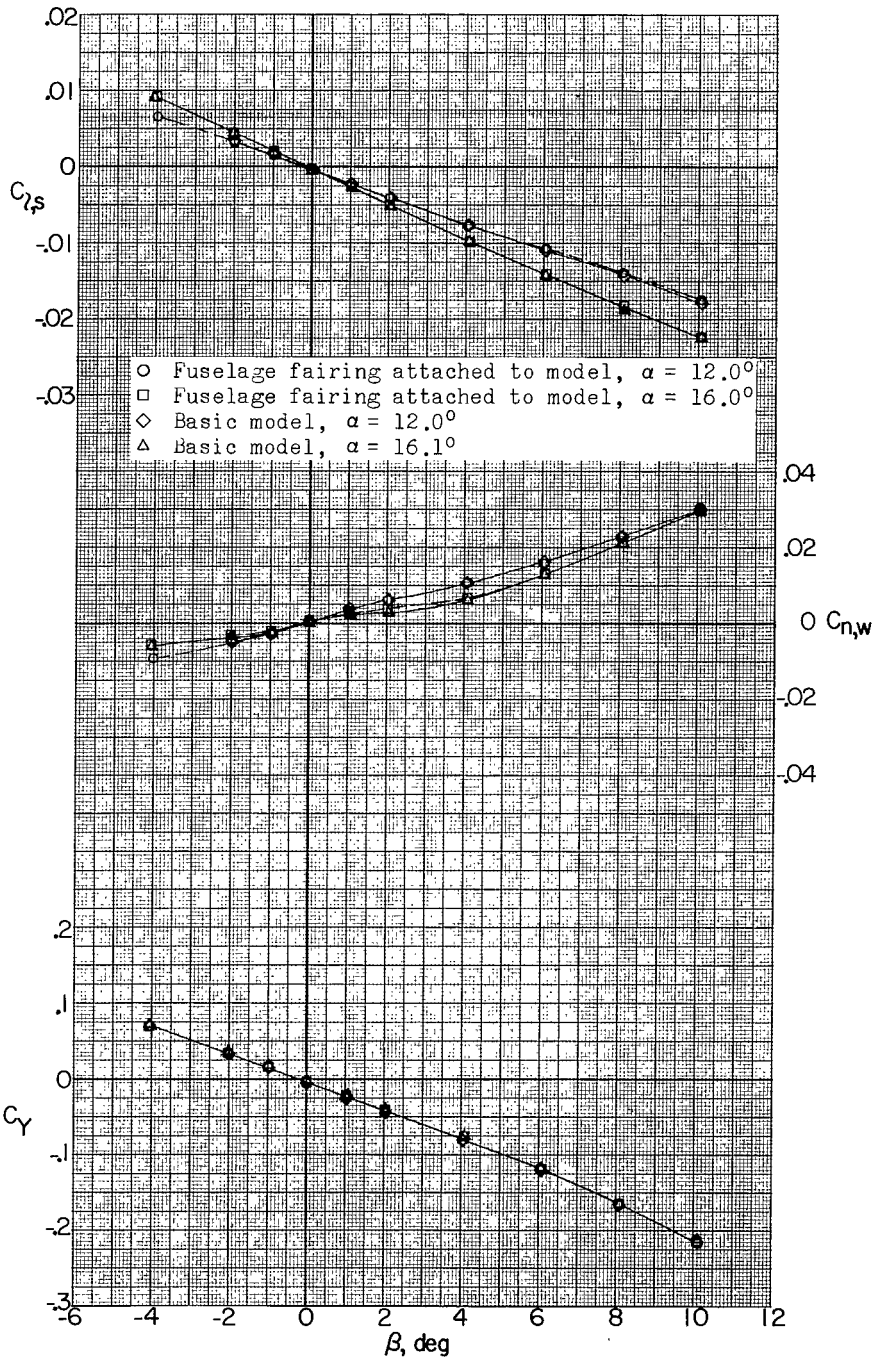

(b) Continued.

Figure 8.- Continued.

[redacted]

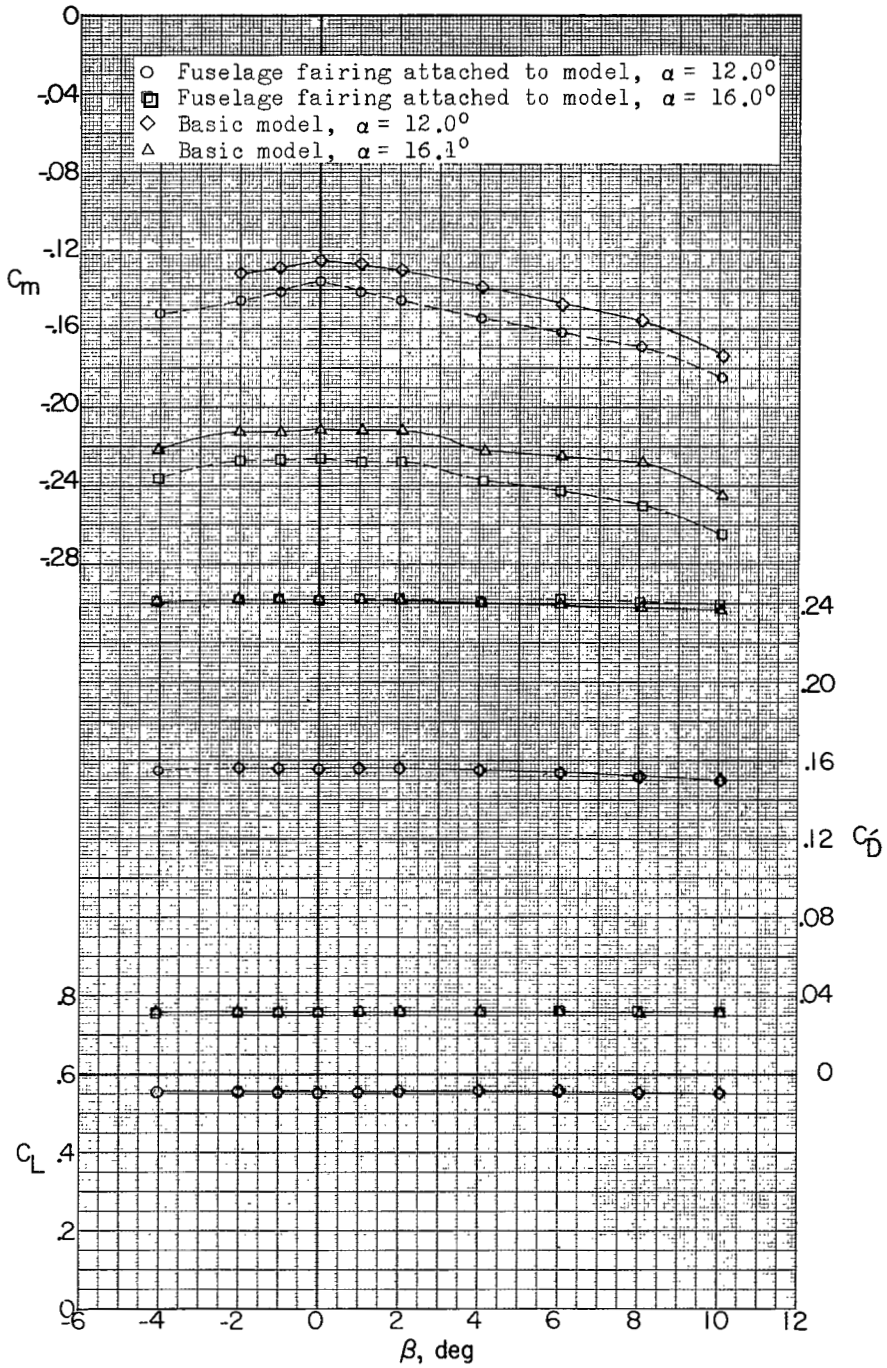

(b) Concluded.

Figure 8.- Concluded.

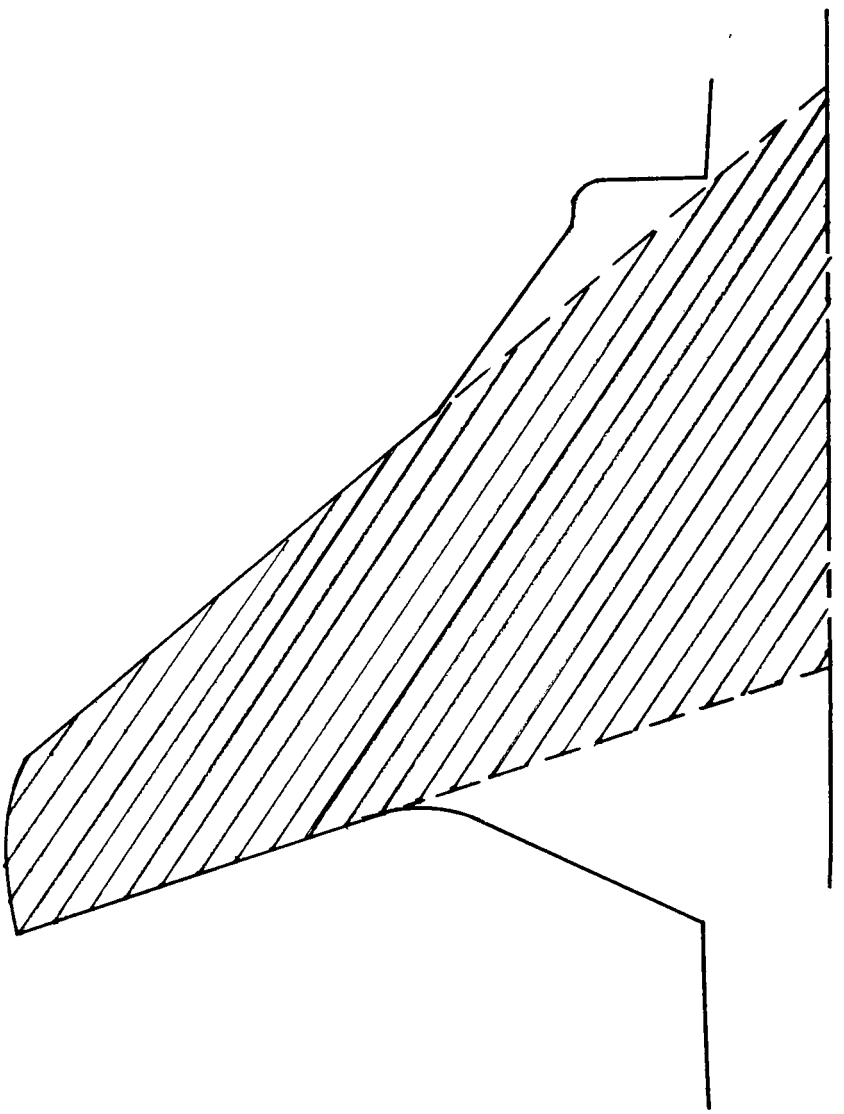

Figure 9.- Wing area used in computation of aerodynamic coefficients.

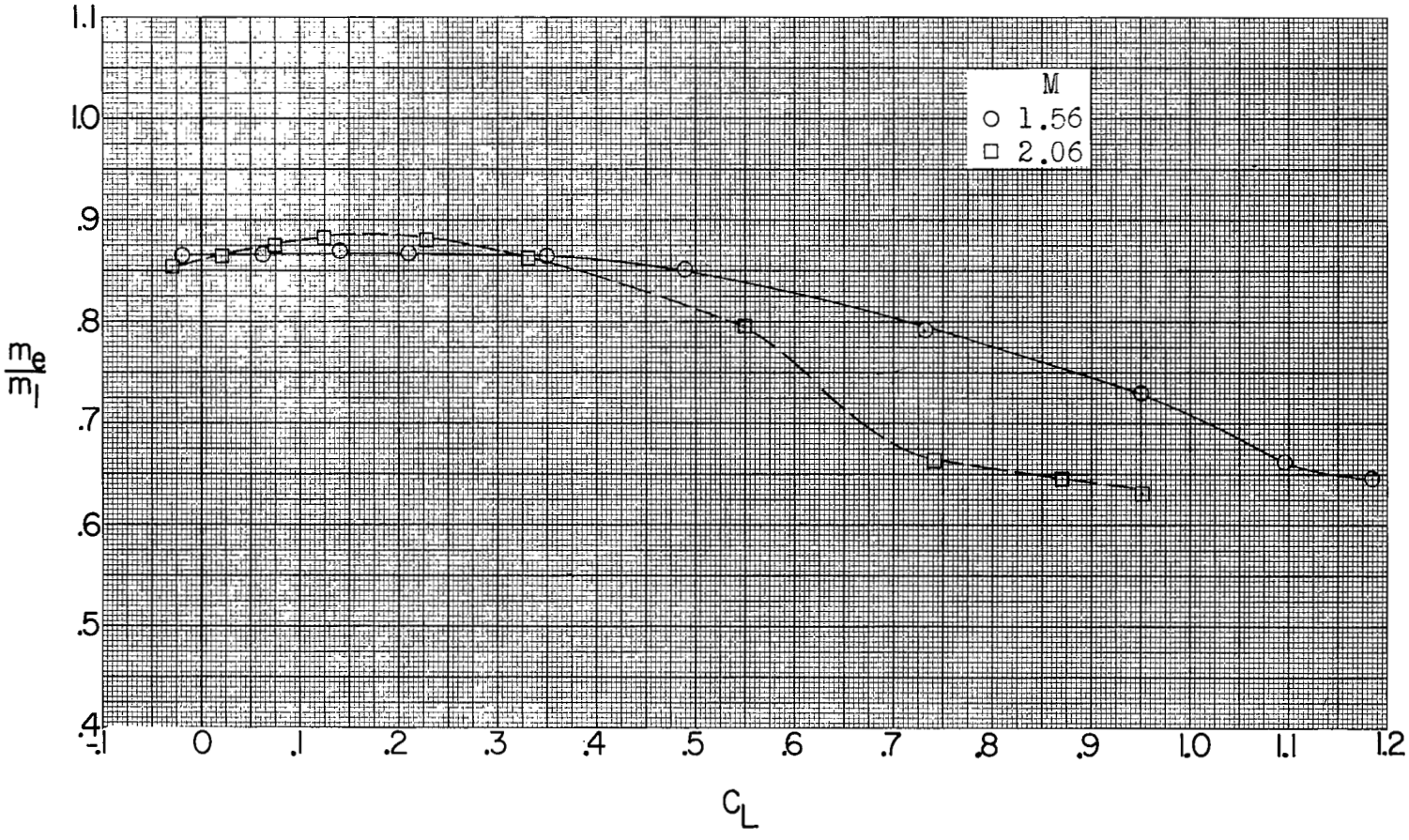

Figure 10.- Effect of duct mass-flow ratio on lift coefficient; $\beta = 0^{\circ}$.

α = .95°
β = .00°

α = 4.01°
β = .00°

α = .92°
β = .03°

α = 9.63°
β = .02°

α = 16.27°
β = .02°

L-95822

(a) Basic model, M = 1.56.

Figure 11.- Typical schlieren photographs of model.

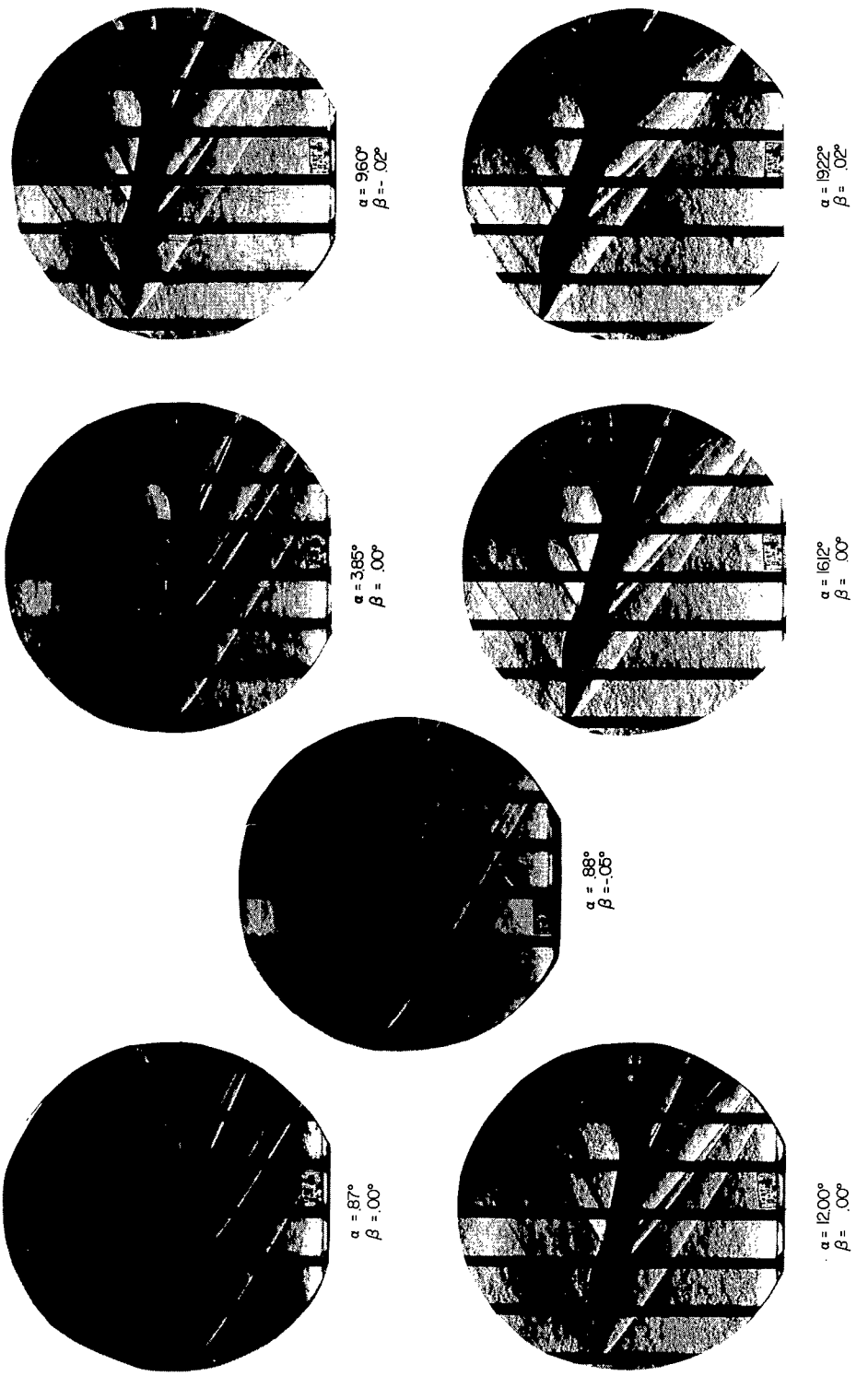

L-95823

(b) Basic model, M = 2.06.

Figure 11.- Continued.

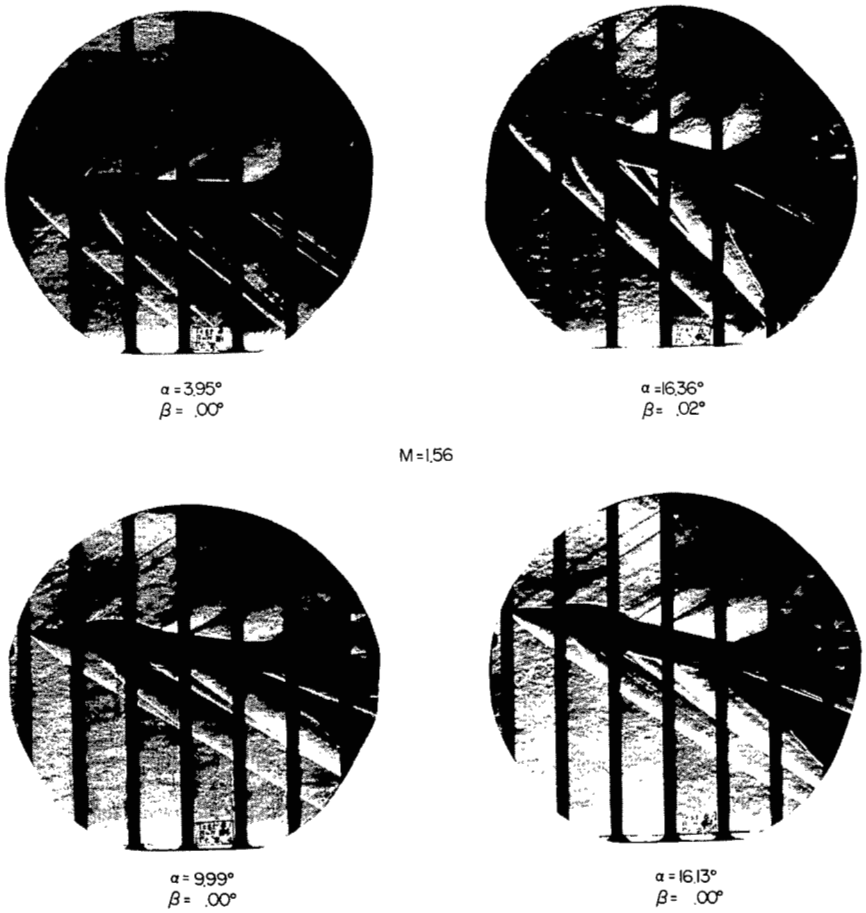

(c) Basic model with missiles.

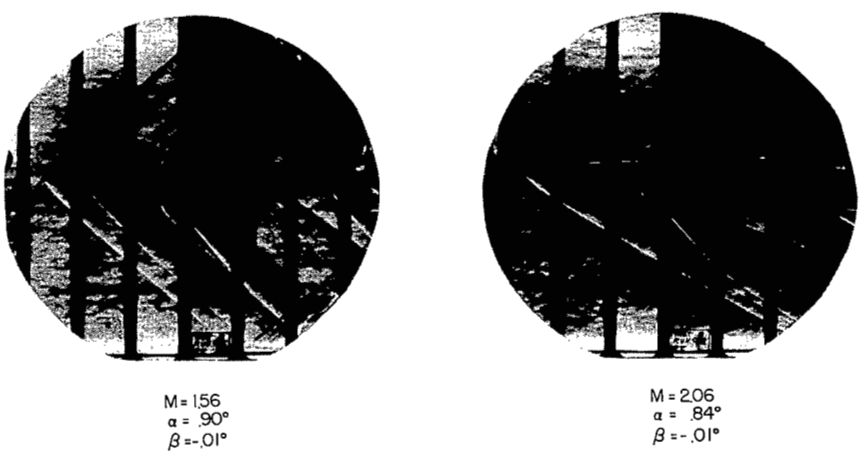

(d) Delta-wing configuration. L-95824

Figure 11.- Concluded.

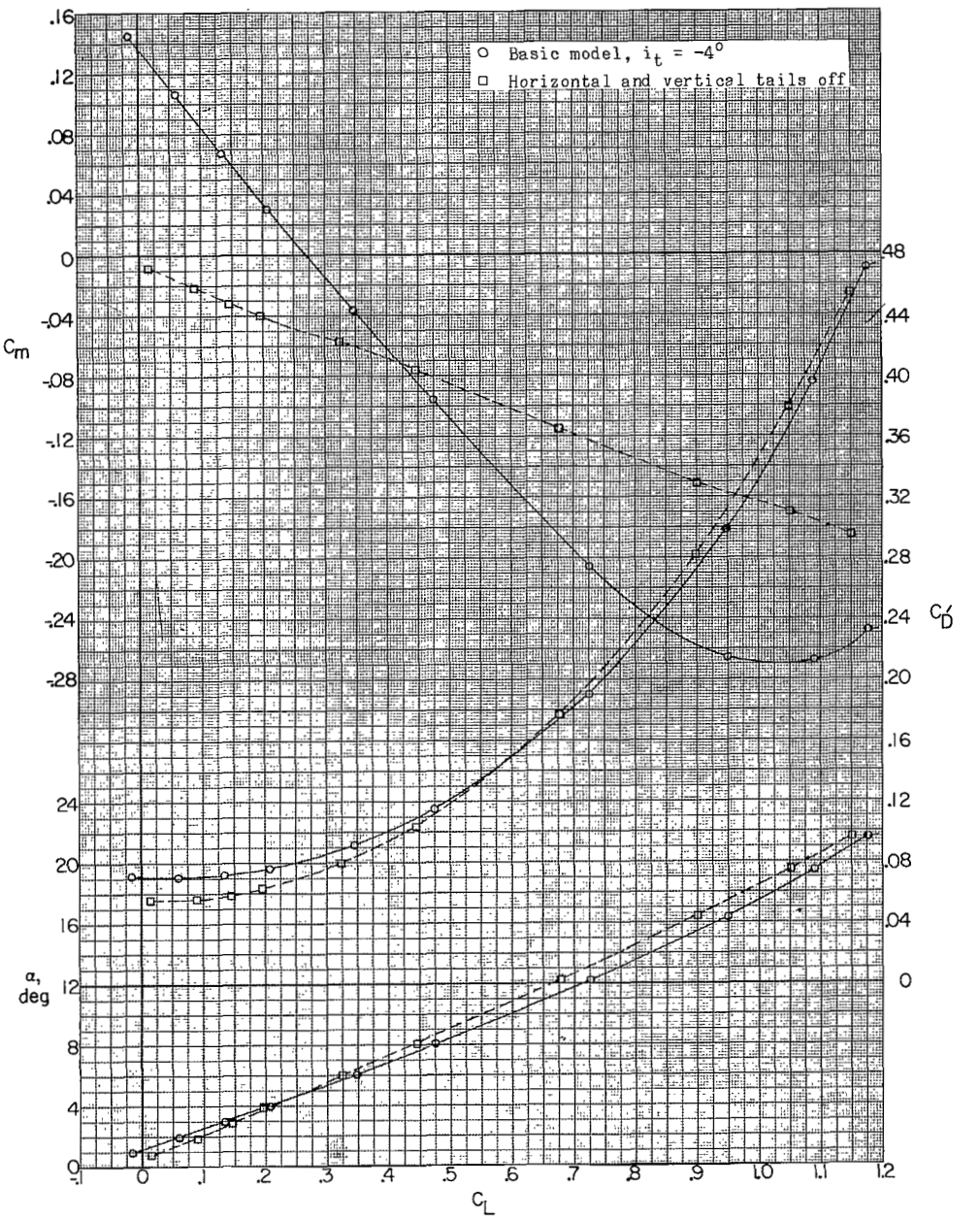

(a) M = 1.56.

Figure 12.- Effects of horizontal and vertical tails on aerodynamic characteristics in pitch; $\beta = 0^\circ$. Data uncorrected for base and internal duct drag. (Flagged symbols denote wall reflected shock waves striking tail.)

[redacted]

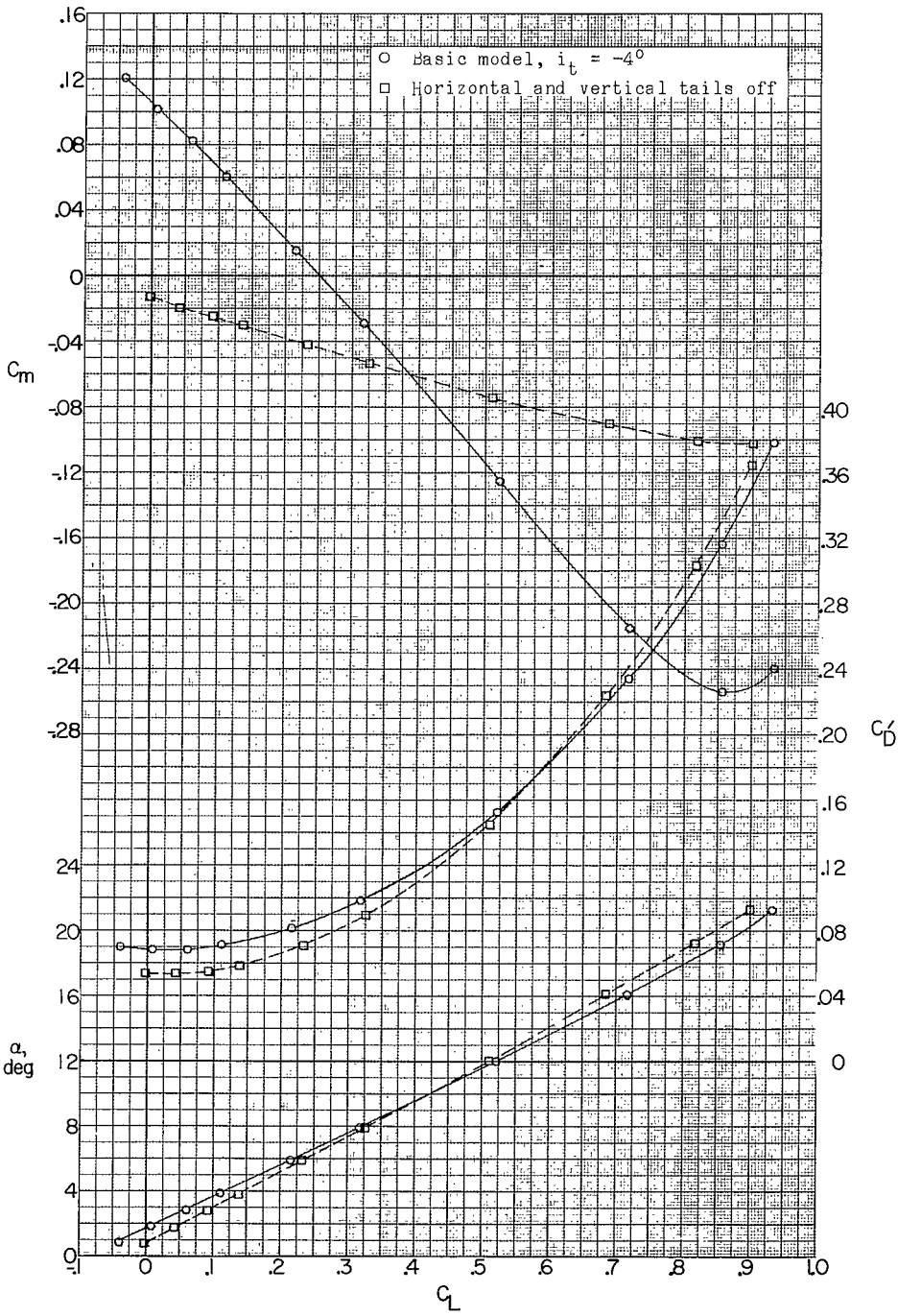

(b) M = 2.06.

Figure 12.- Concluded.

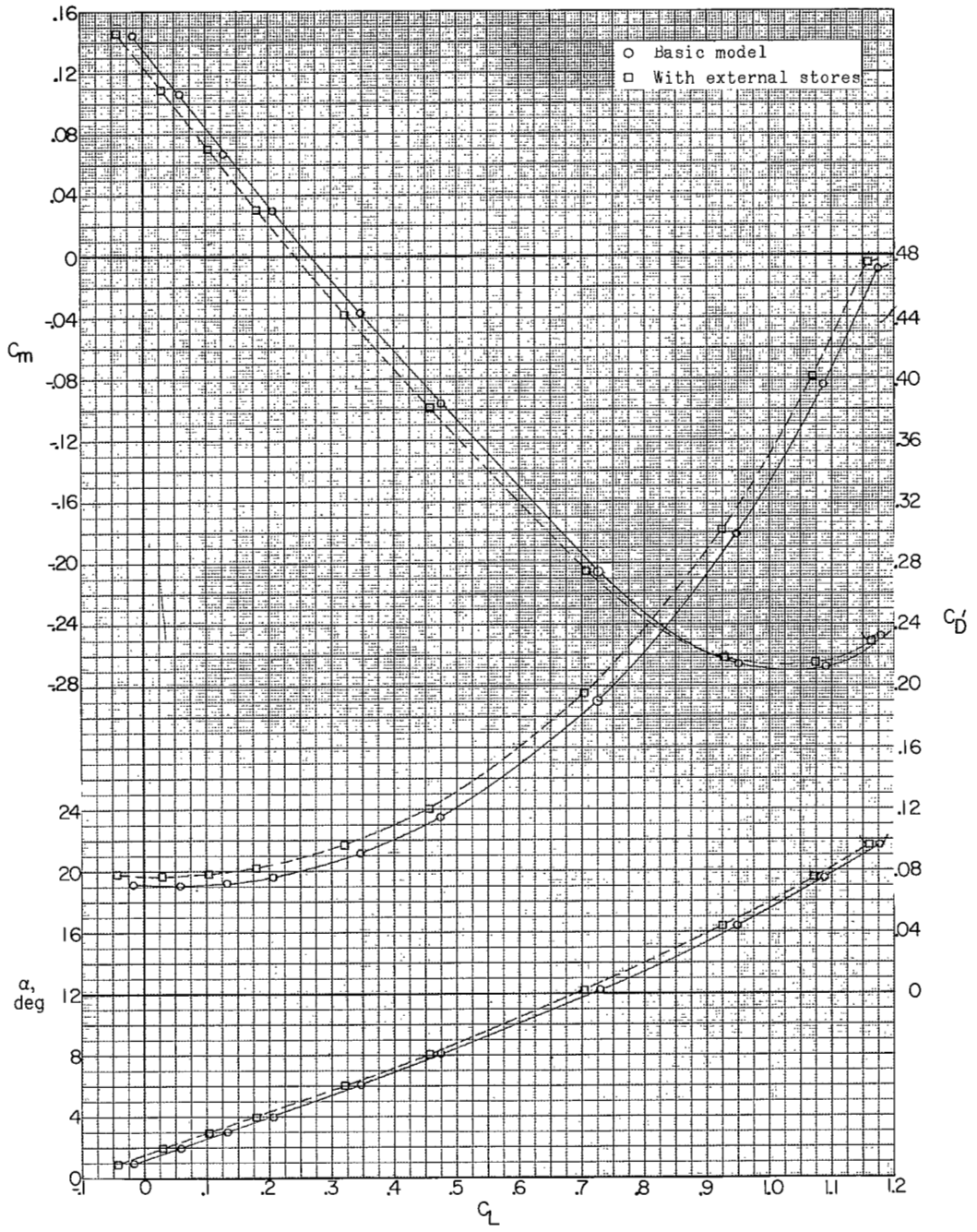

(a) M = 1.56.

Figure 13.- Effect of external stores on aerodynamic characteristics in pitch; $\beta = 0^{\circ}$. Data uncorrected for base and internal duct drag. (Flagged symbols denote wall reflected shock waves striking tail.)

[redacted]

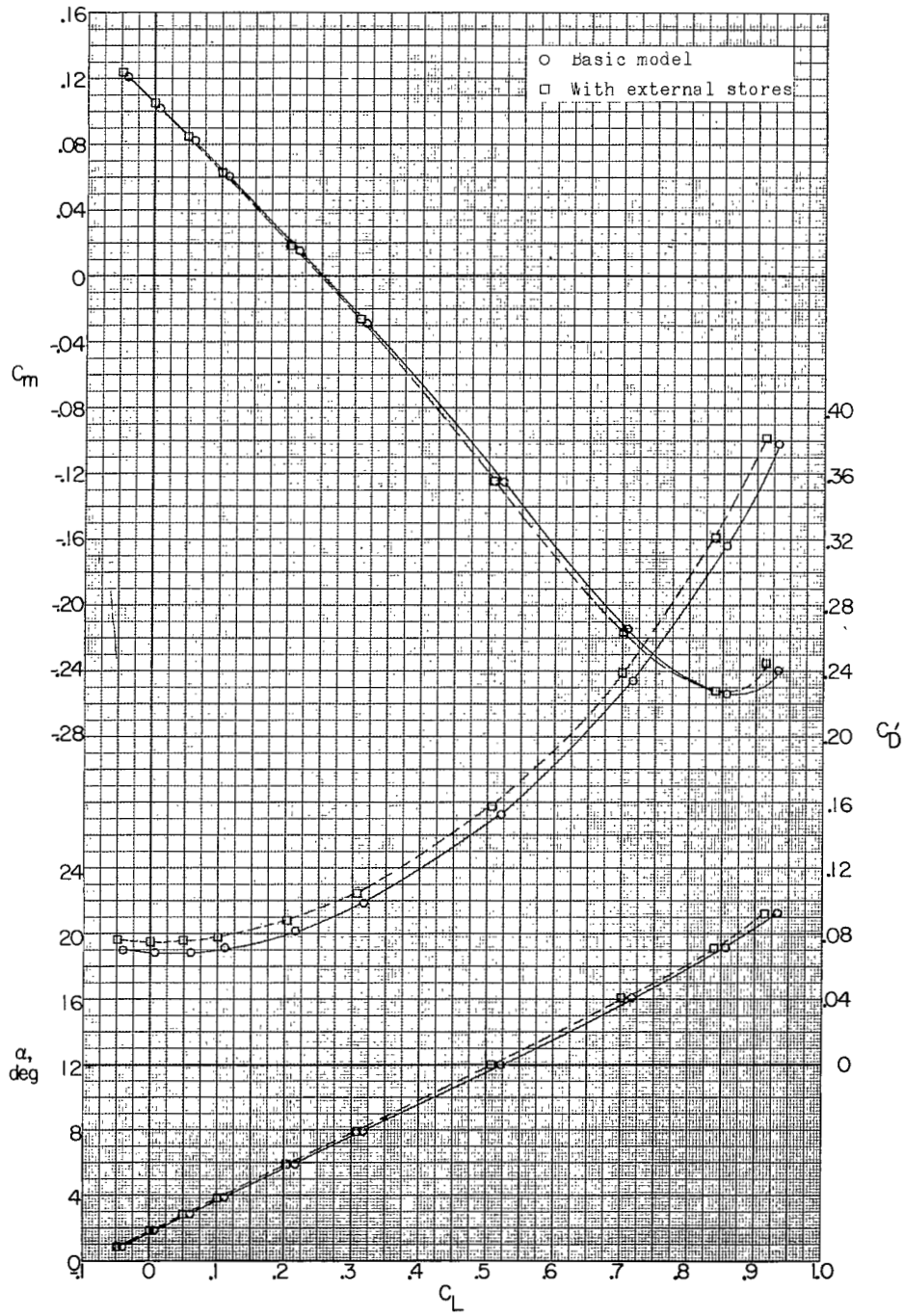

(b) M = 2.06.

Figure 13.- Concluded.

[redacted]

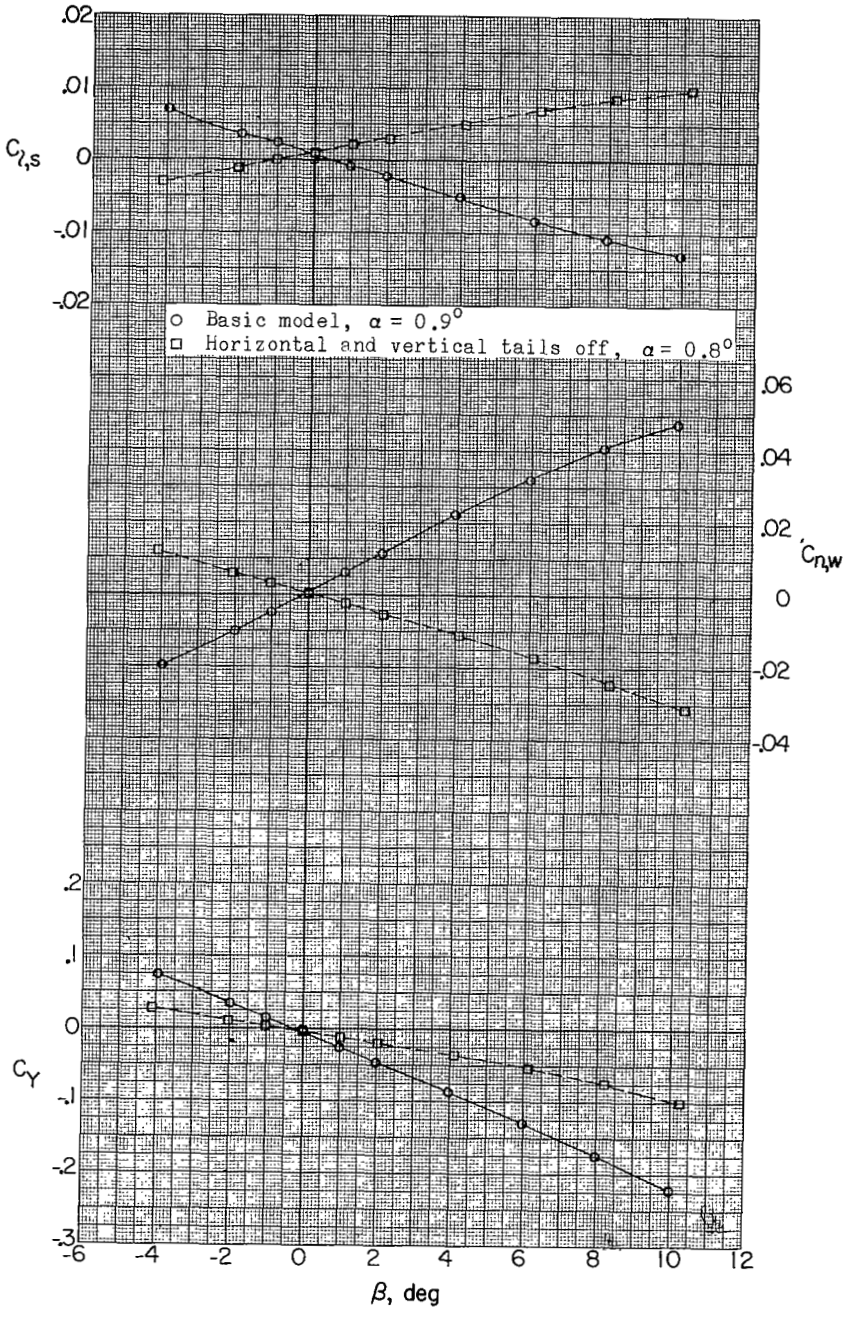

(a) M = 1.56.

Figure 14.- Effects of horizontal and vertical tails on aerodynamic characteristics in sideslip.

[redacted]

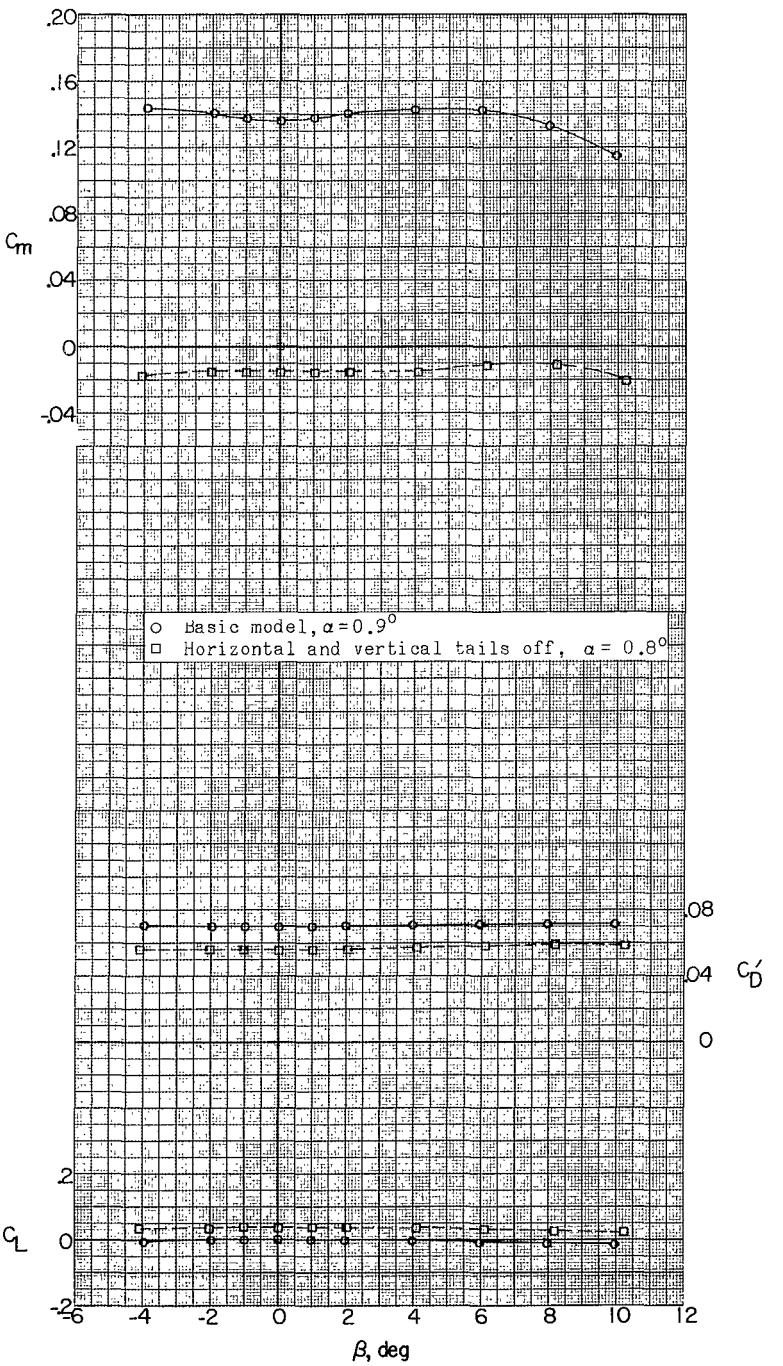

(a) Continued.

Figure 14.- Continued.

[redacted]

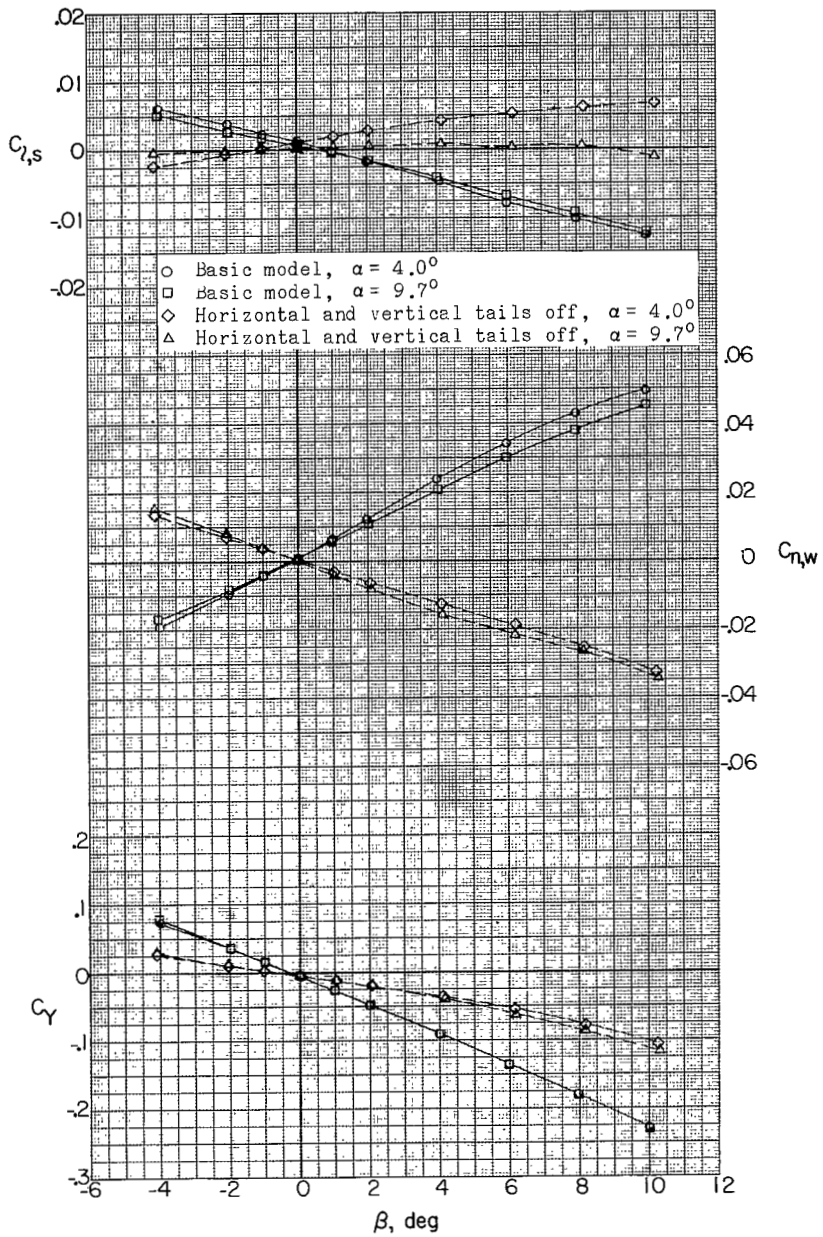

(a) Continued.

Figure 14.- Continued.

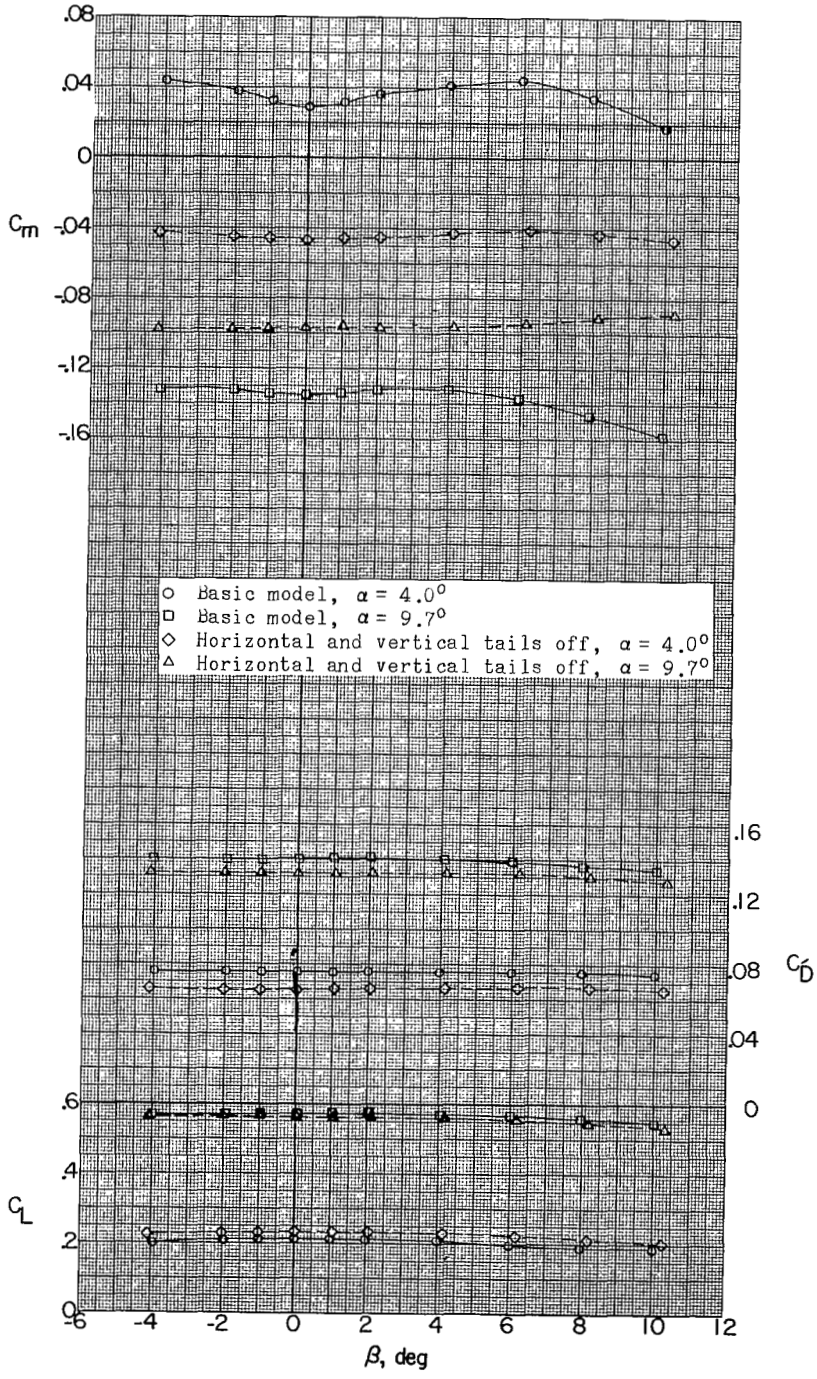

(a) Continued.

Figure 14.- Continued.

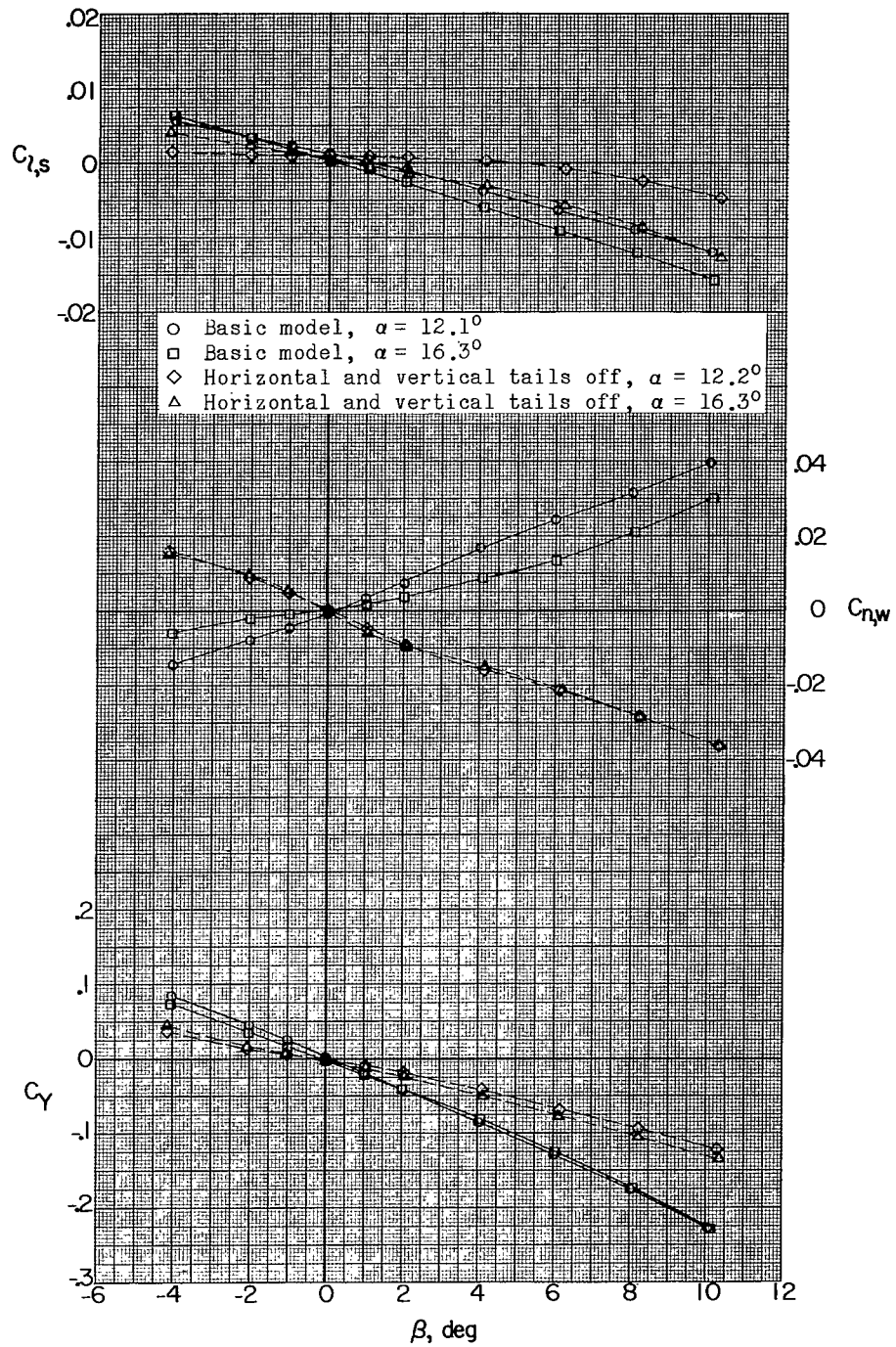

(a) Continued.

Figure 14.- Continued.

[redacted]

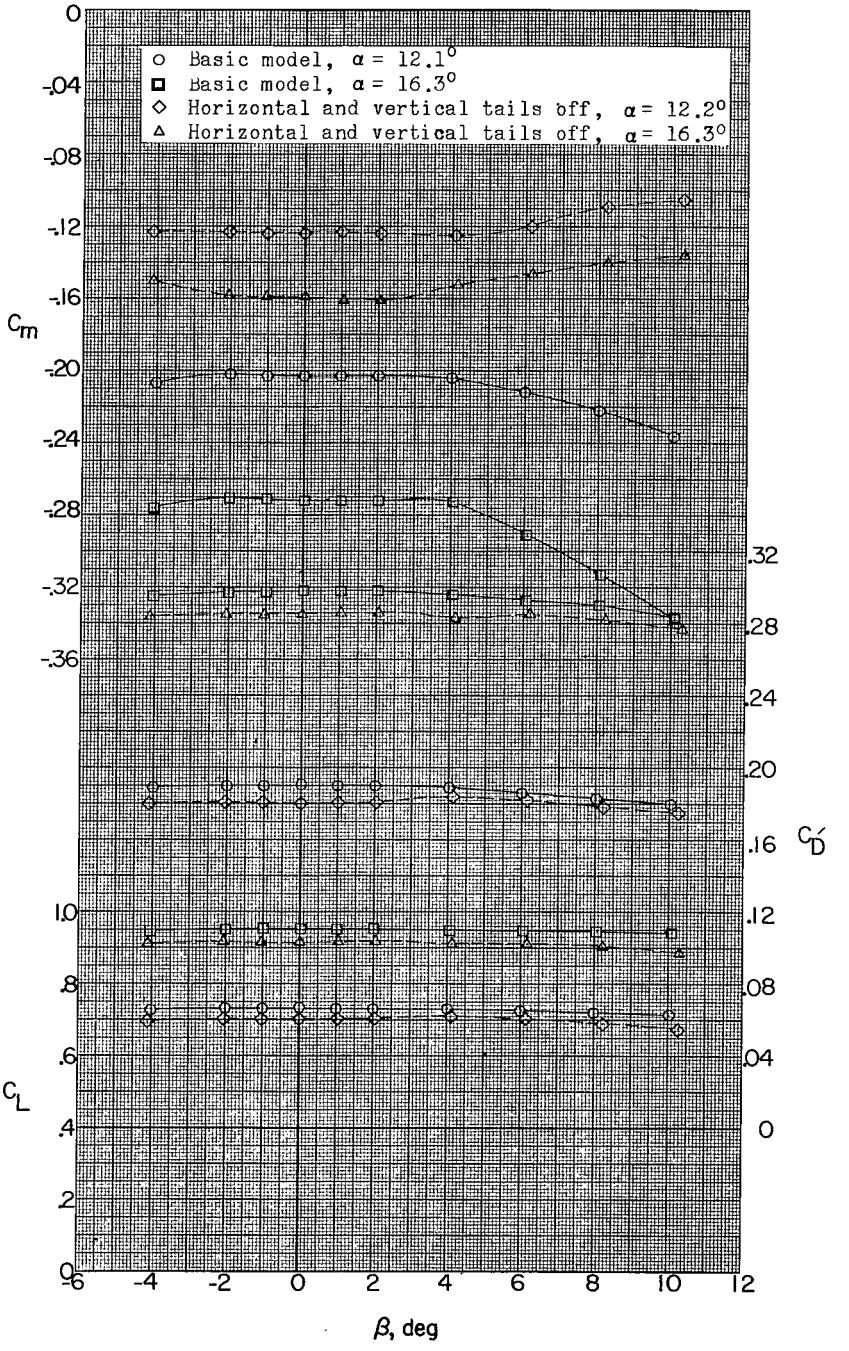

(a) Concluded.

Figure 14.- Continued.

[redacted]

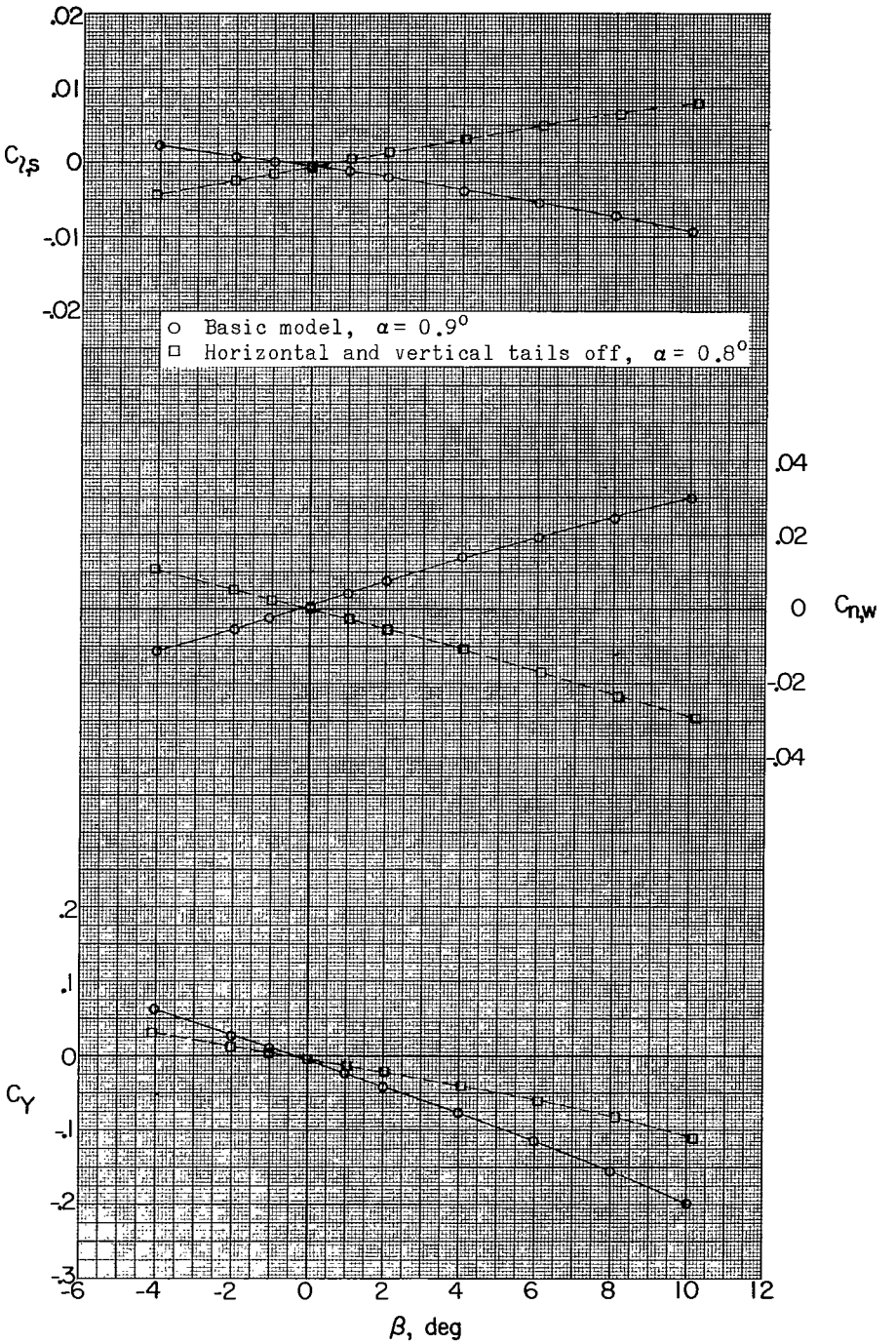

(b) M = 2.06.

Figure 14.- Continued.

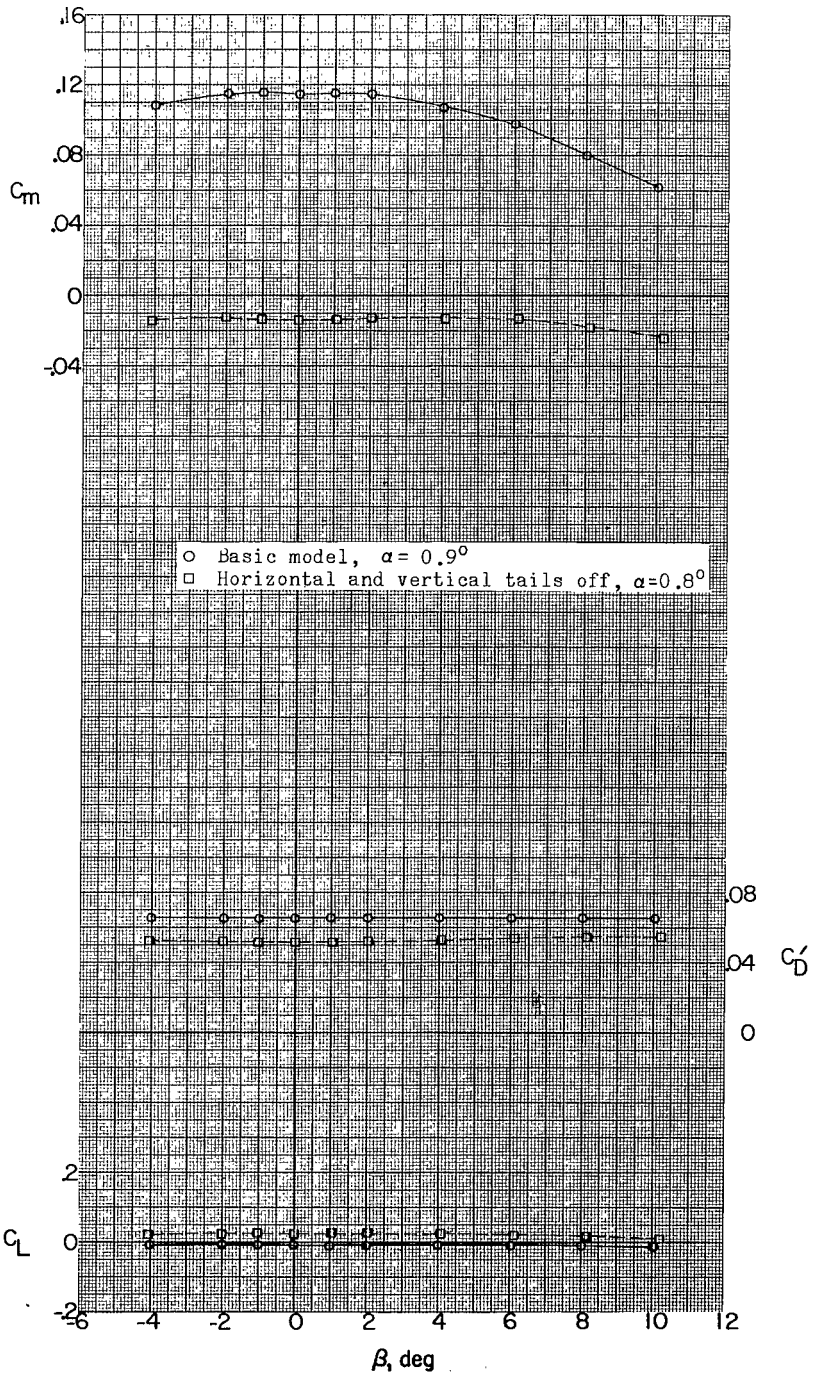

(b) Continued.

Figure 14.- Continued.

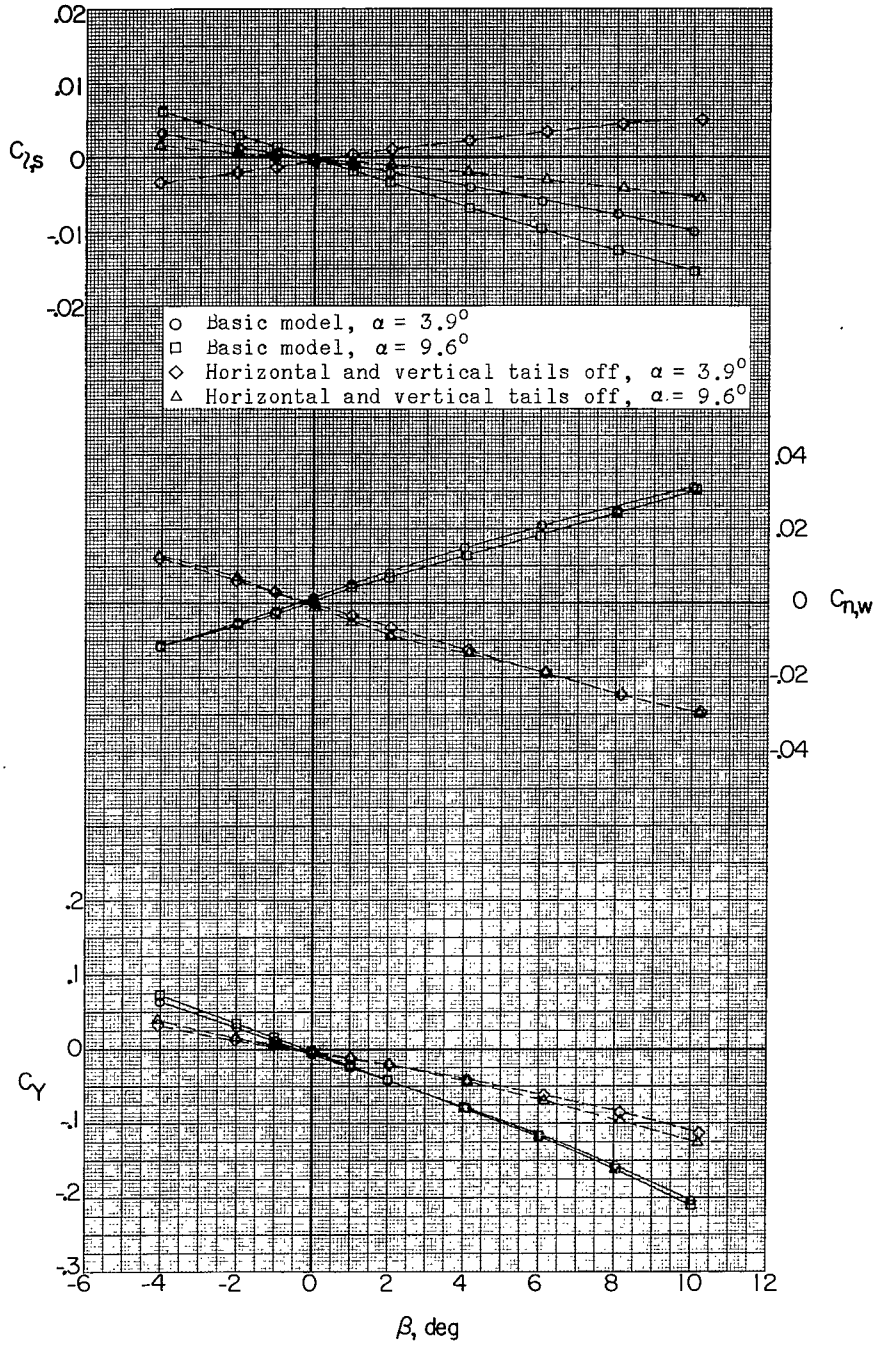

(b) Continued.

Figure 14.- Continued.

[redacted]

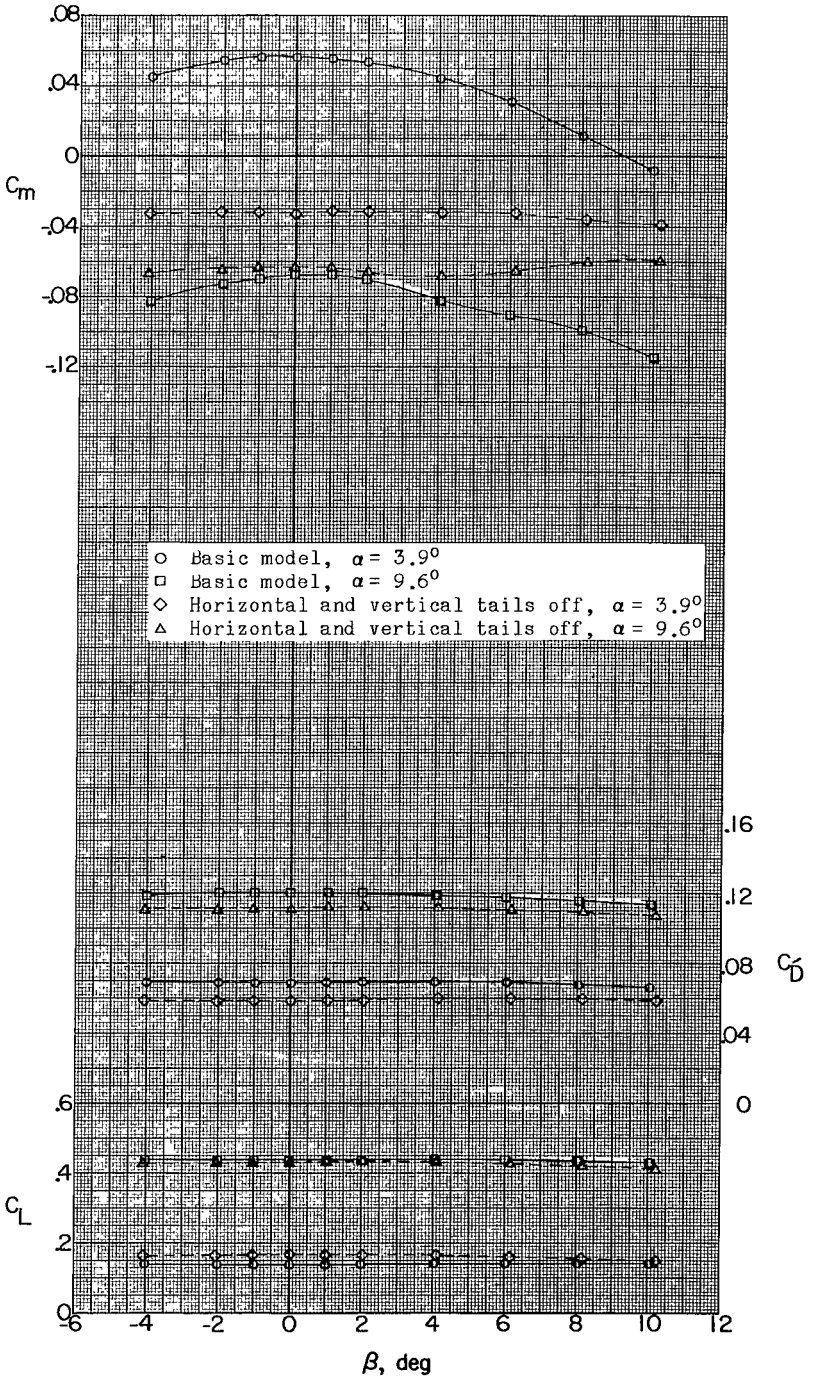

(b) Continued.

Figure 14.- Continued.

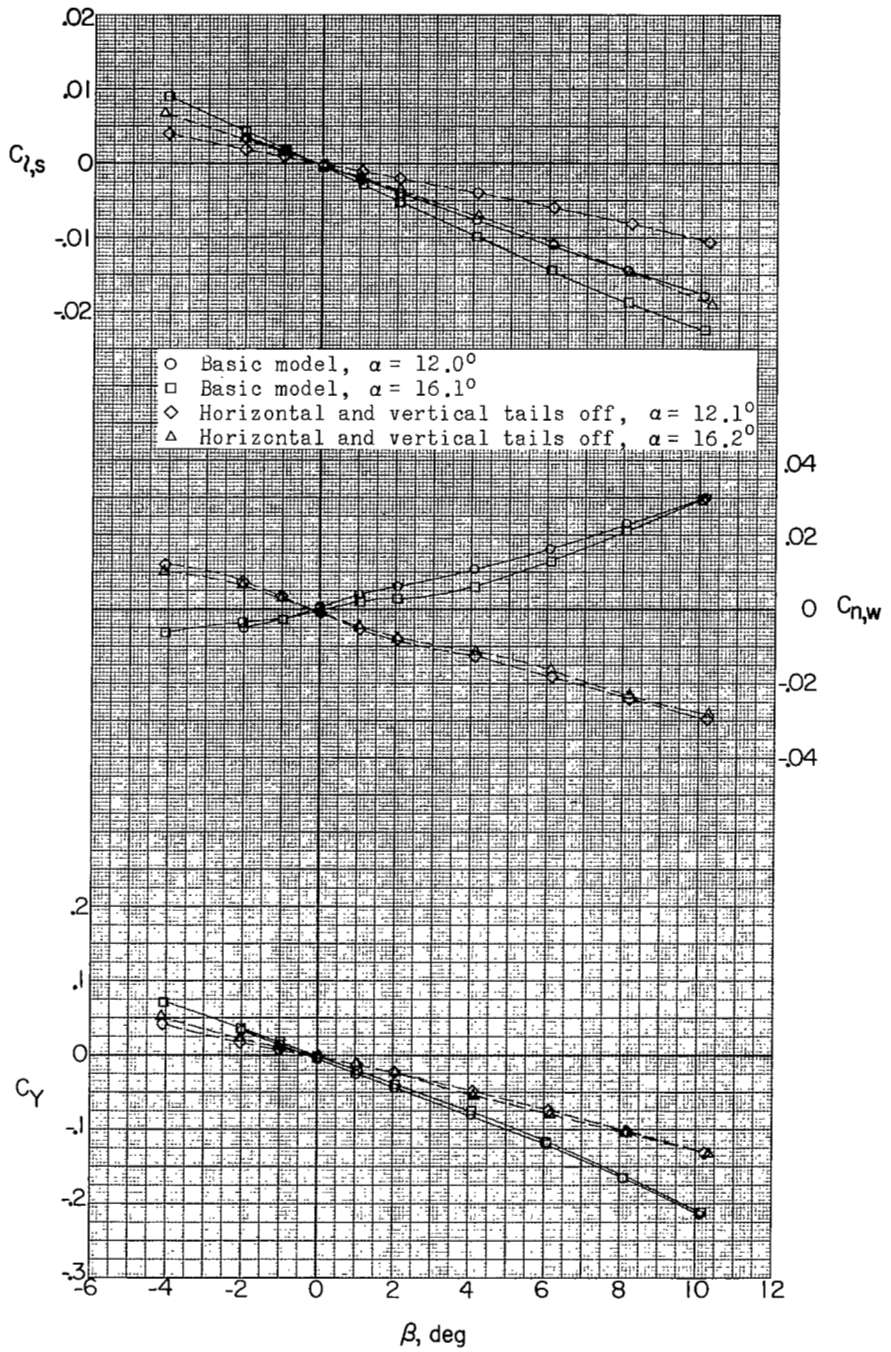

(b) Continued.

Figure 14.- Continued.

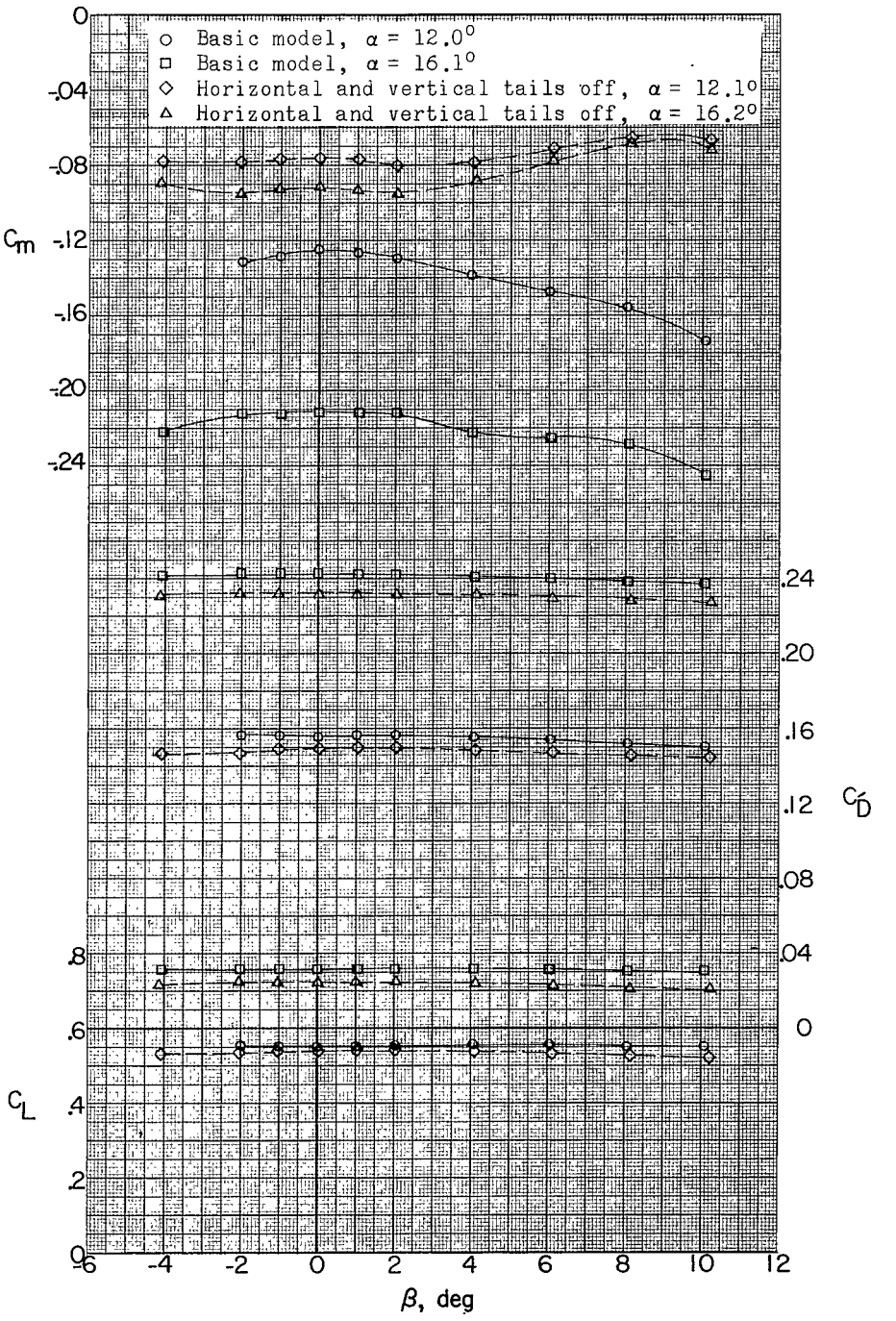

(b) Continued.

Figure 14.- Continued.

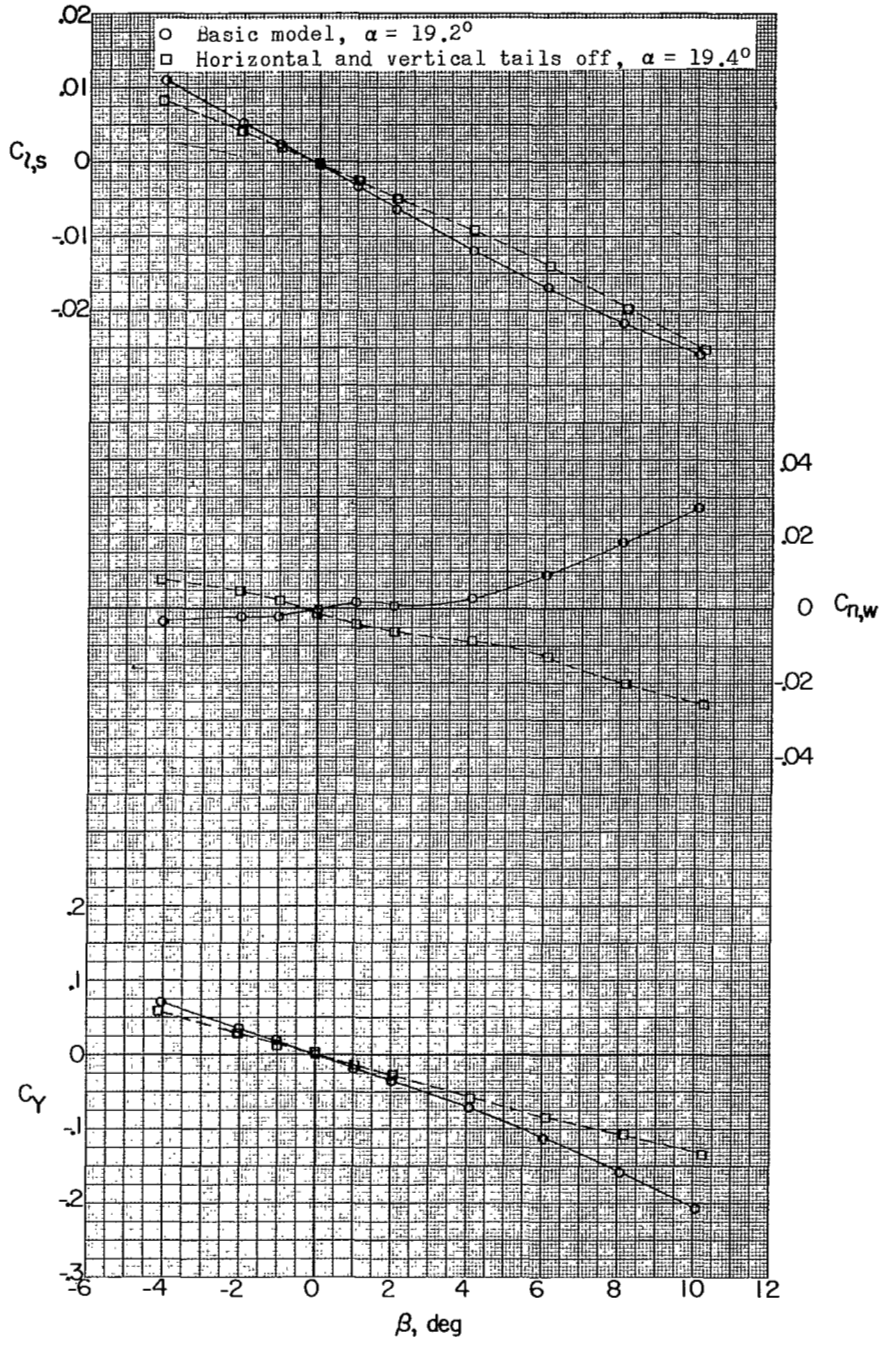

(b) Continued.

Figure 14.- Continued.

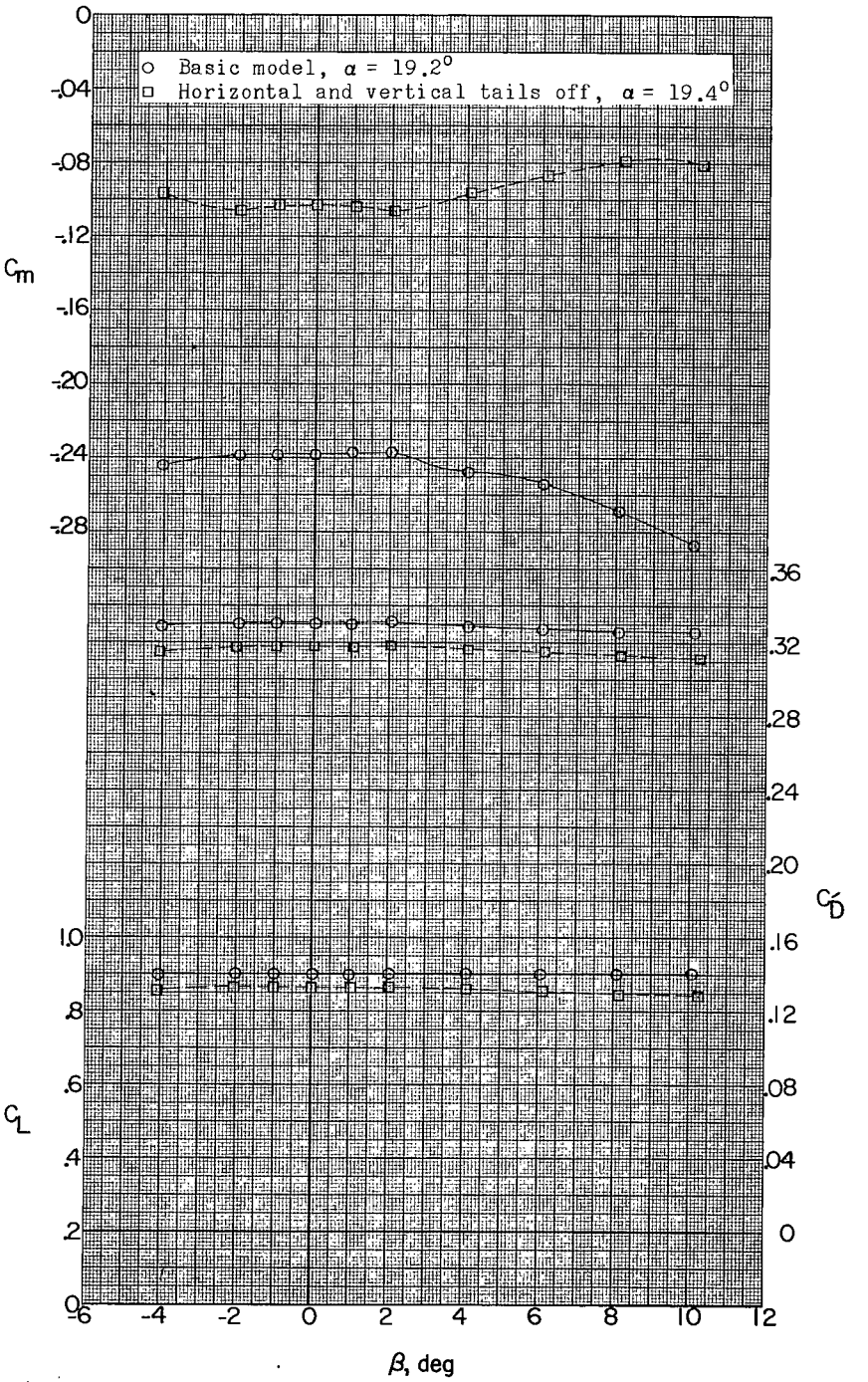

(b) Concluded.

Figure 14.- Concluded.

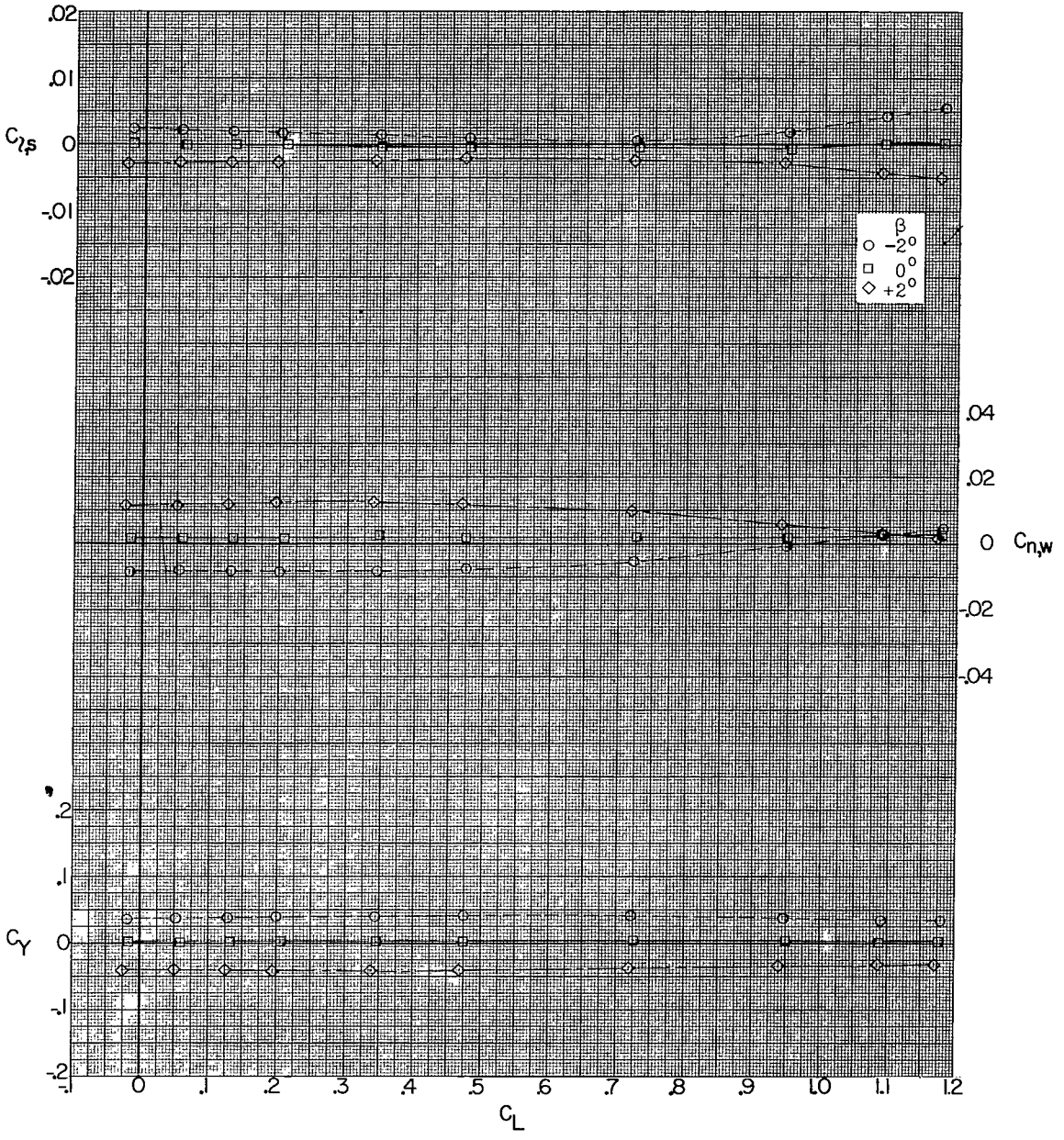

(a) M = 1.56.

Figure 15.- Effect of sideslip on lateral stability for basic-model configuration in pitch.

[redacted]

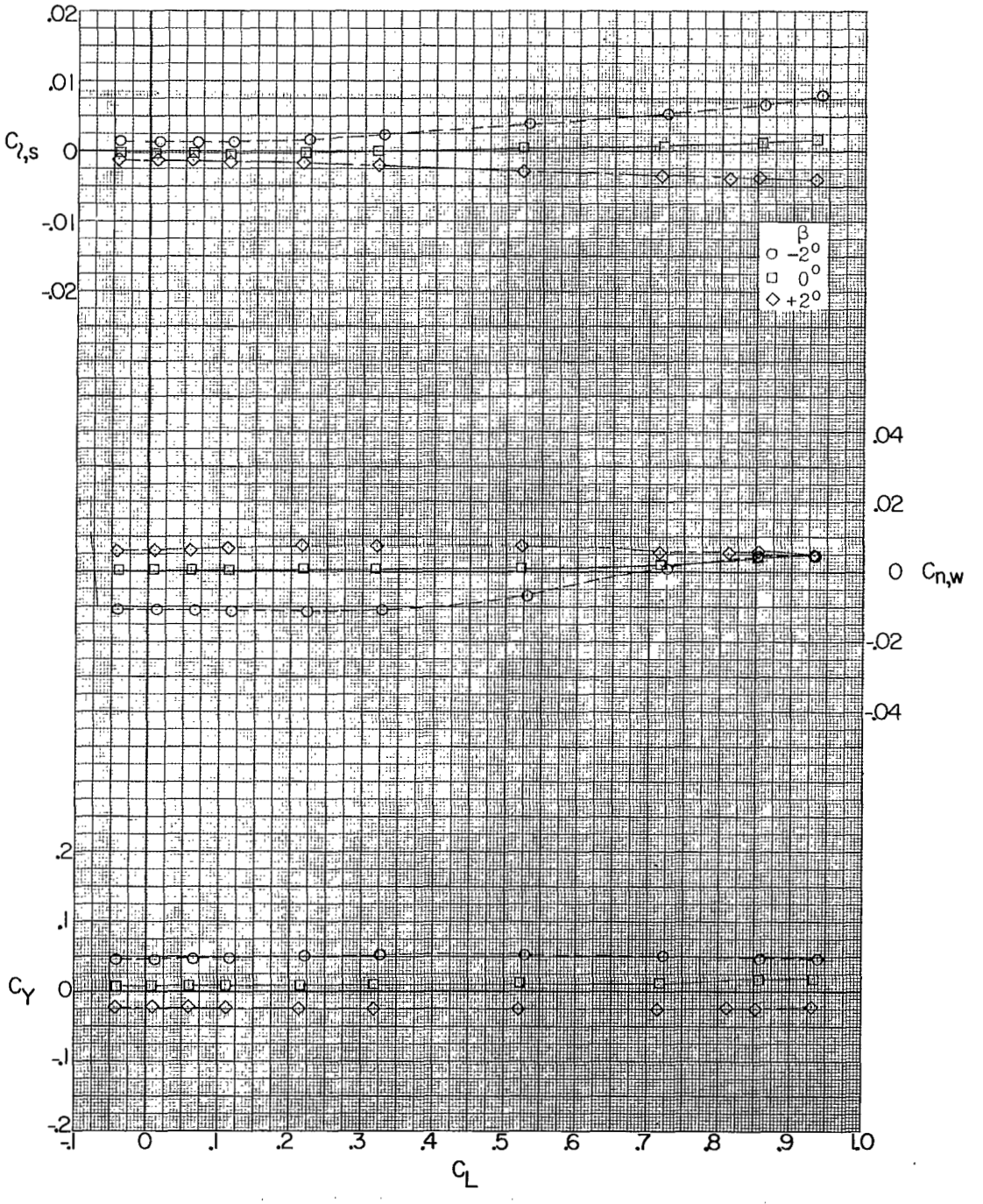

(b) M = 2.06.

Figure 15.- Concluded.

[redacted]

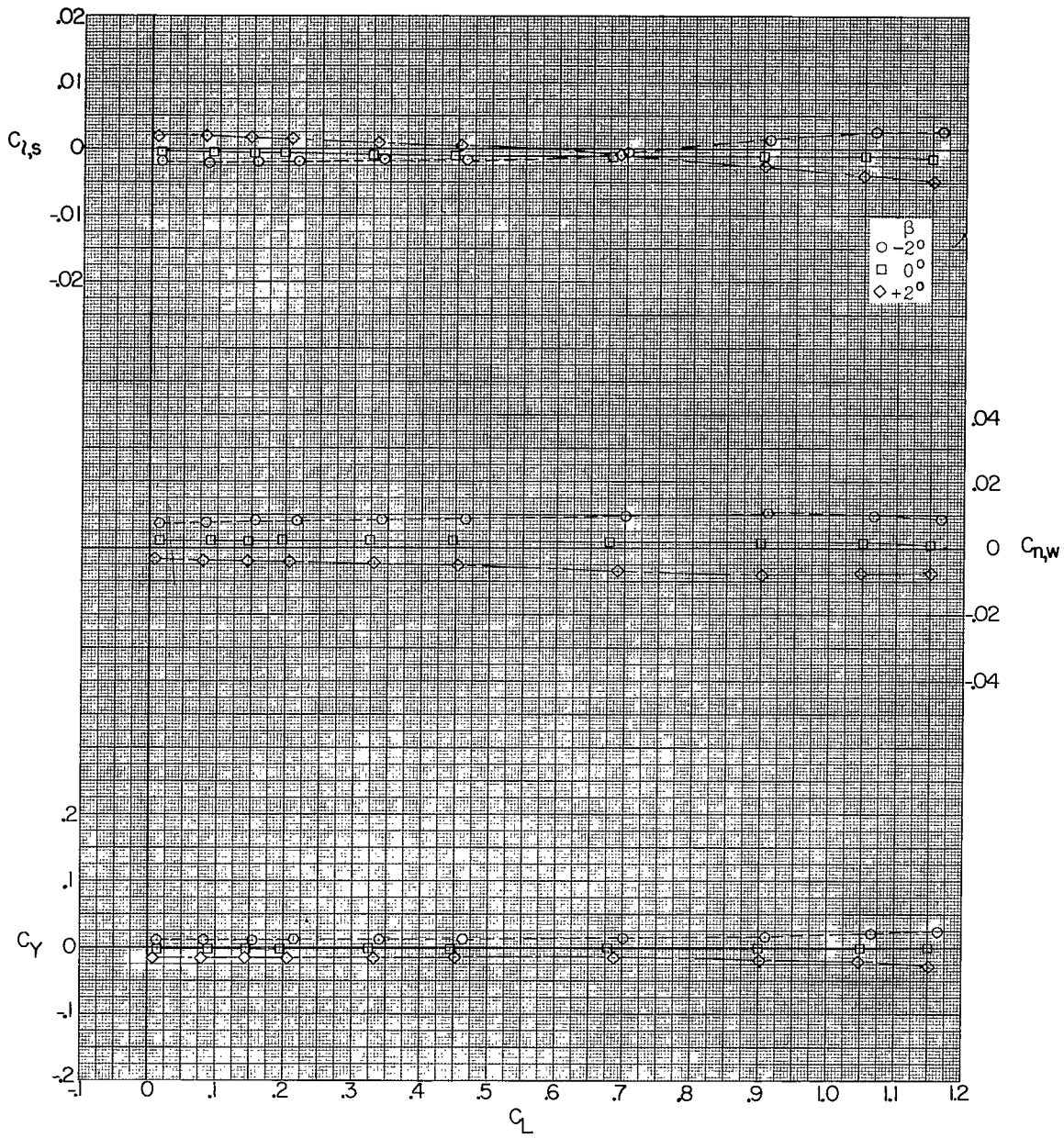

(a) M = 1.56.

Figure 16.- Effect of sideslip on lateral stability for model configuration with tails off in pitch.

[redacted]

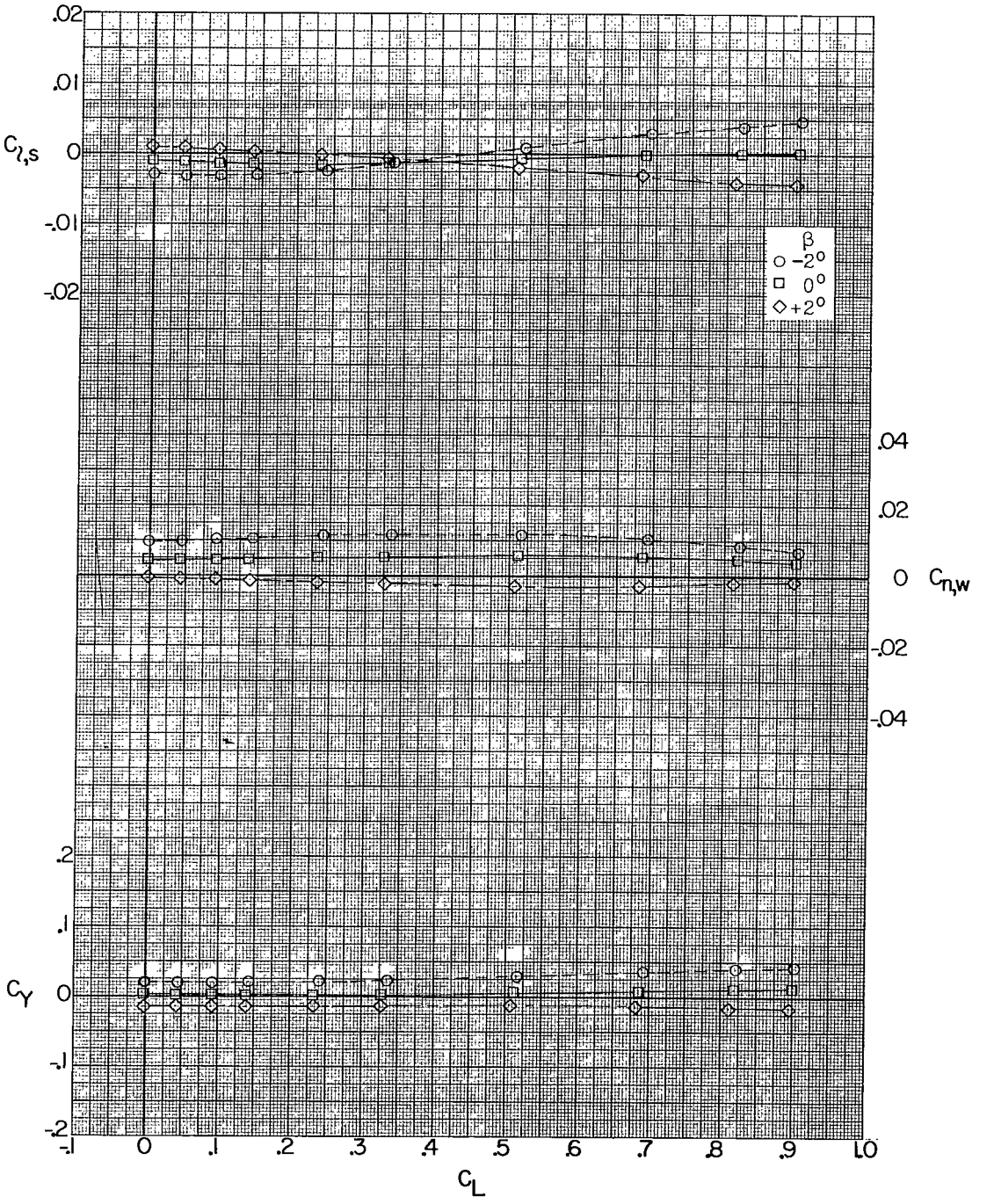

(b) M = 2.06.

Figure 16.- Concluded.

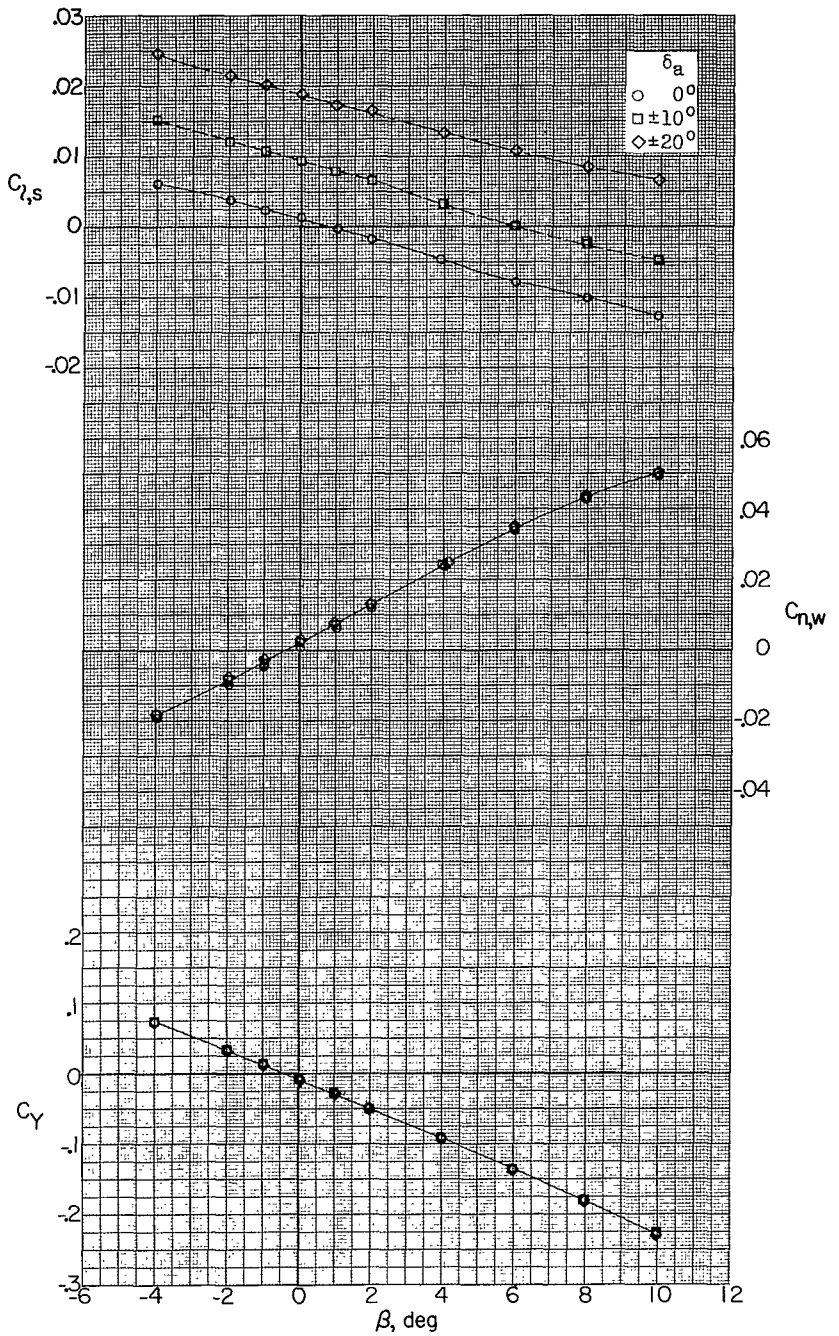

(a) M = 1.56; $\alpha = 4.0^\circ$.

Figure 17.- Effect of aileron deflection on aerodynamic characteristics in sideslip.

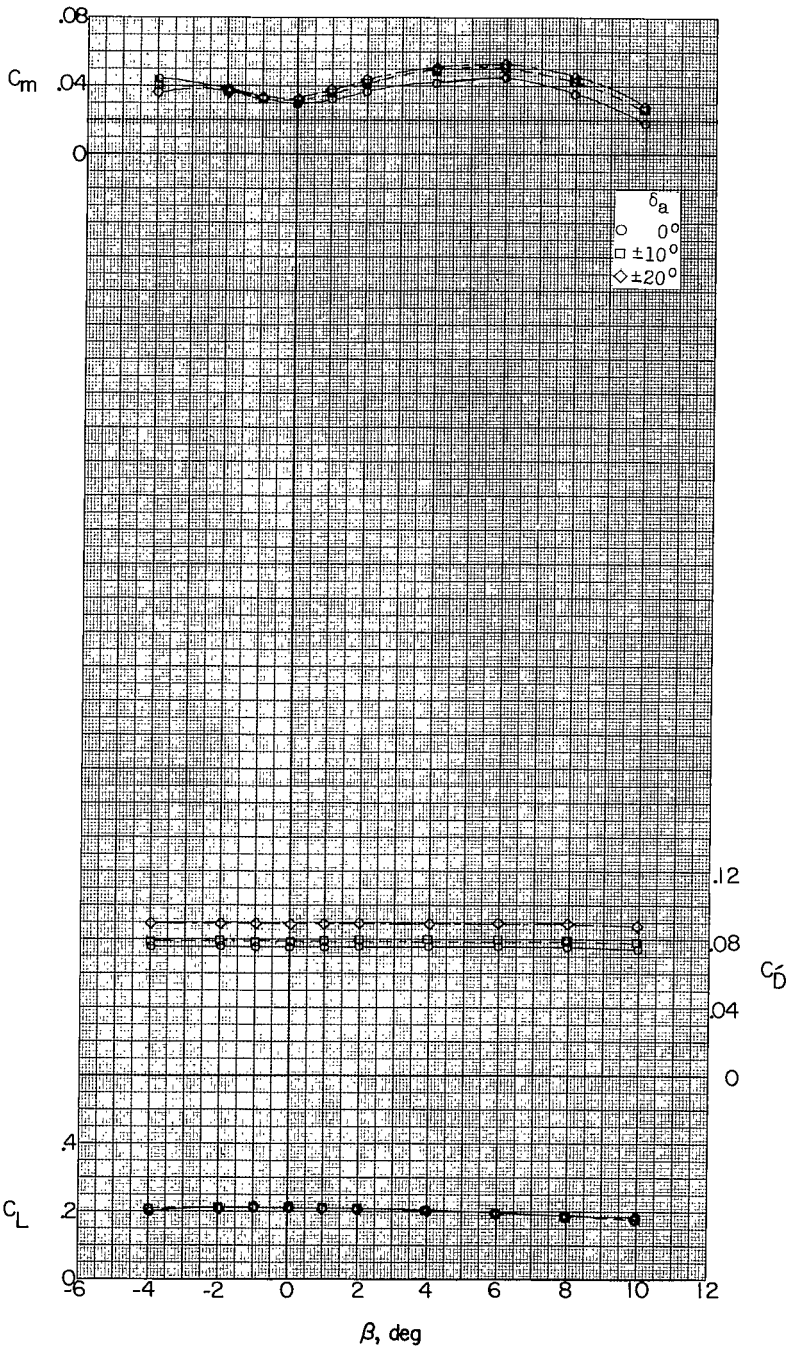

(a) Concluded.

Figure 17.- Continued.

[redacted]

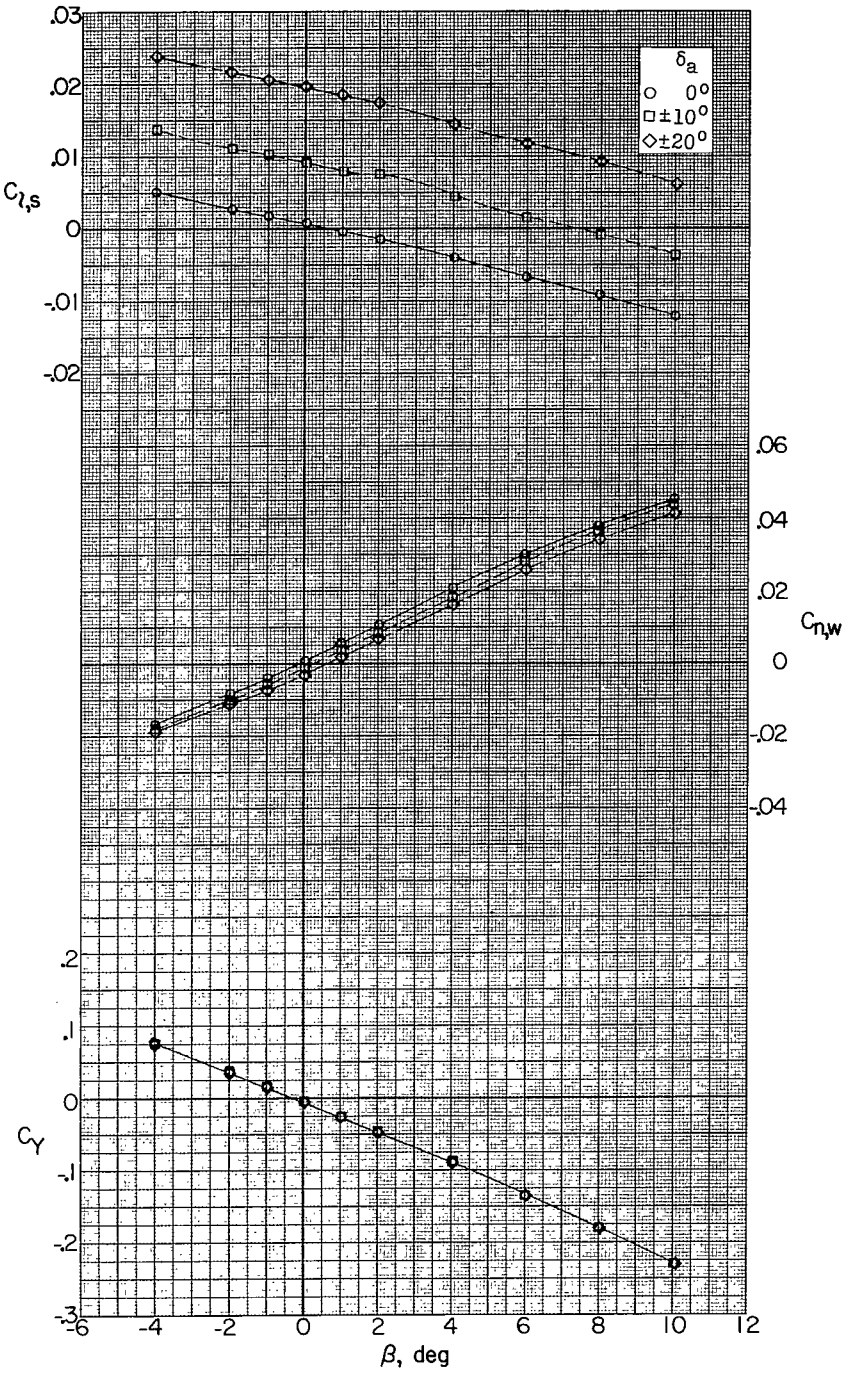

(b) M = 1.56; $\alpha = 9.7^\circ$.

Figure 17.- Continued.

[redacted]

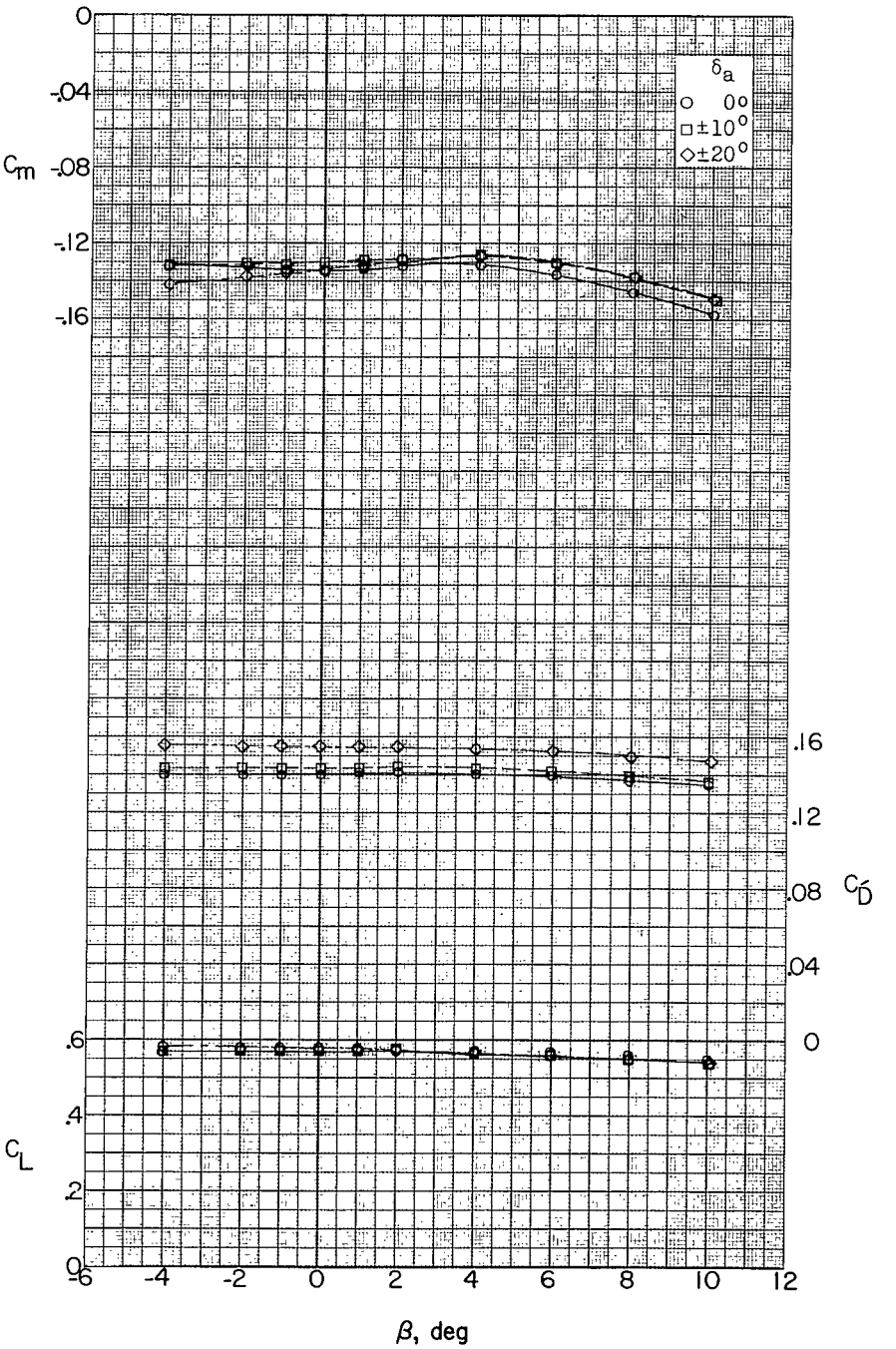

(b) Concluded.

Figure 17.- Continued.

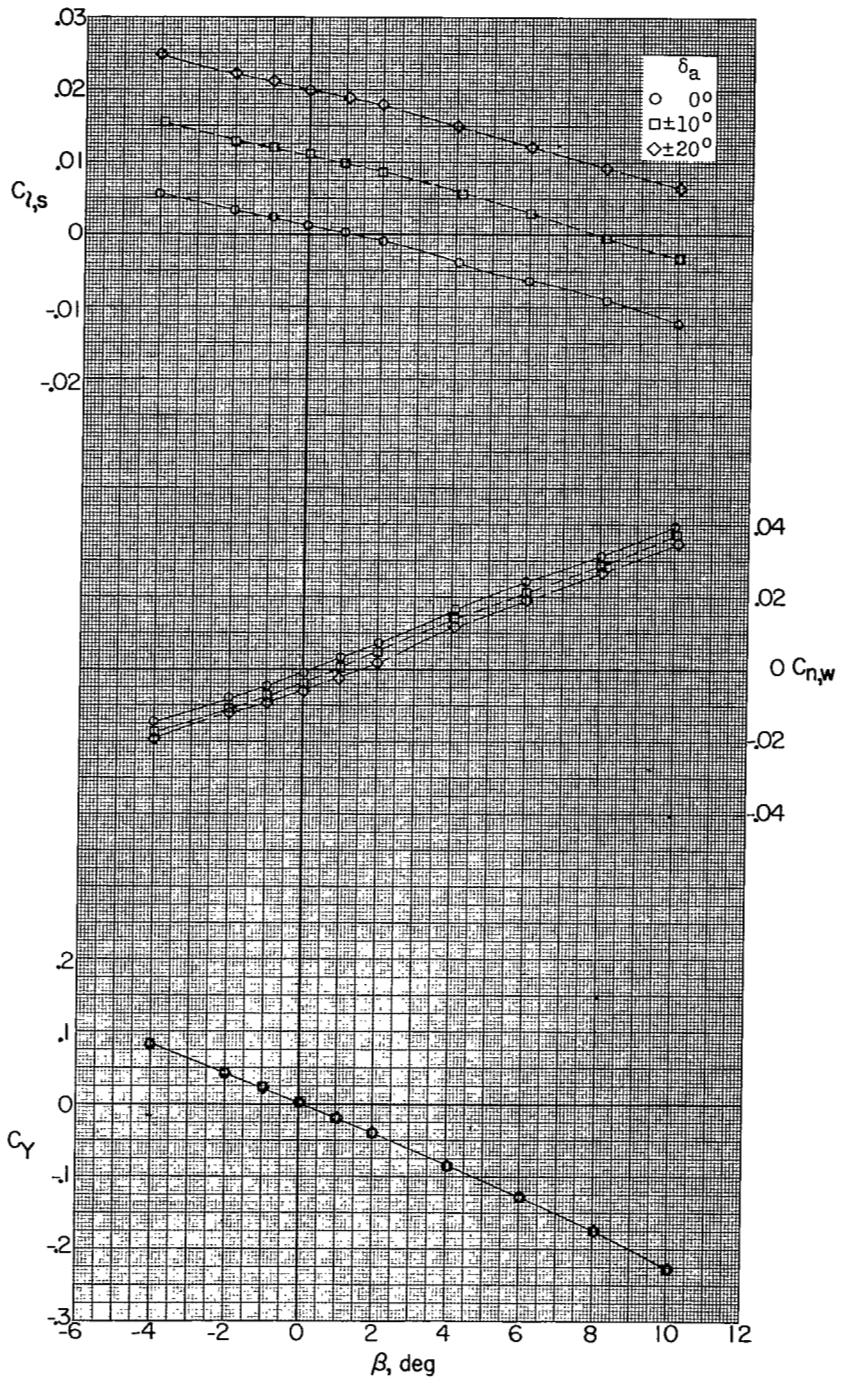

(c) M = 1.56; $\alpha \approx 12.1^\circ$.

Figure 17.- Continued.

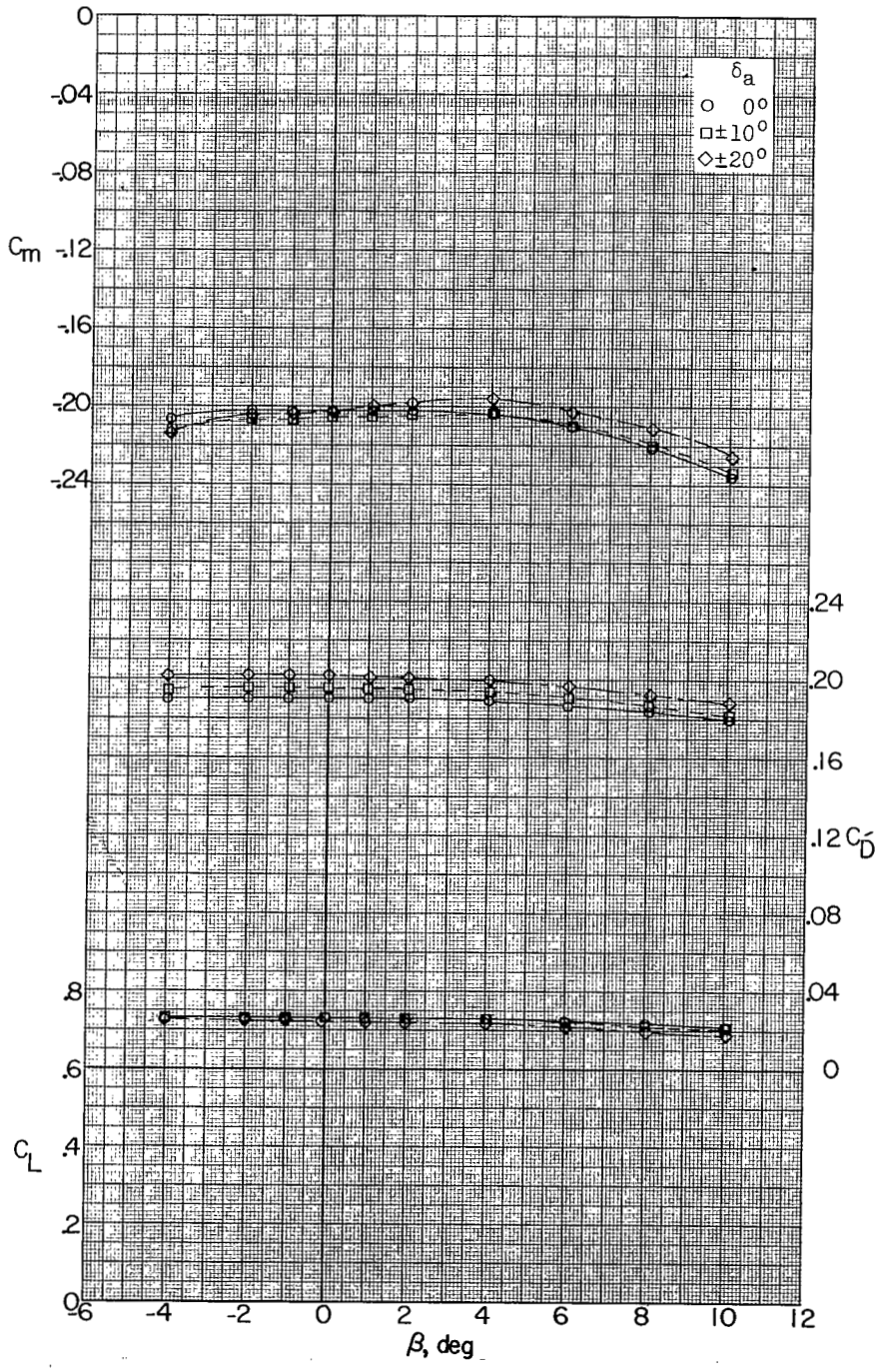

(c) Concluded.

Figure 17.- Continued.

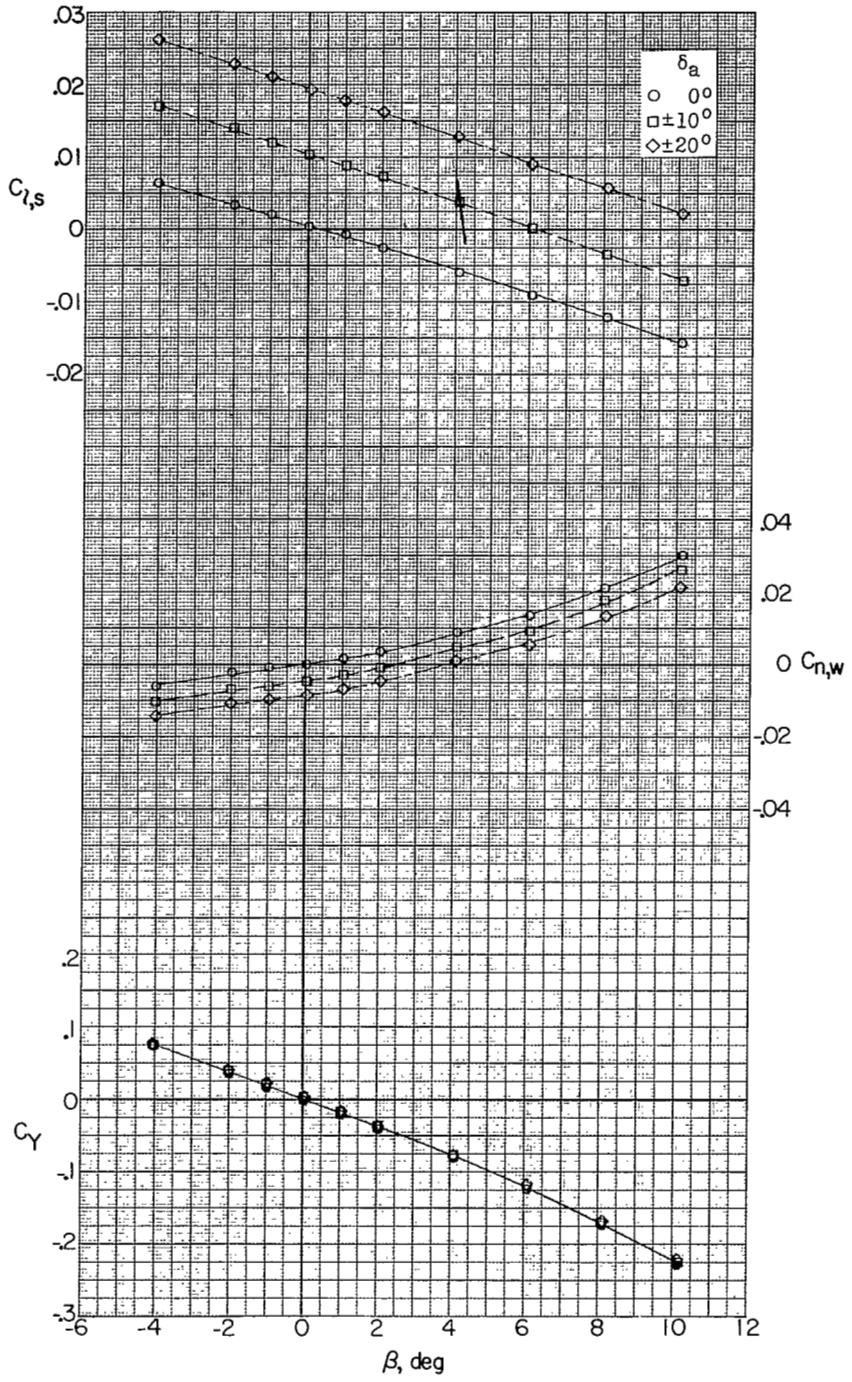

(d) M = 1.56; $\alpha \approx 16.2^{\circ}$.

Figure 17.- Continued.

[redacted]

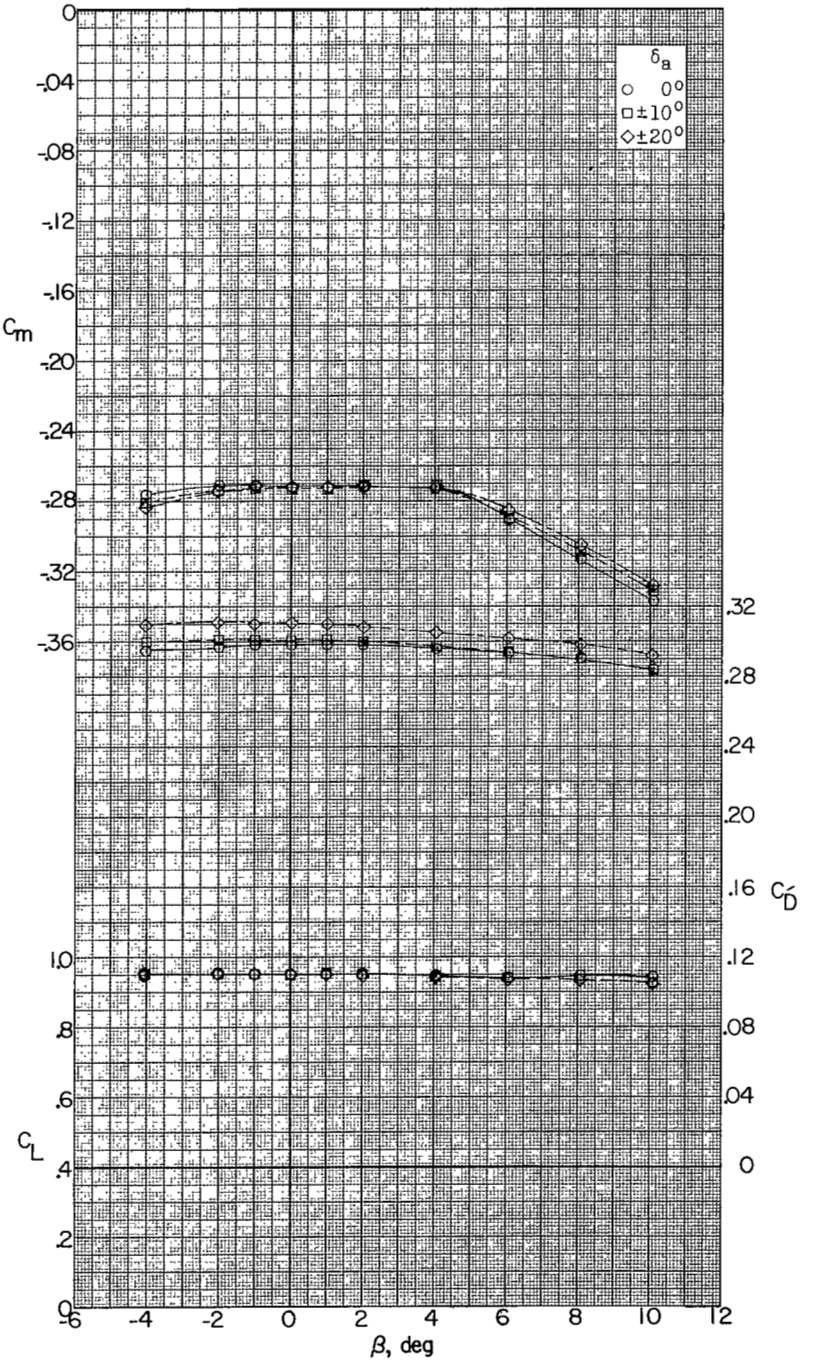

(d) Concluded.

Figure 17.- Continued.

[redacted]

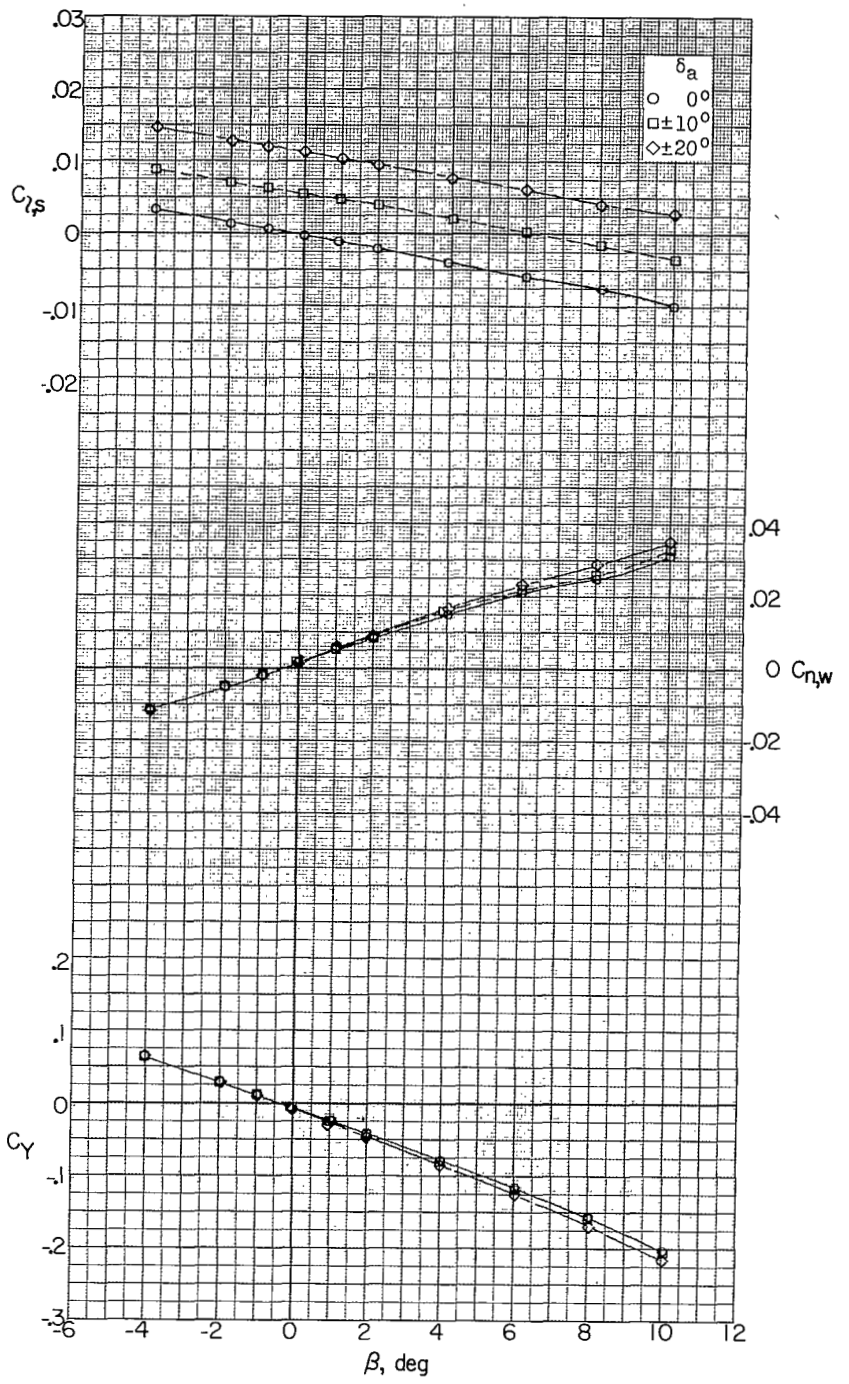

(e) M = 2.06; $\alpha \approx 3.8^{\circ}$.

Figure 17.- Continued.

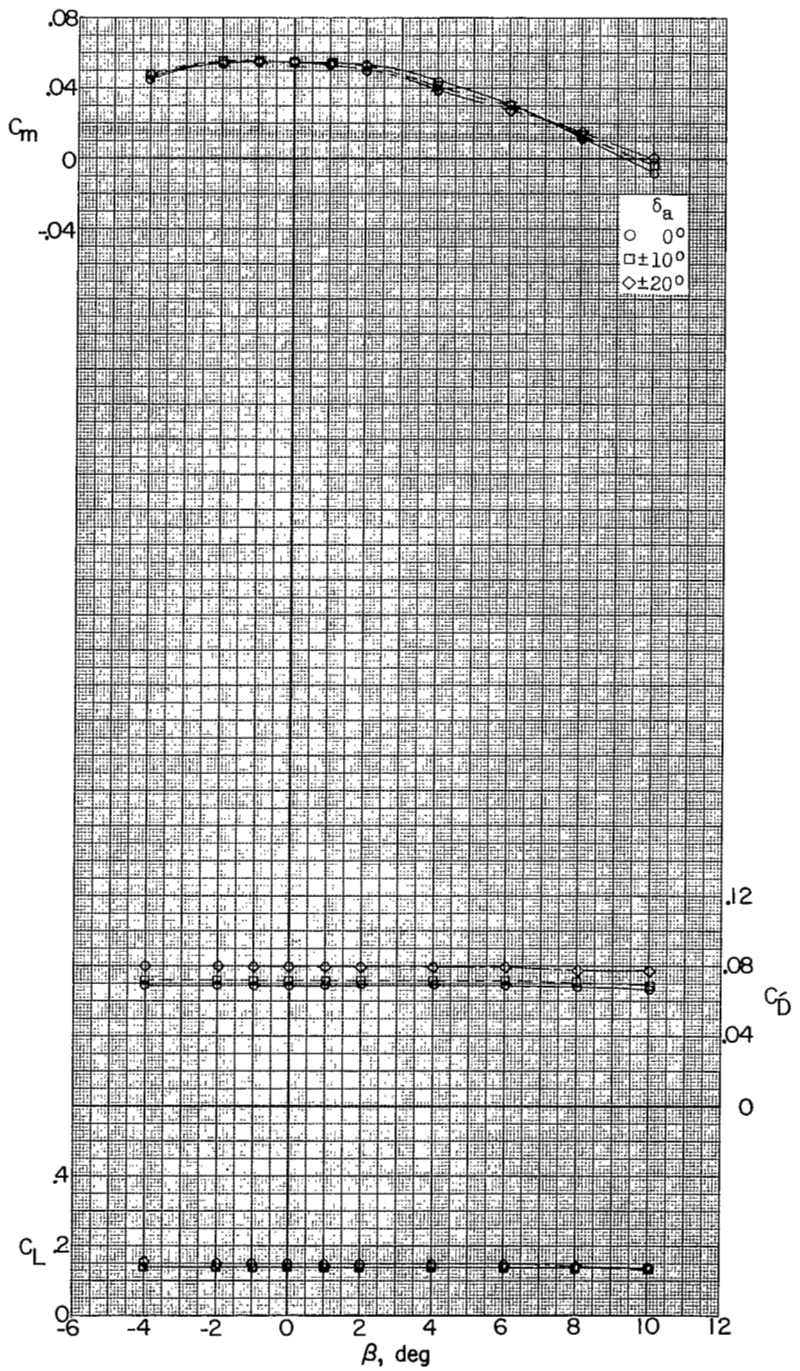

(e) Concluded.

Figure 17.- Continued.

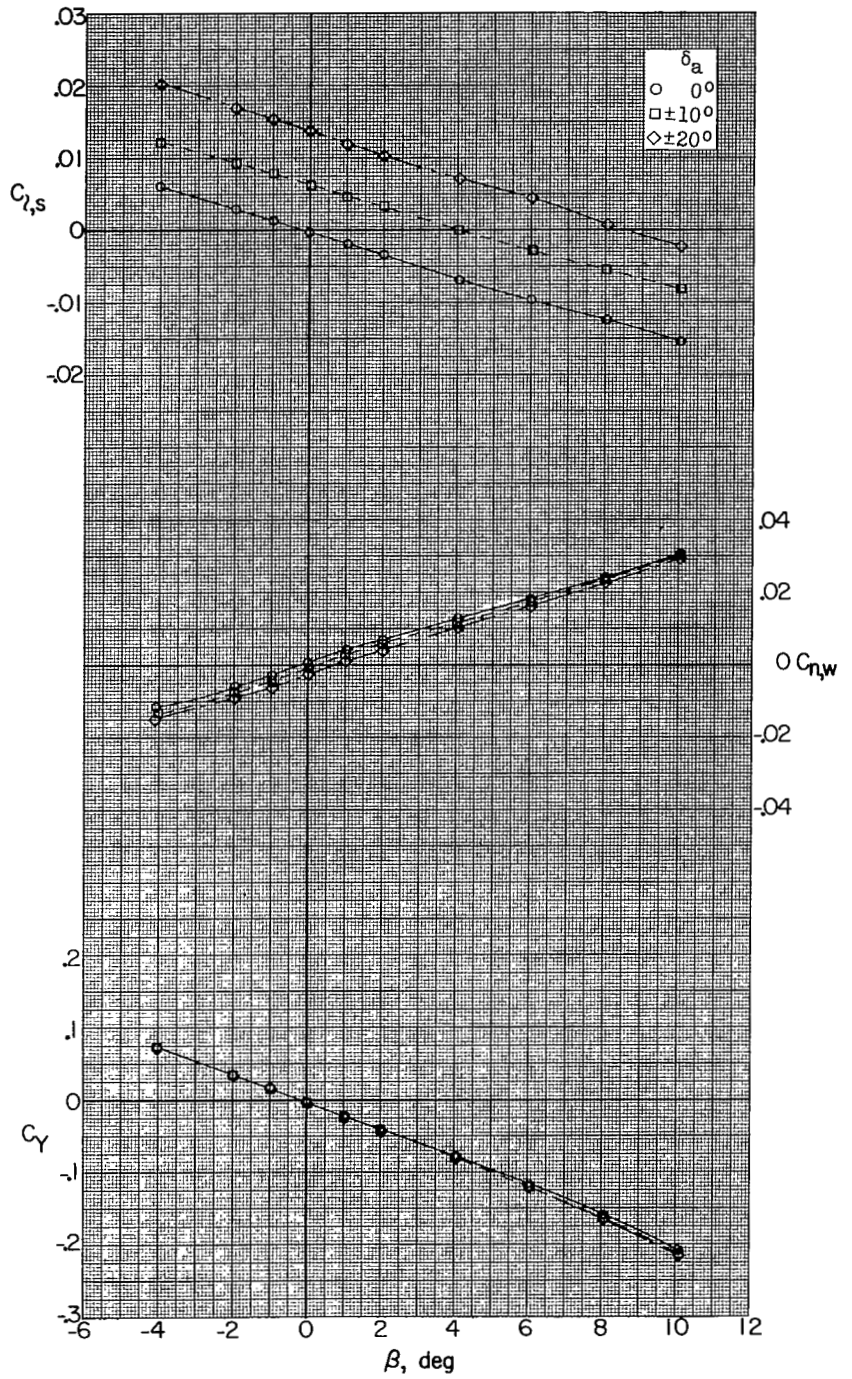

(f) M = 2.06; $\alpha \approx 9.6^\circ$.

Figure 17.- Continued.

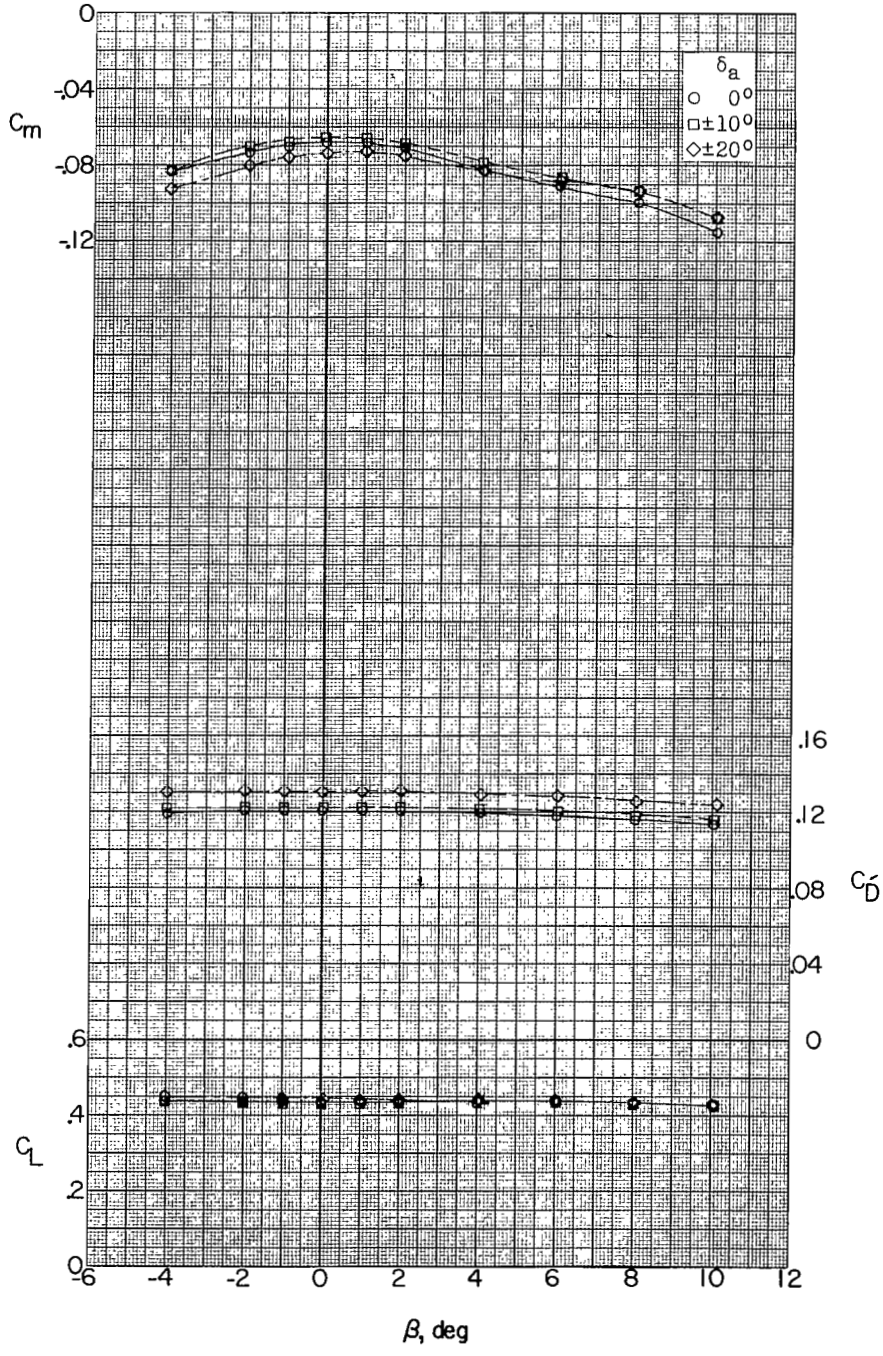

(f) Concluded.

Figure 17.- Continued.

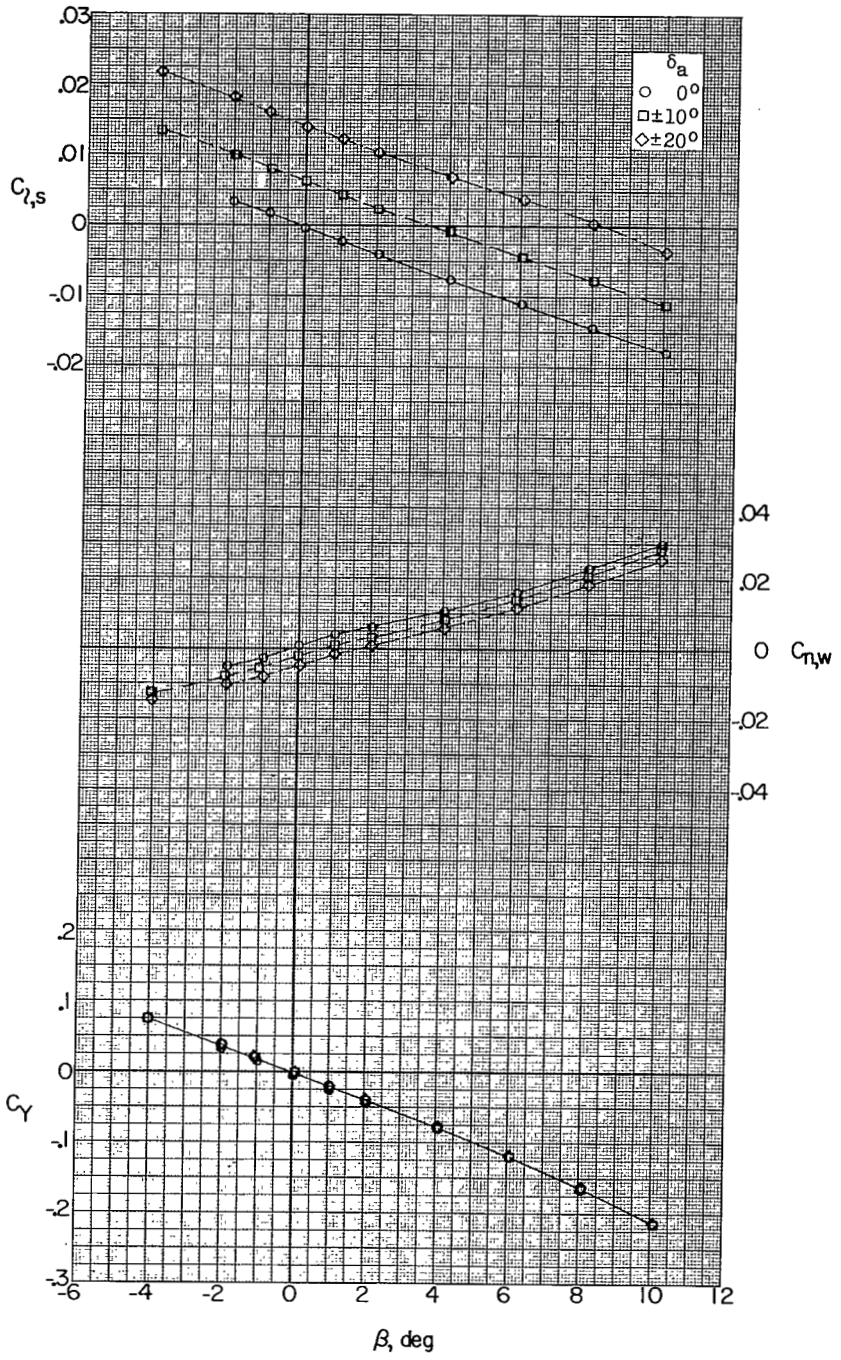

(g) M = 2.06; $\alpha \approx 12.0^\circ$.

Figure 17.- Continued.

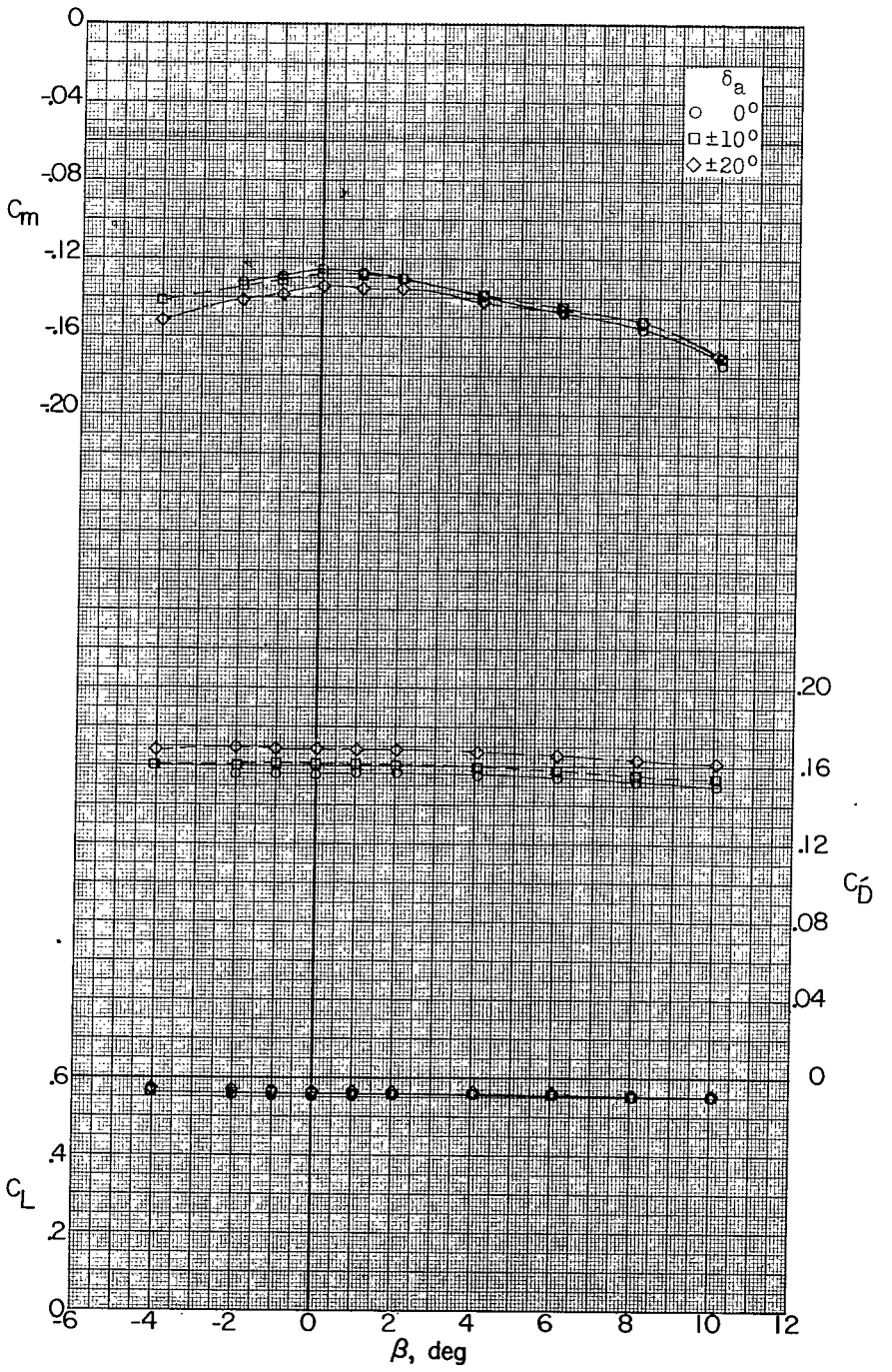

(g) Concluded.

Figure 17.- Continued.

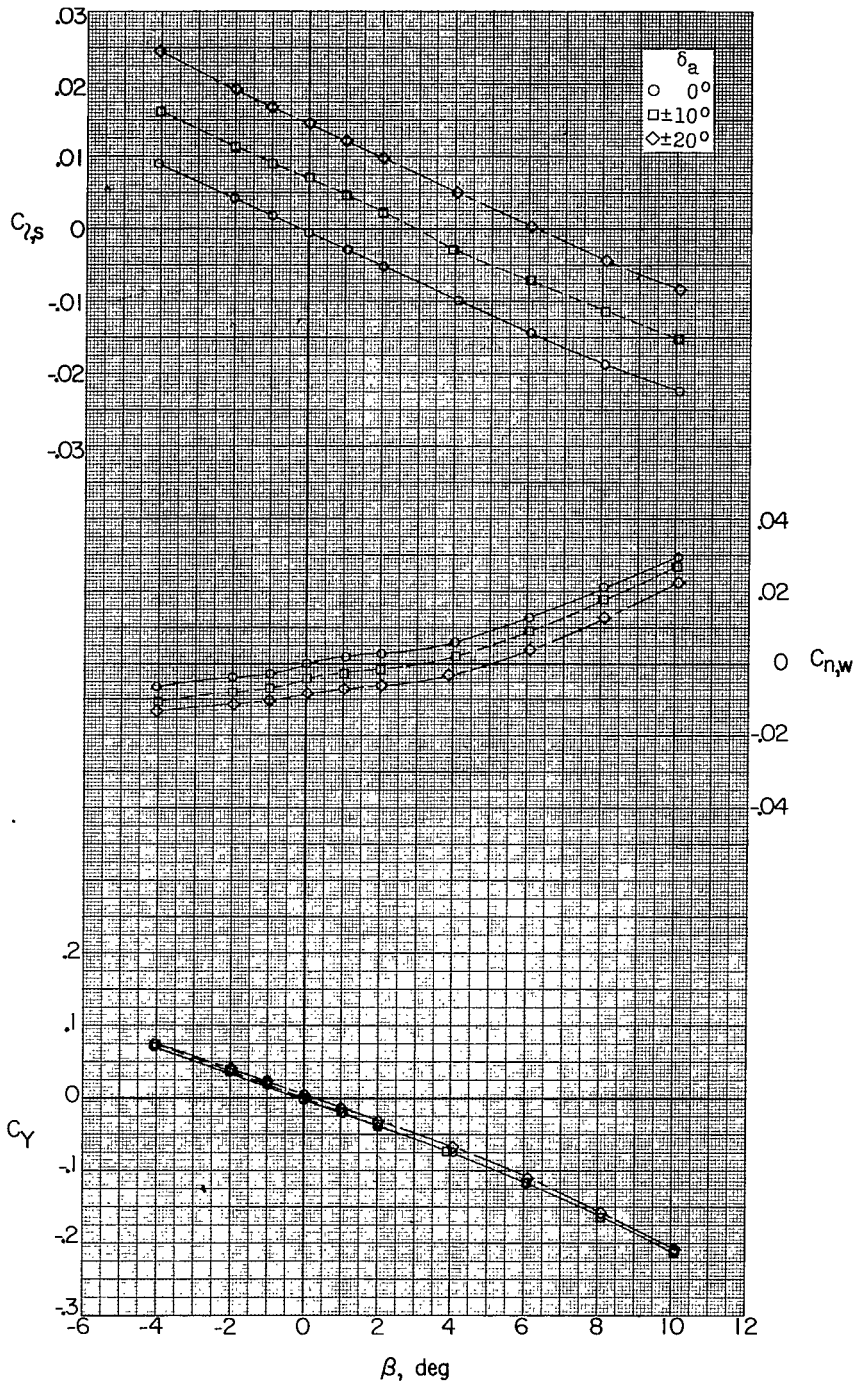

(h) M = 2.06; $\alpha = 16.1^\circ$.

Figure 17.- Continued.

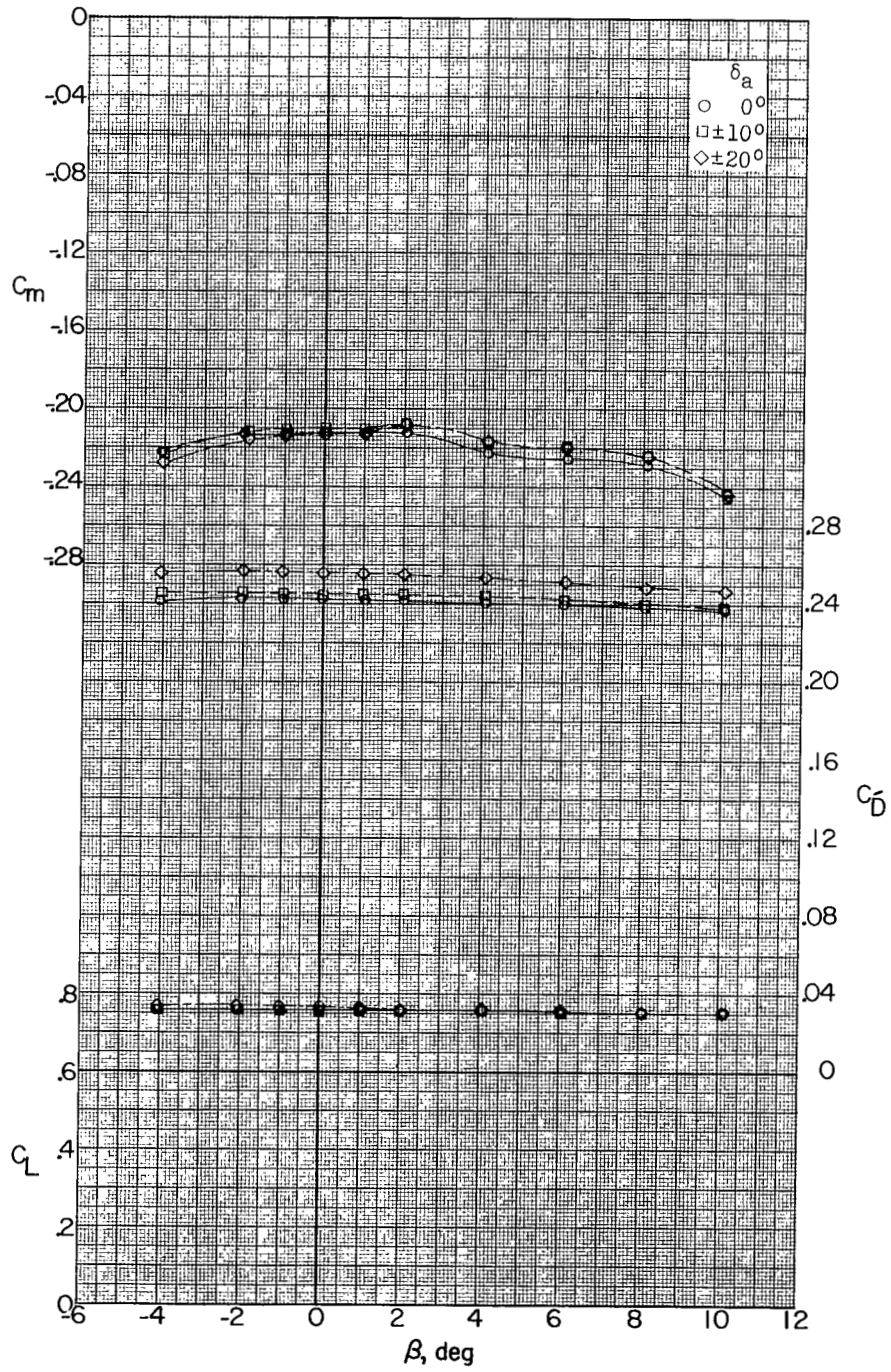

(h) Concluded.

Figure 17.- Concluded.

[redacted]

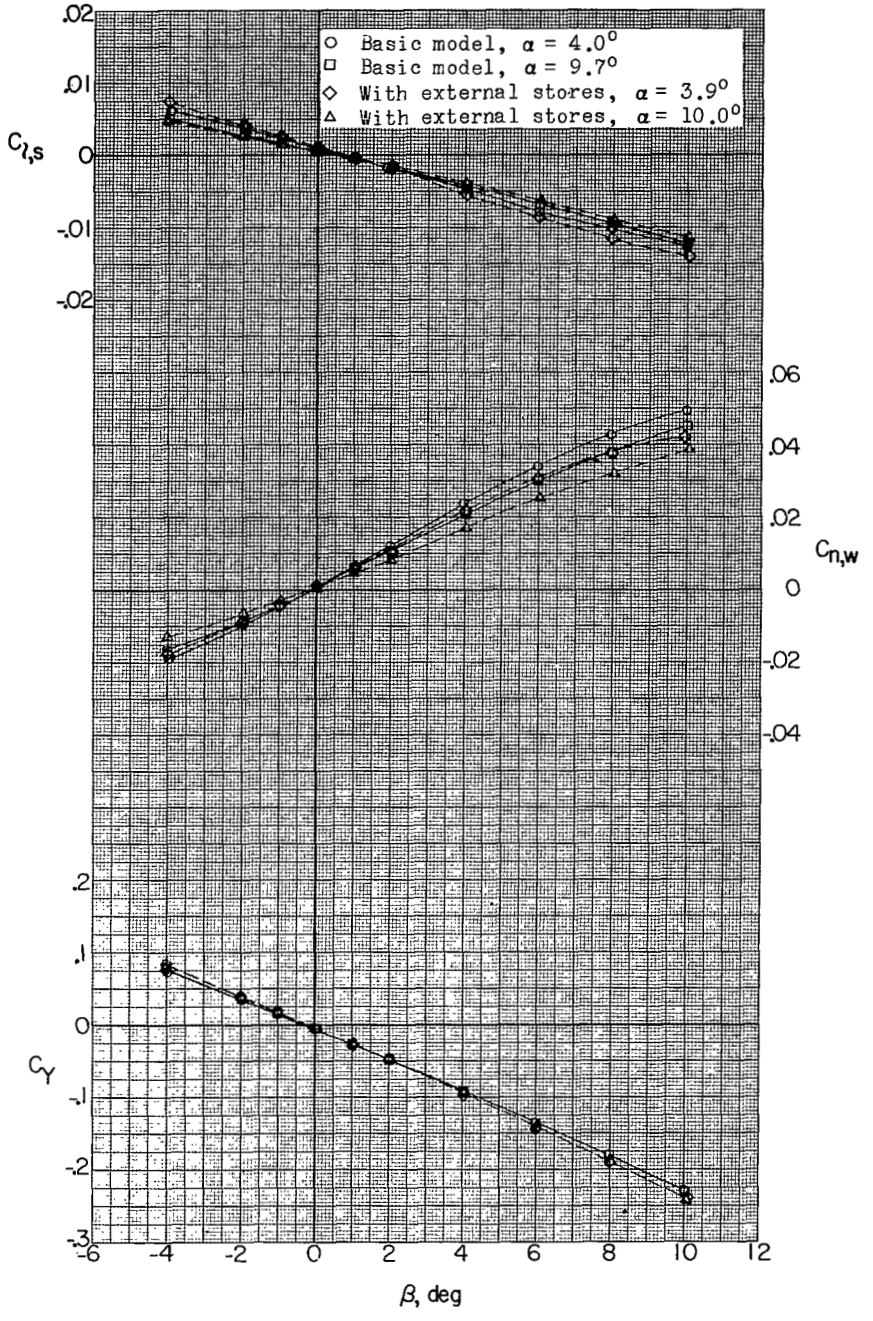

(a) M = 1.56.

Figure 18.- Effect of external stores on aerodynamic characteristics in sideslip.

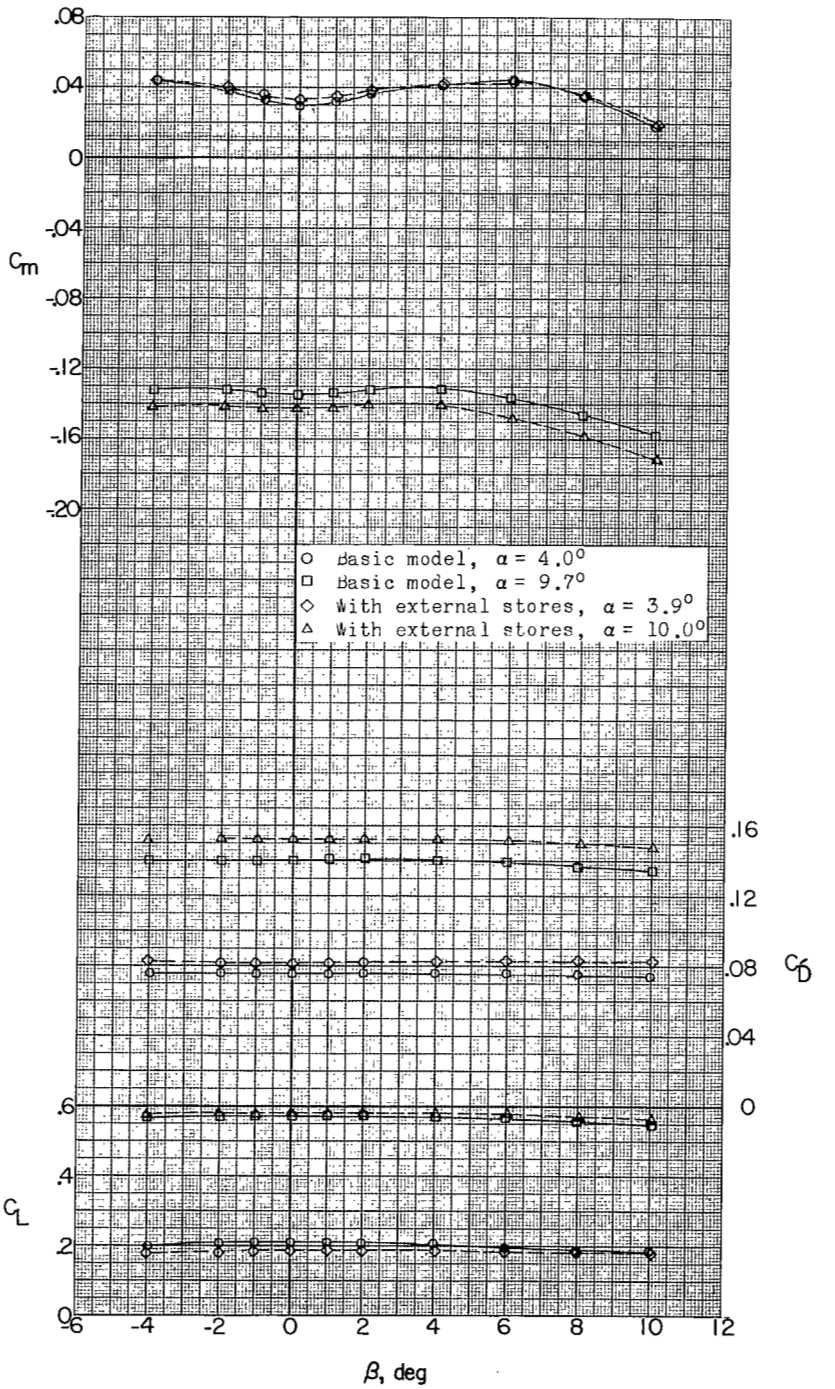

(a) Continued.

Figure 18.- Continued.

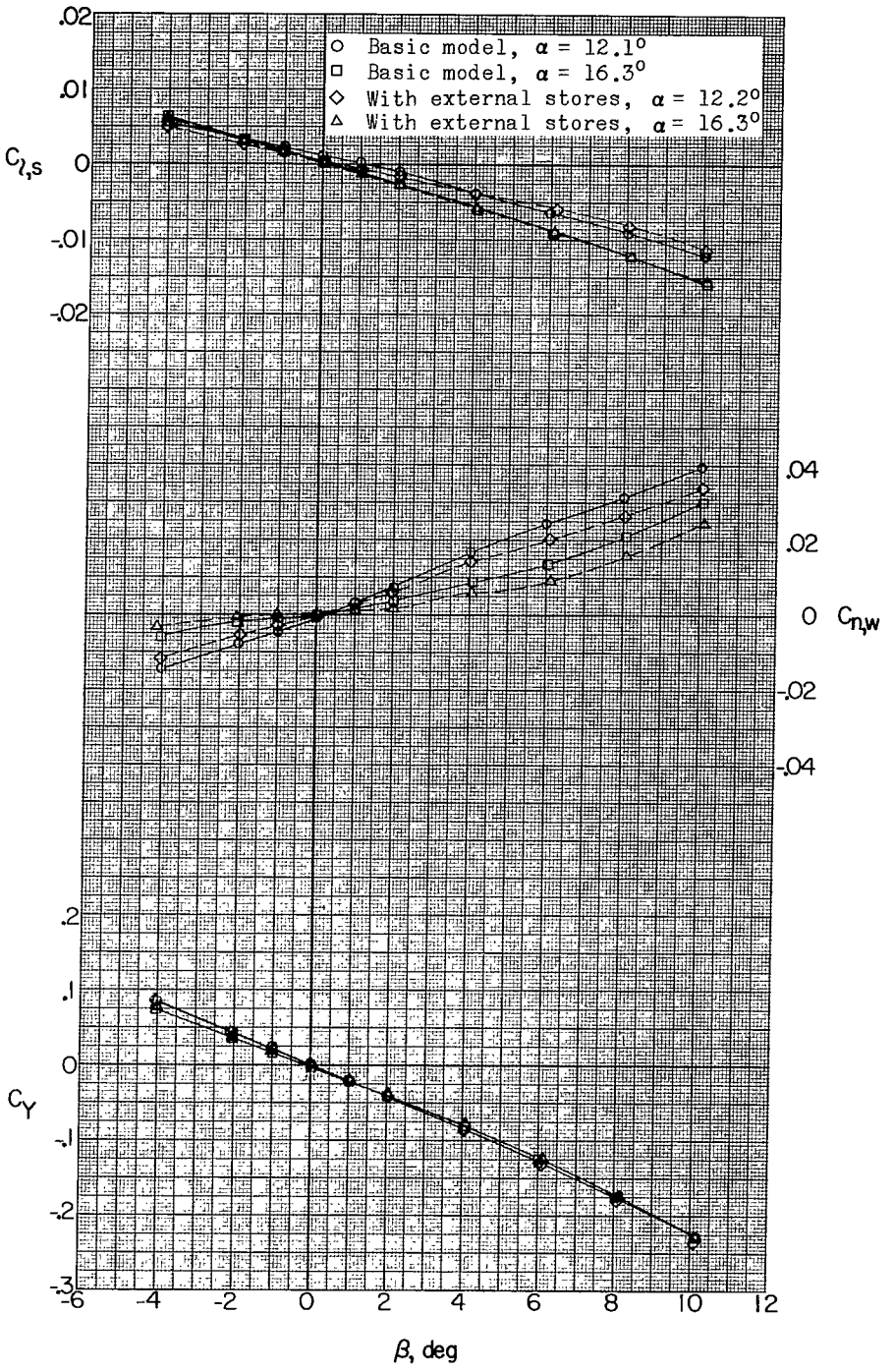

(a) Continued.

Figure 18.- Continued.

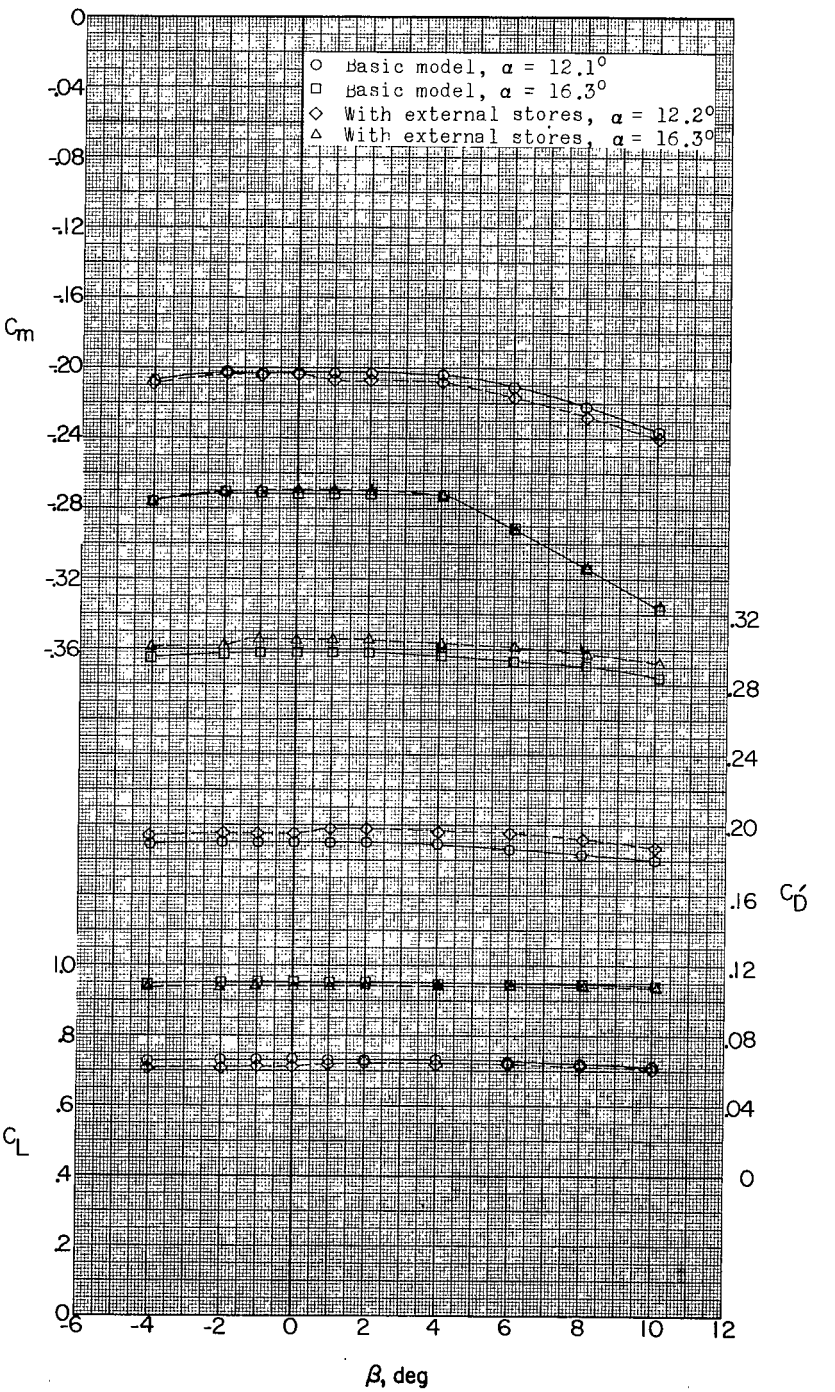

(a) Concluded.

Figure 18.- Continued.

[redacted]

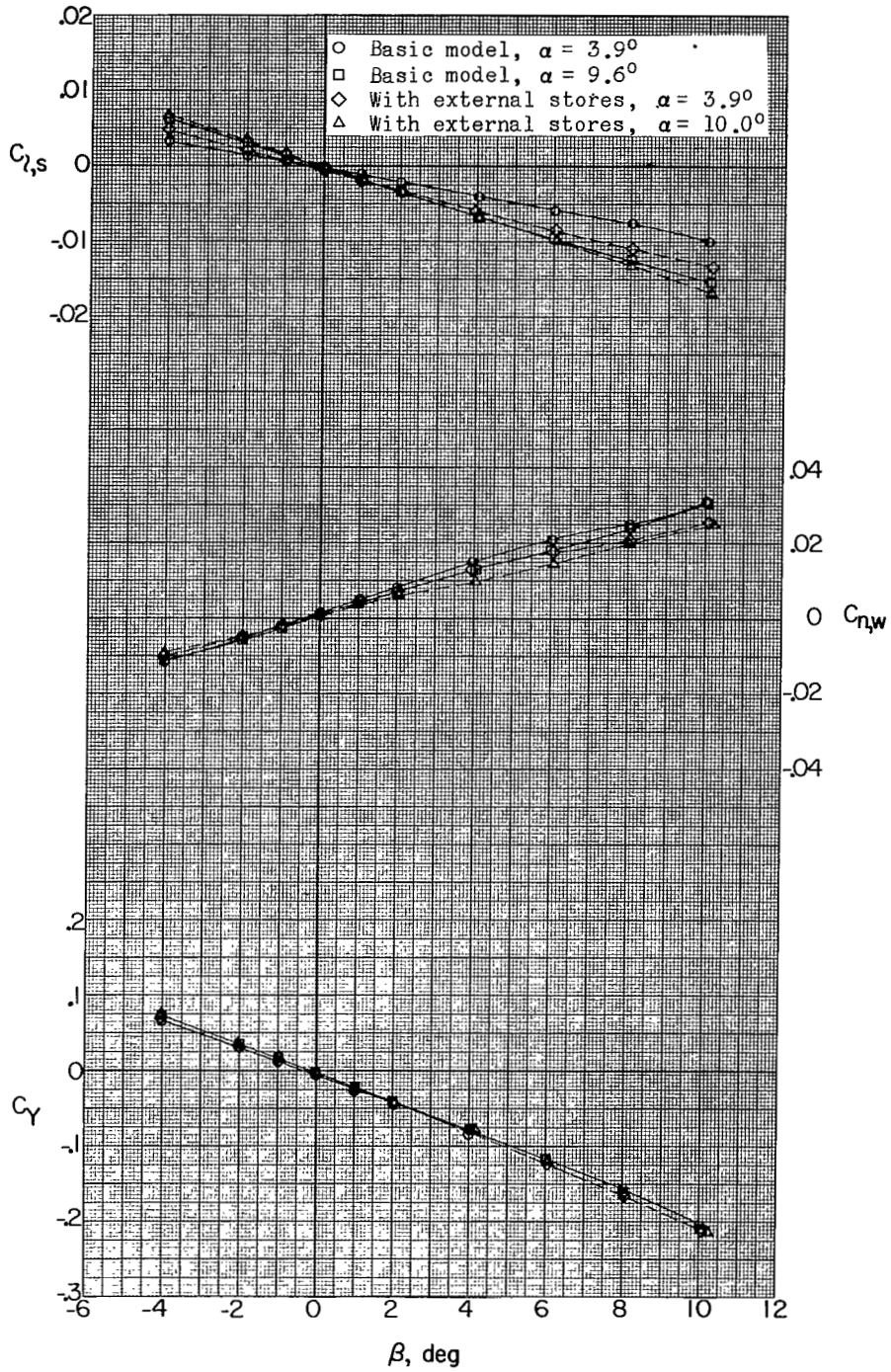

(b) M = 2.06.

Figure 18.- Continued.

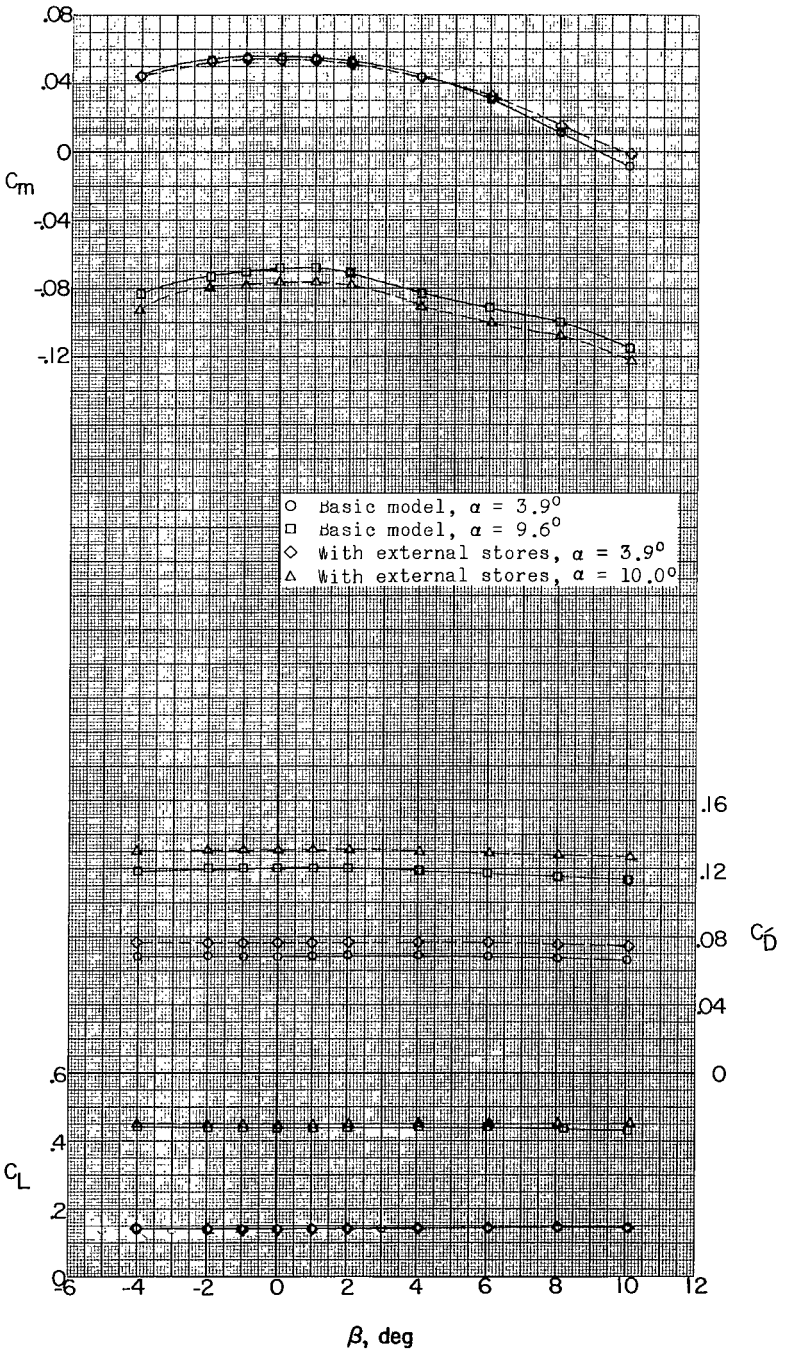

(b) Continued.

Figure 18.- Continued.

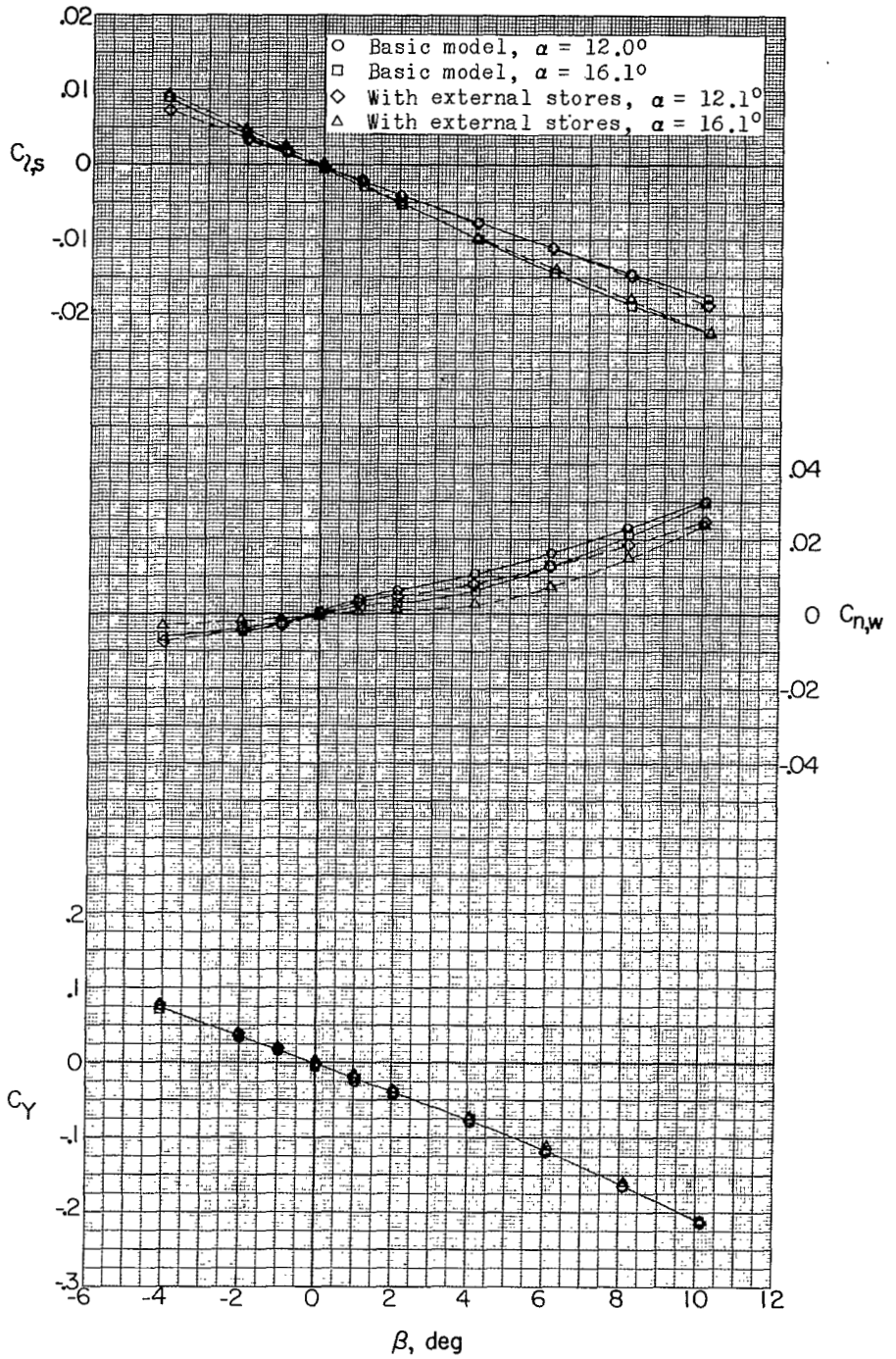

(b) Continued.

Figure 18.- Continued.

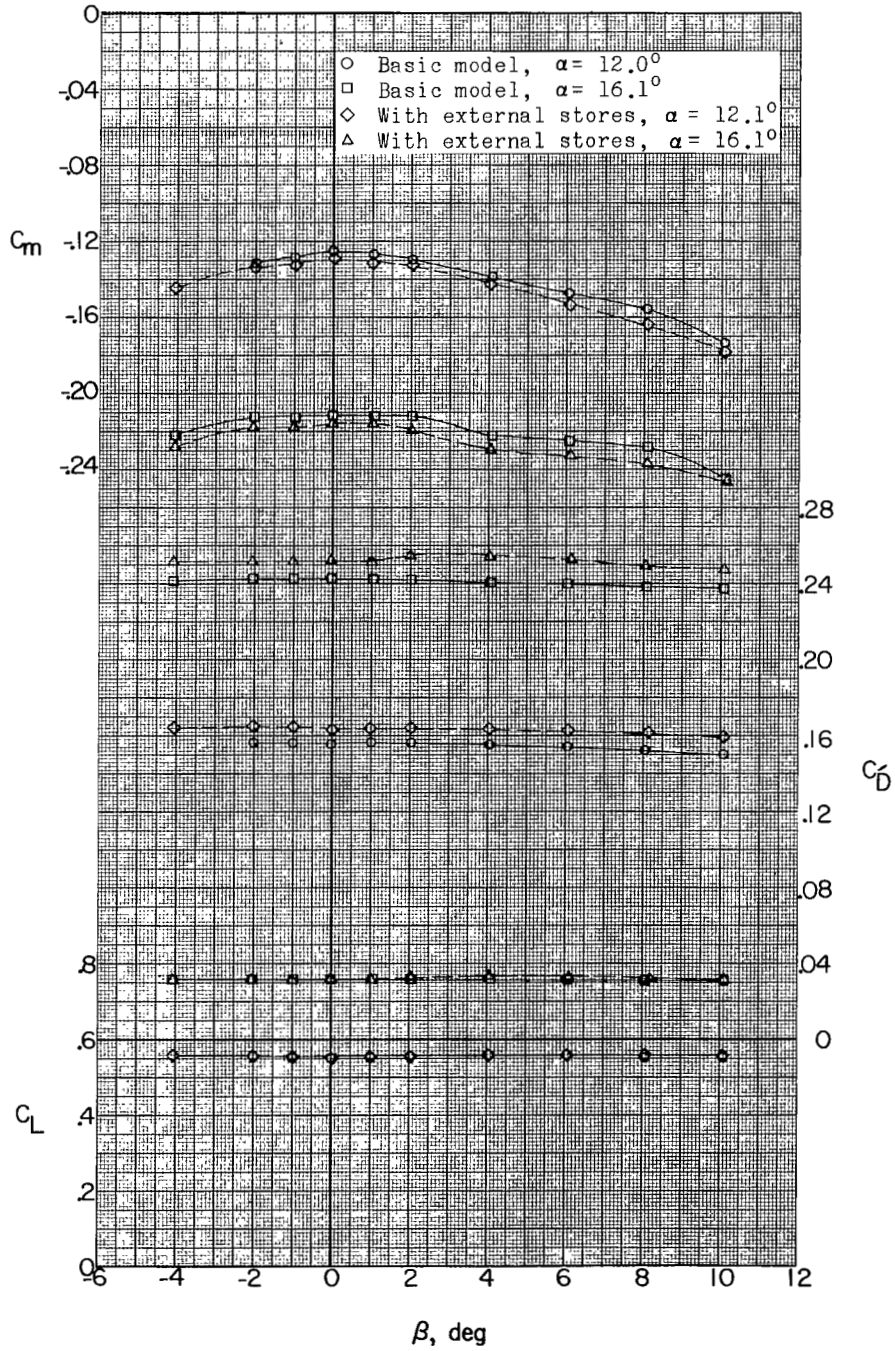

(b) Concluded.

Figure 18.- Concluded.

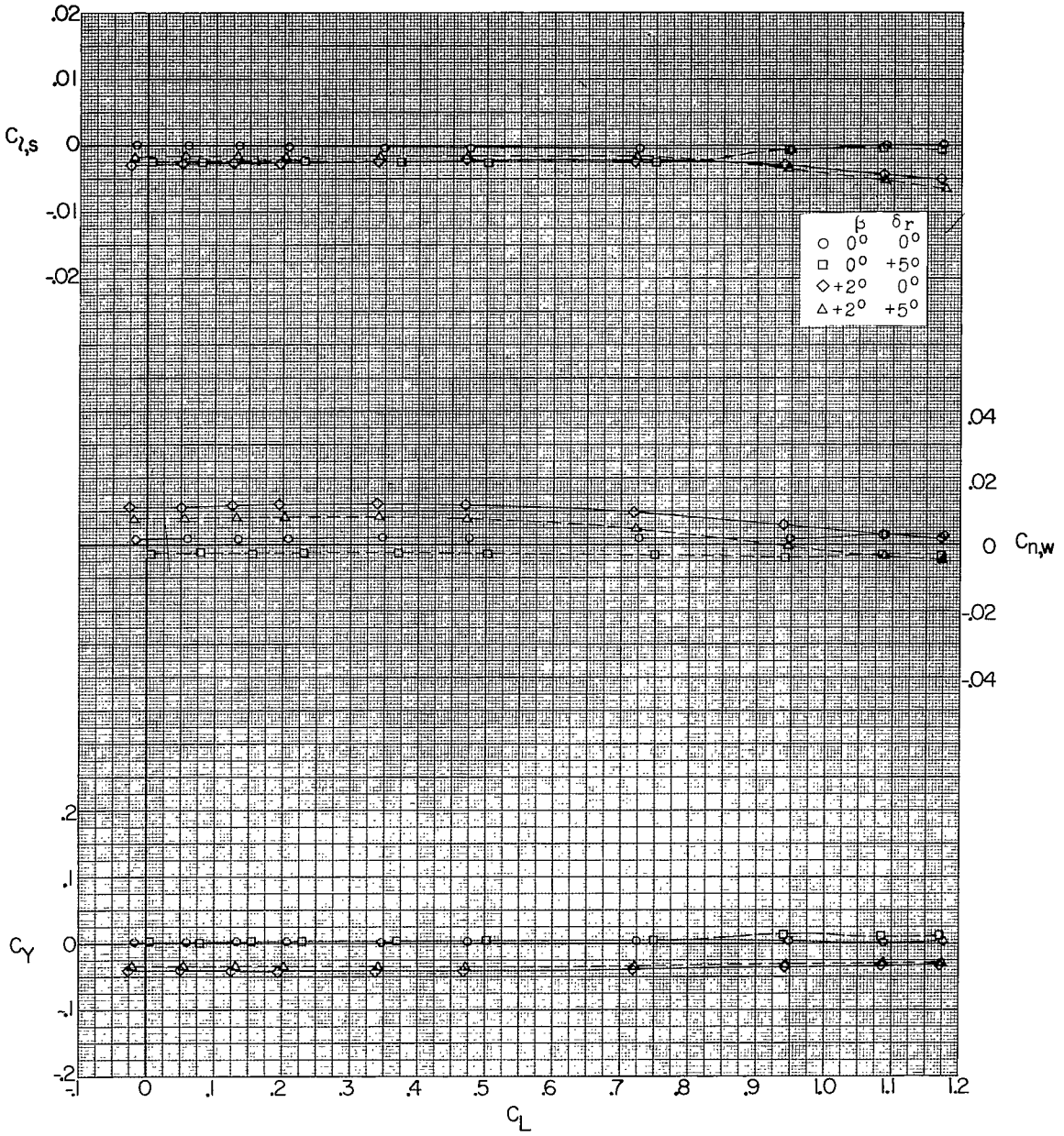

(a) M = 1.56.

Figure 19.- Effect of rudder deflection on aerodynamic characteristics in pitch.

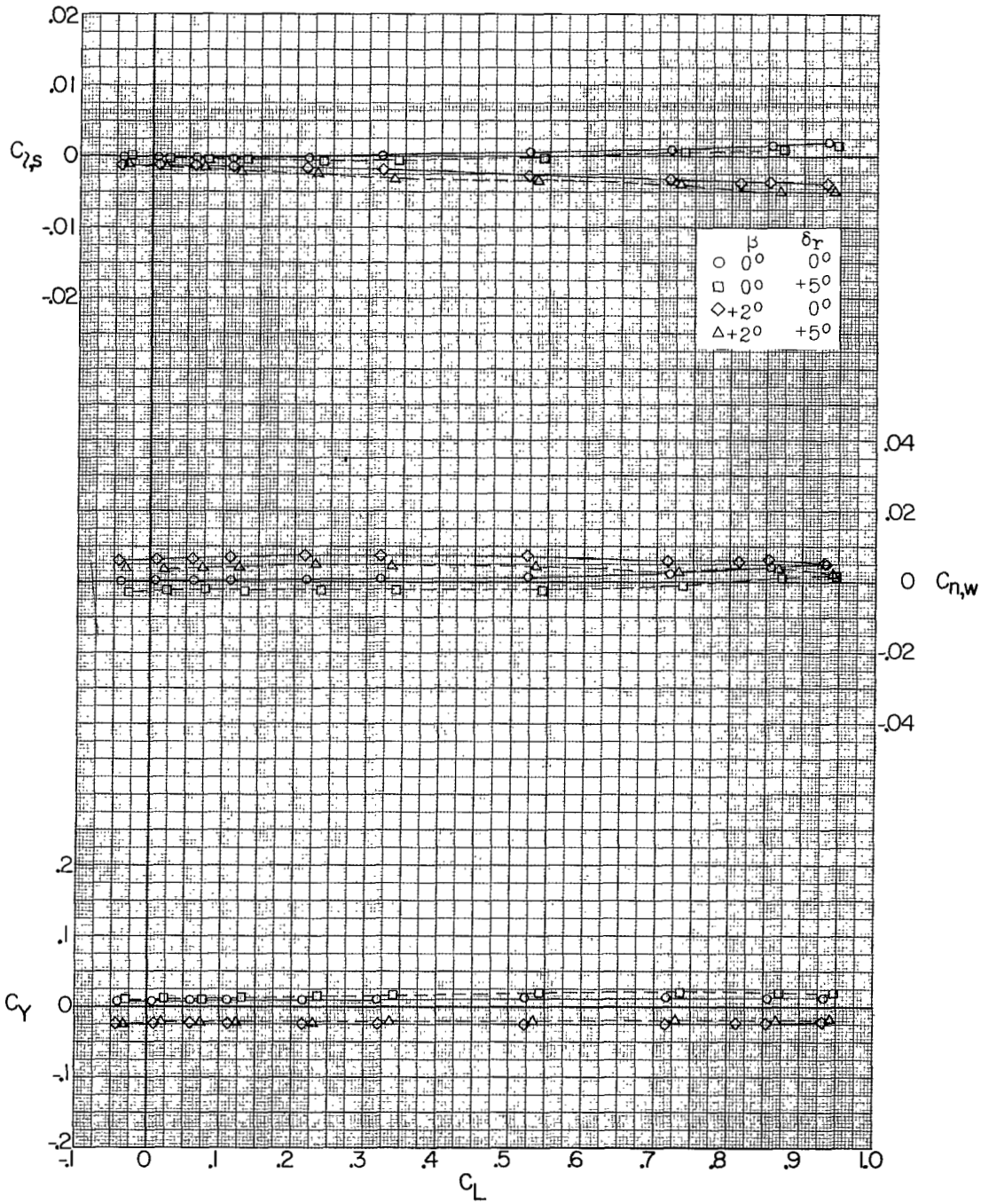

(b) M = 2.06.

Figure 19.- Concluded.

[redacted]

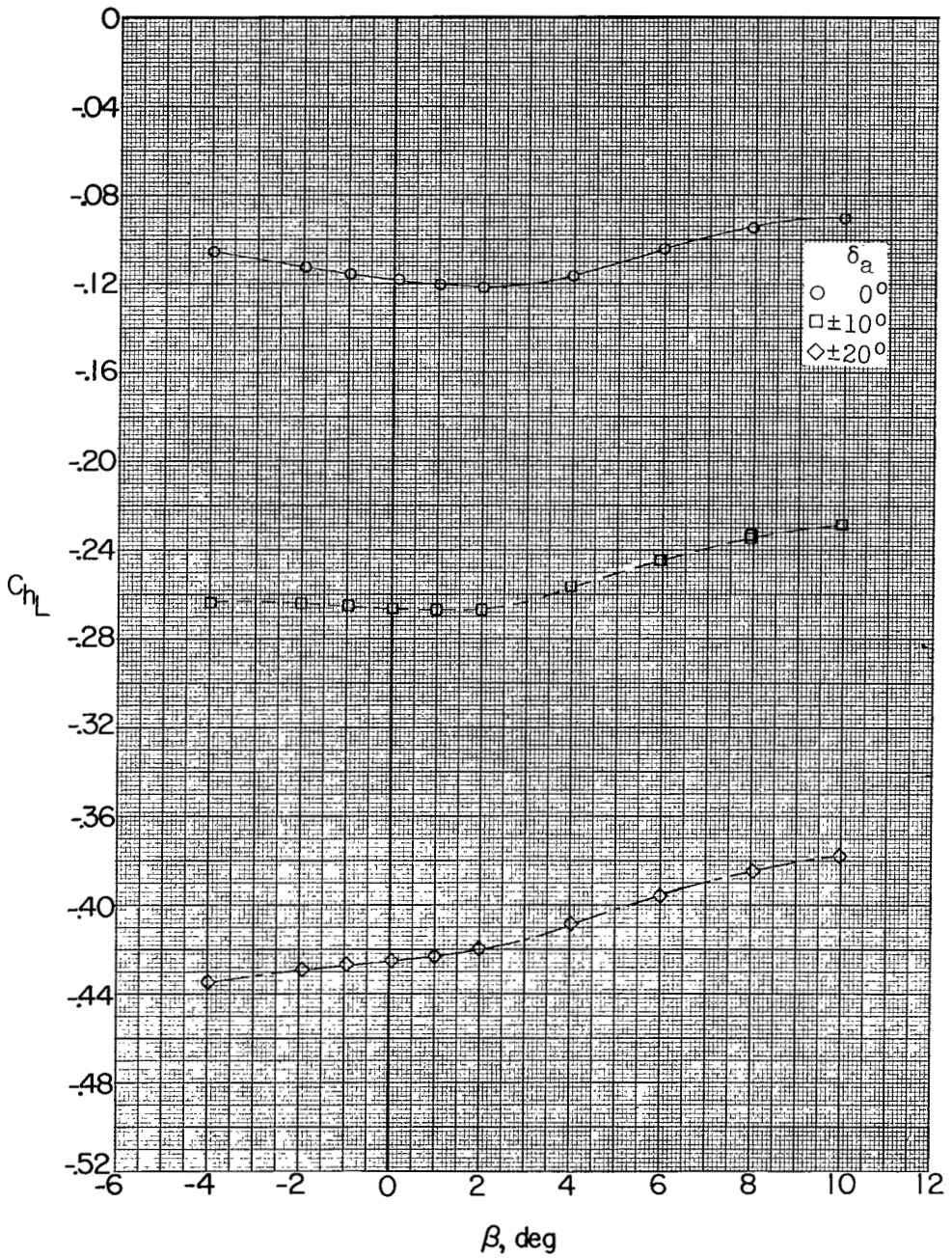

(a) M = 1.56; $\alpha = 4.0^\circ$.

Figure 20.- Effect of sideslip on aileron hinge-moment coefficient.

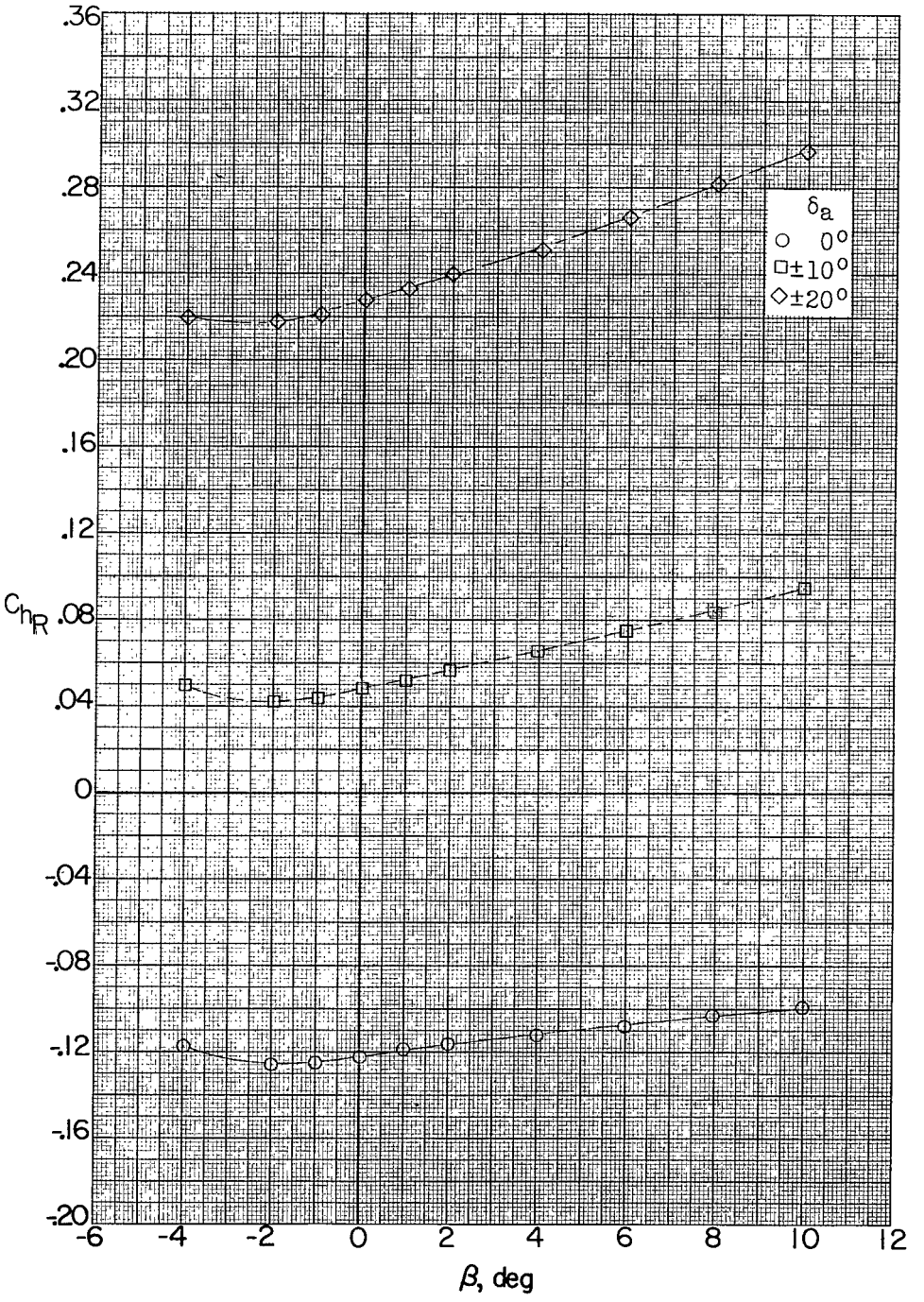

(a) Concluded.

Figure 20.- Continued.

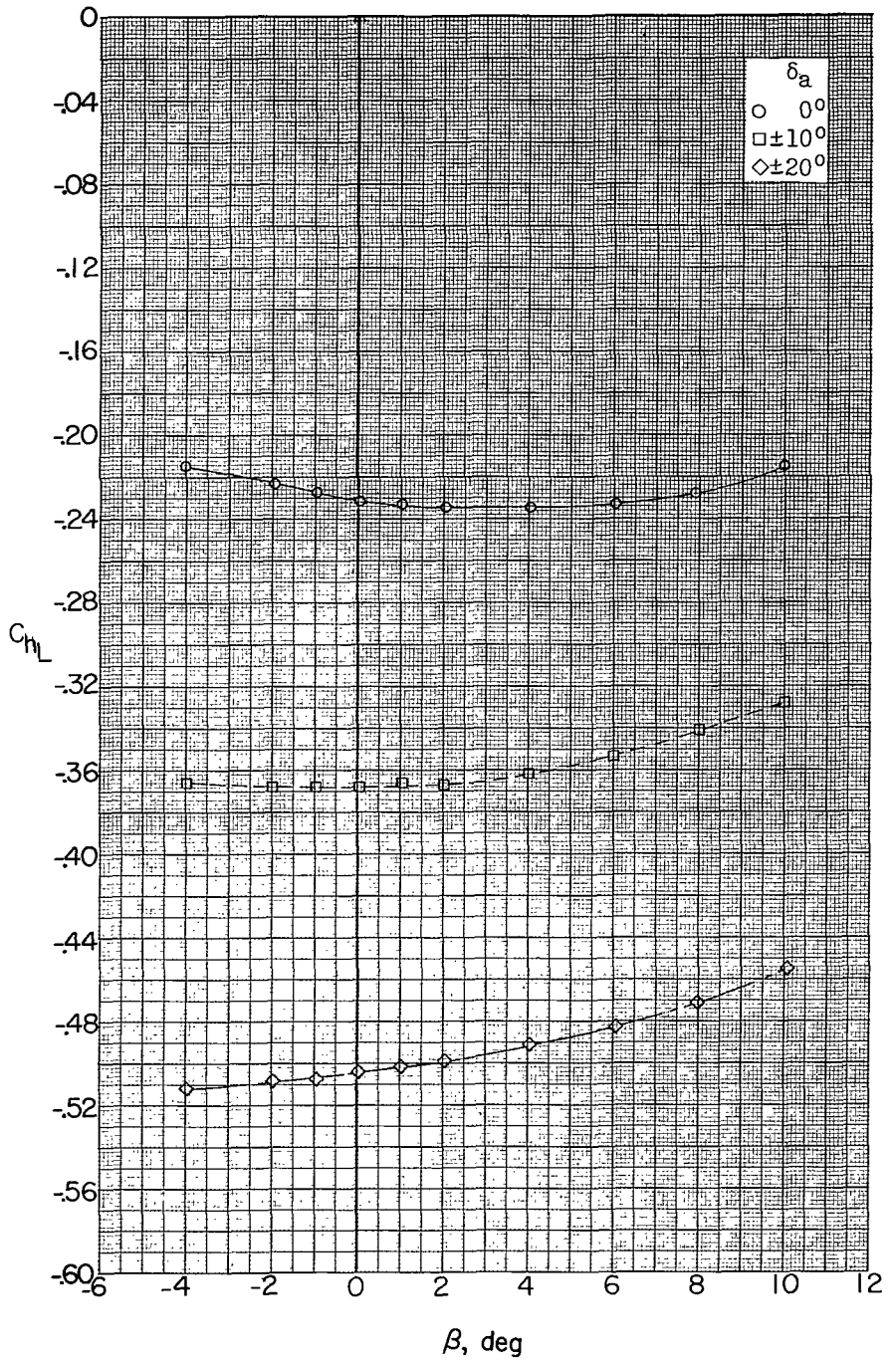

(b) M = 1.56; $\alpha = 9.7^\circ$.

Figure 20.- Continued.

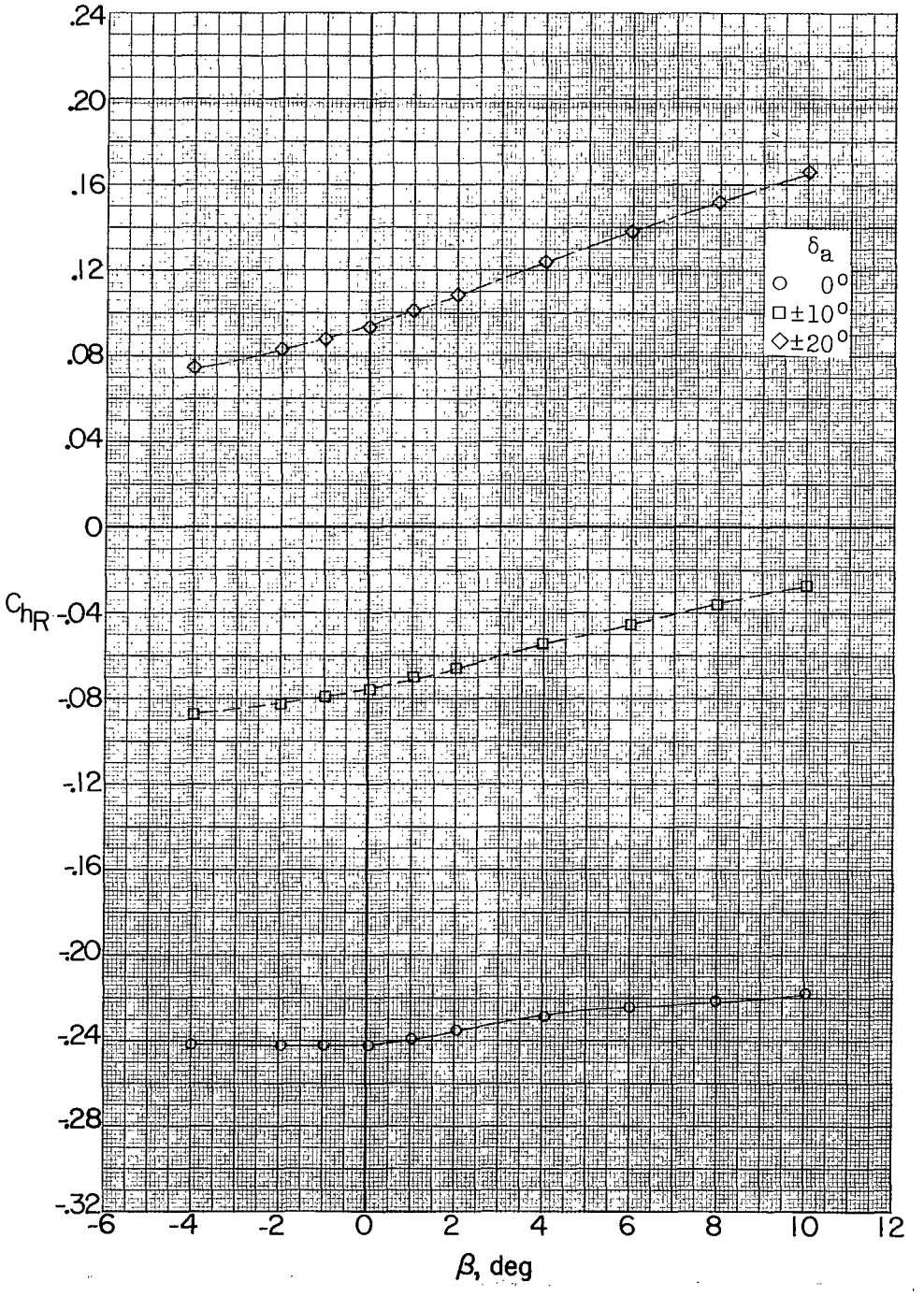

(b) Concluded.

Figure 20.- Continued.

[redacted]

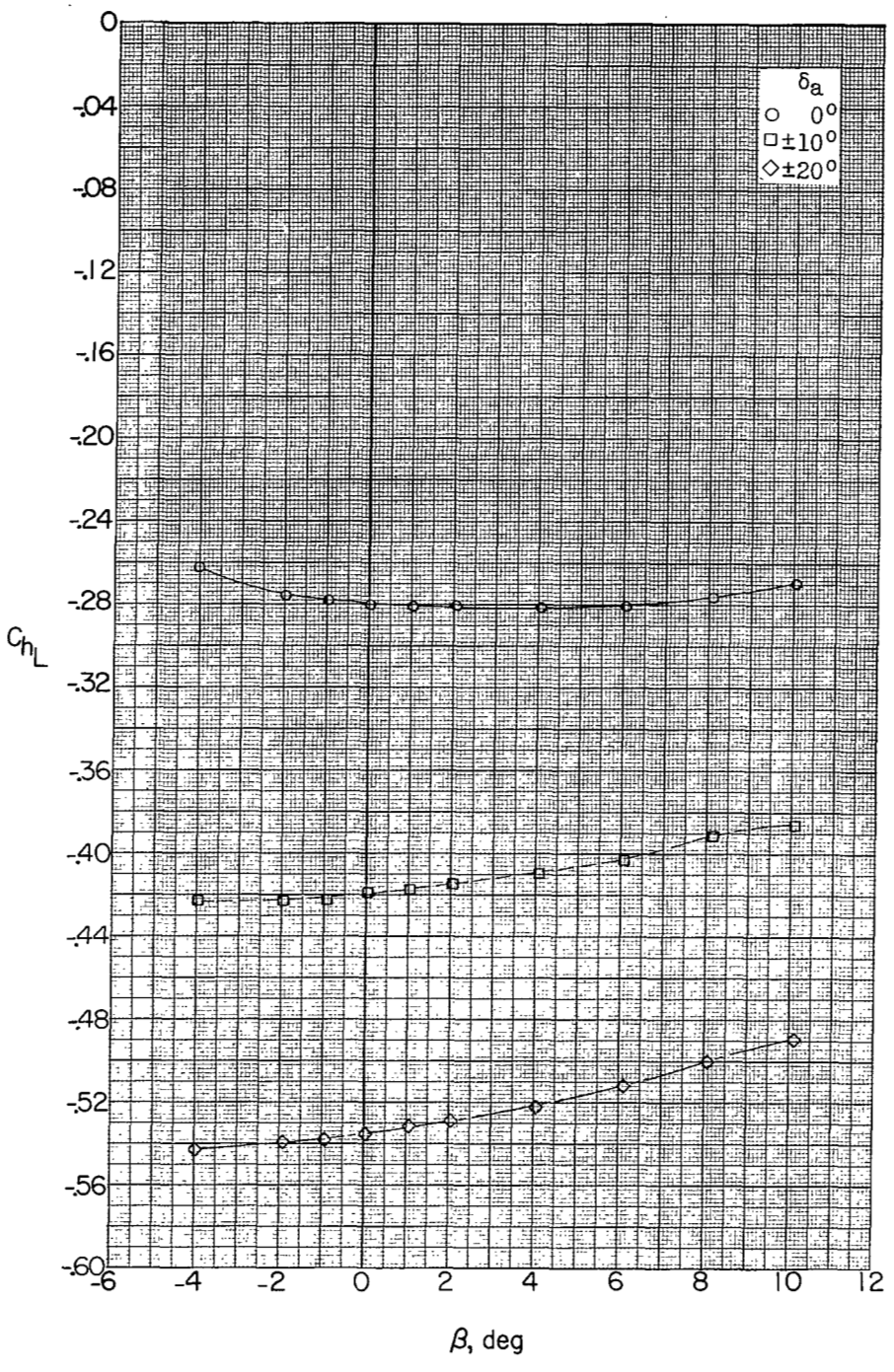

(c) M = 1.56; $\alpha \approx 12.1^{\circ}$.

Figure 20.- Continued.

[redacted]

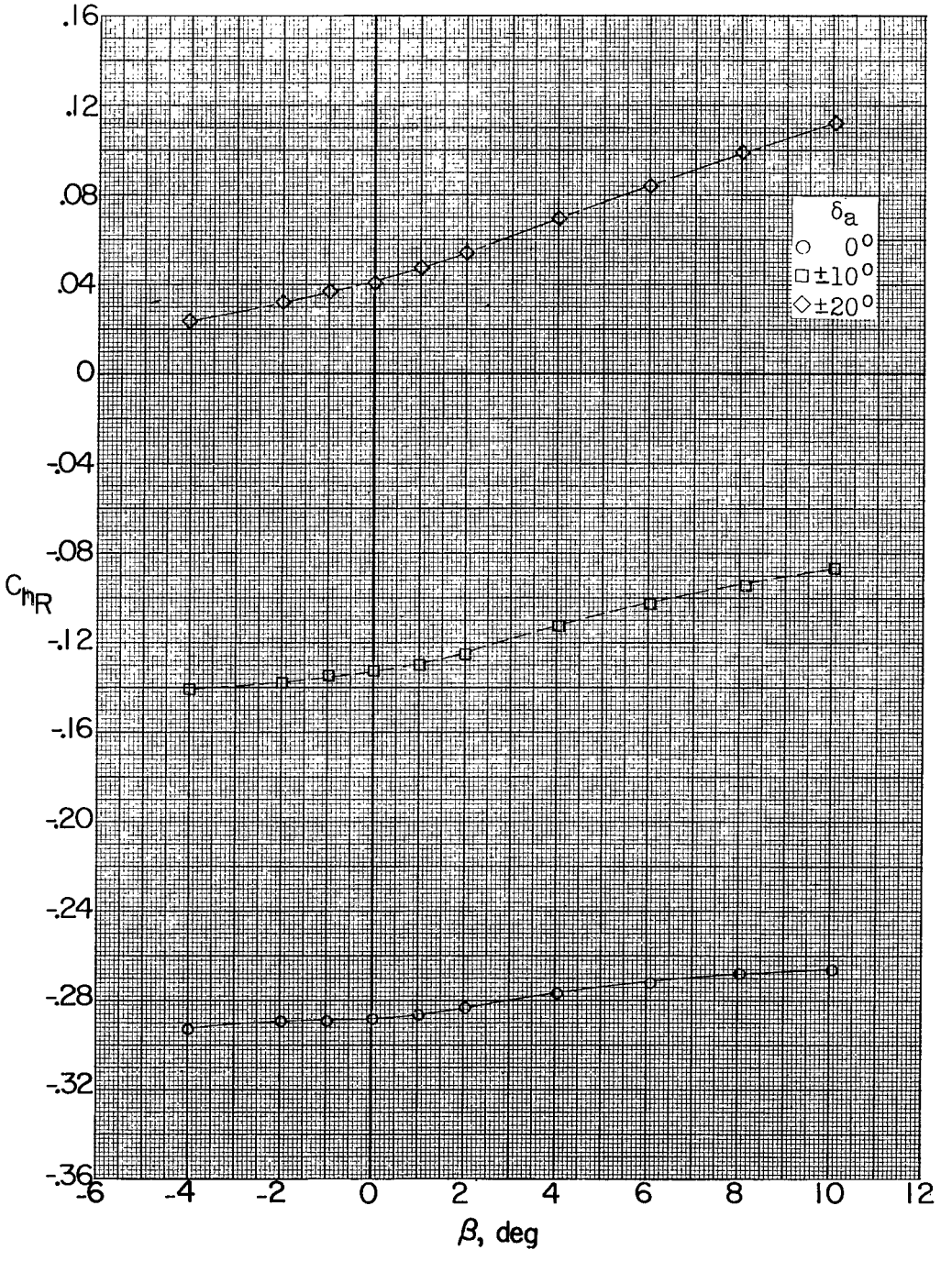

(c) Concluded.

Figure 20.- Continued.

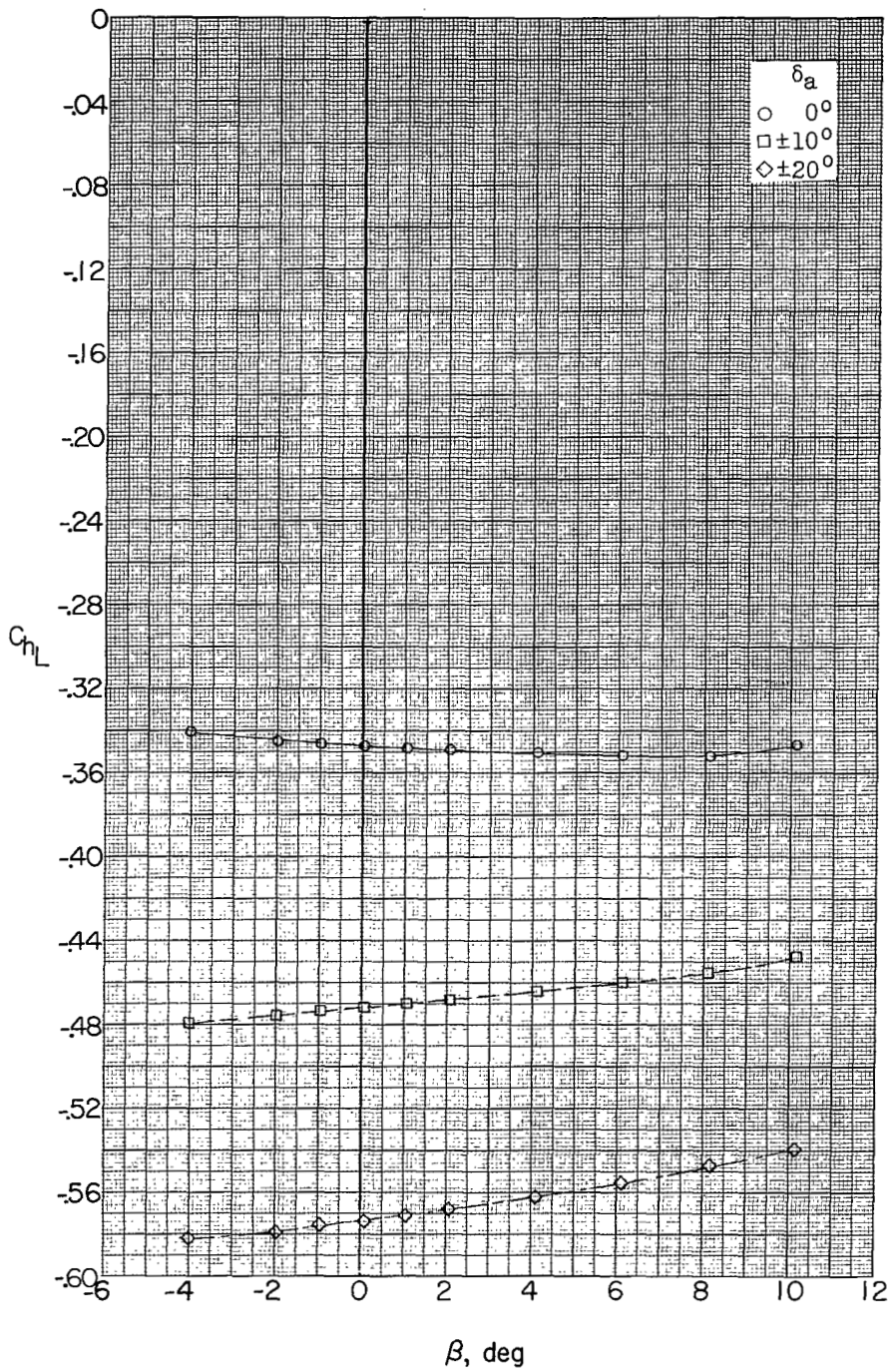

(d) M = 1.56; $\alpha \approx 16.2^{\circ}$.

Figure 20.- Continued.

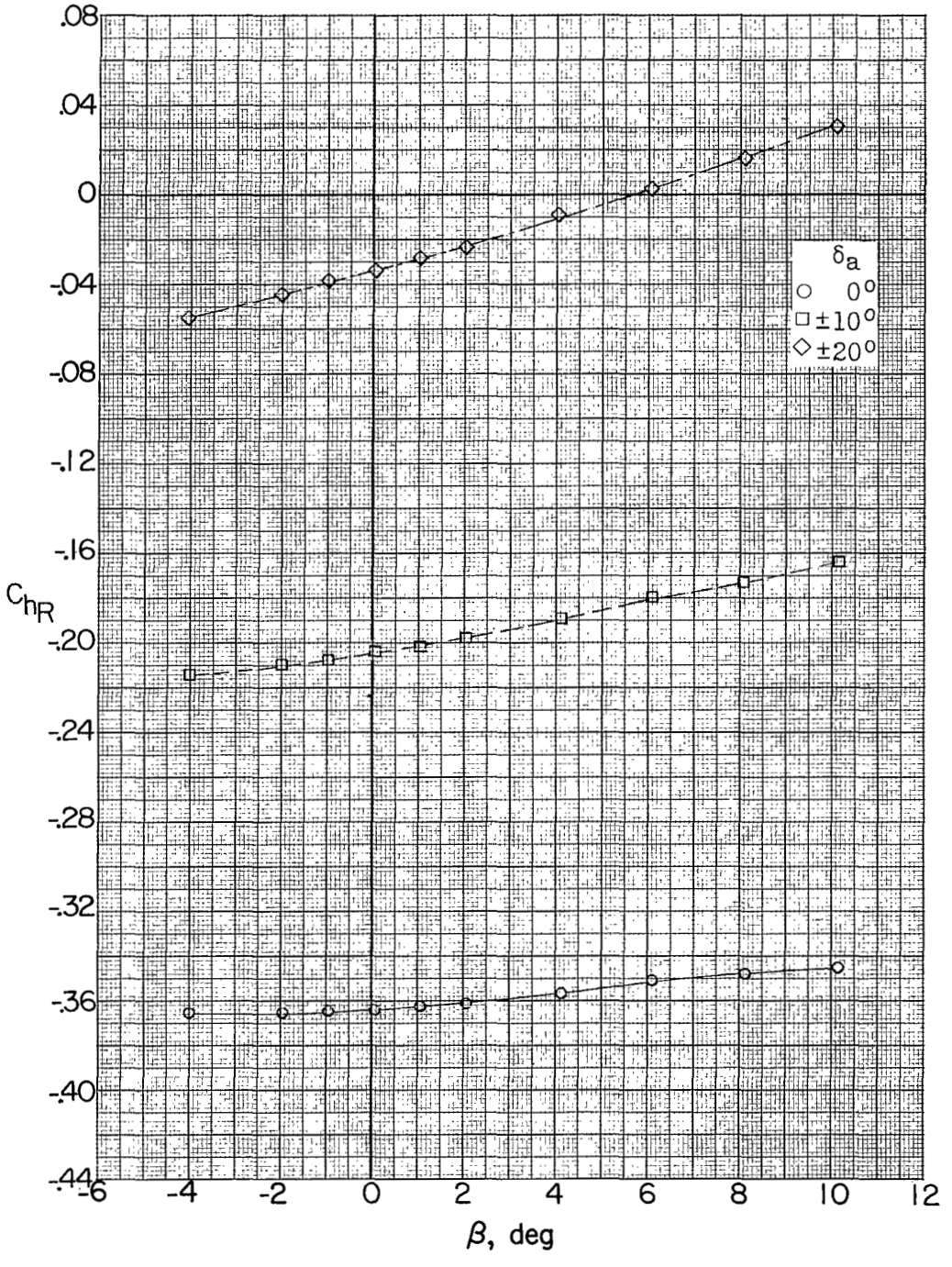

(d) Concluded.

Figure 20.- Continued.

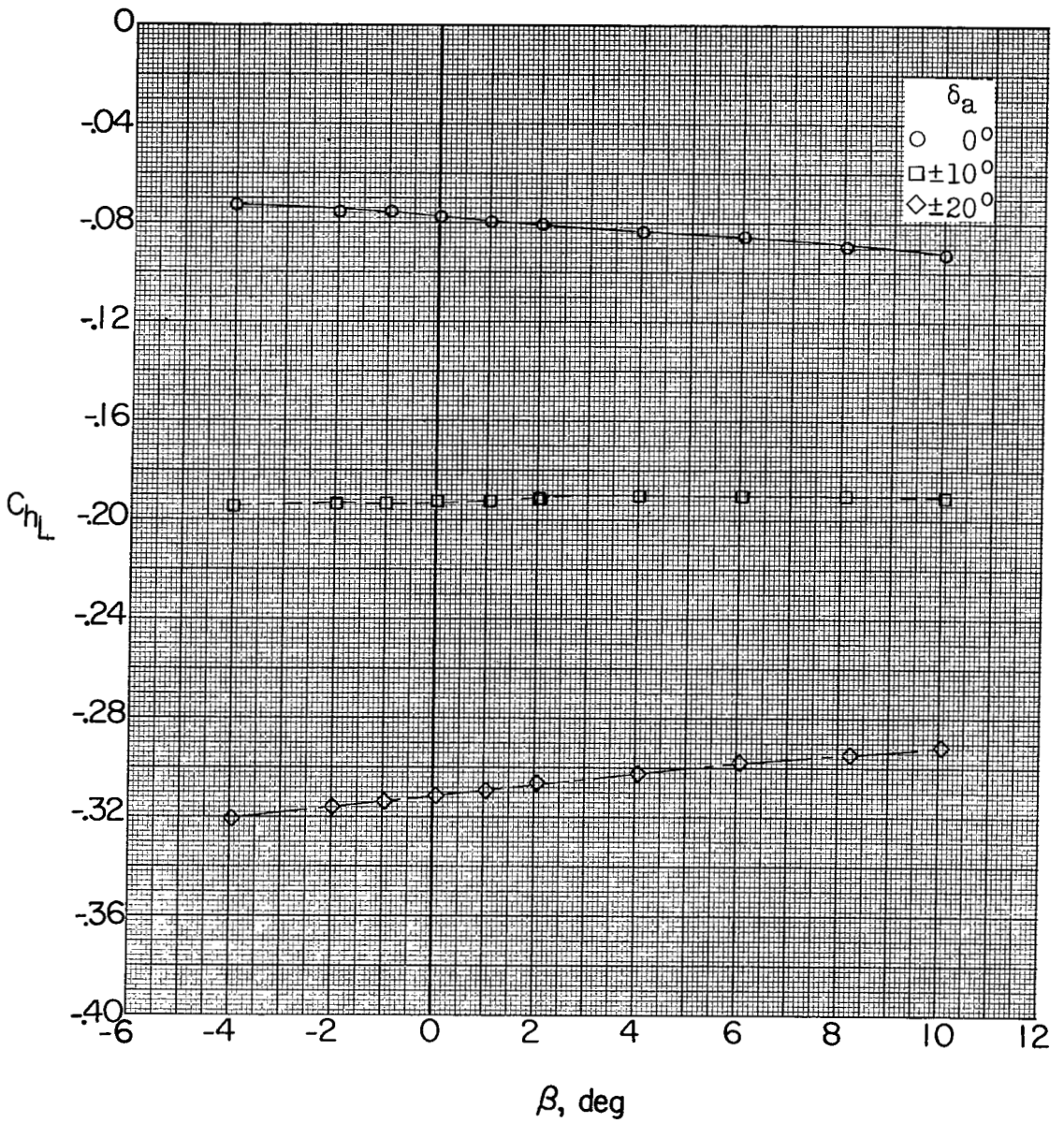

(e) M = 2.06; $\alpha \approx 3.8^\circ$.

Figure 20.- Continued.

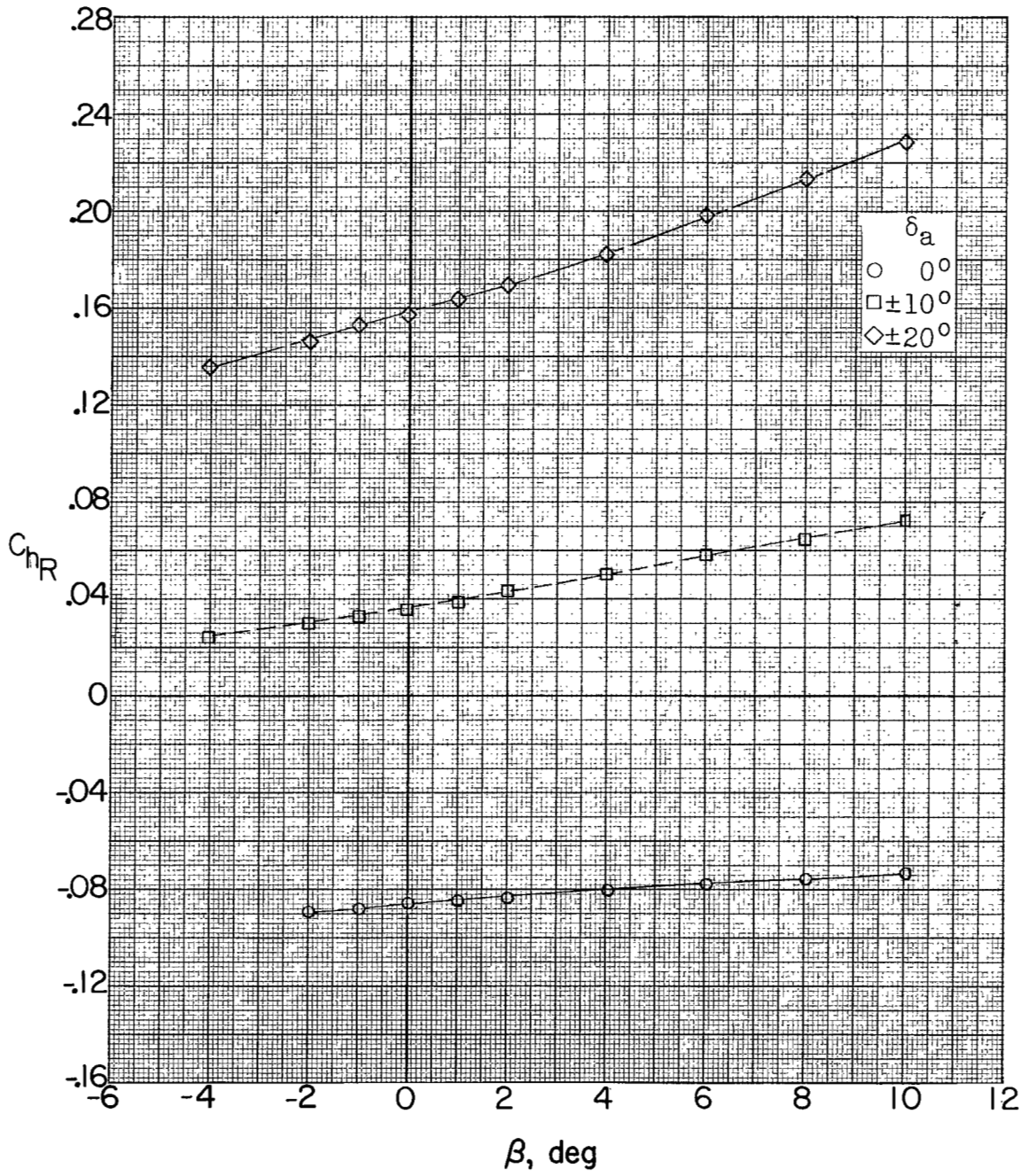

(e) Concluded.

Figure 20.- Continued.

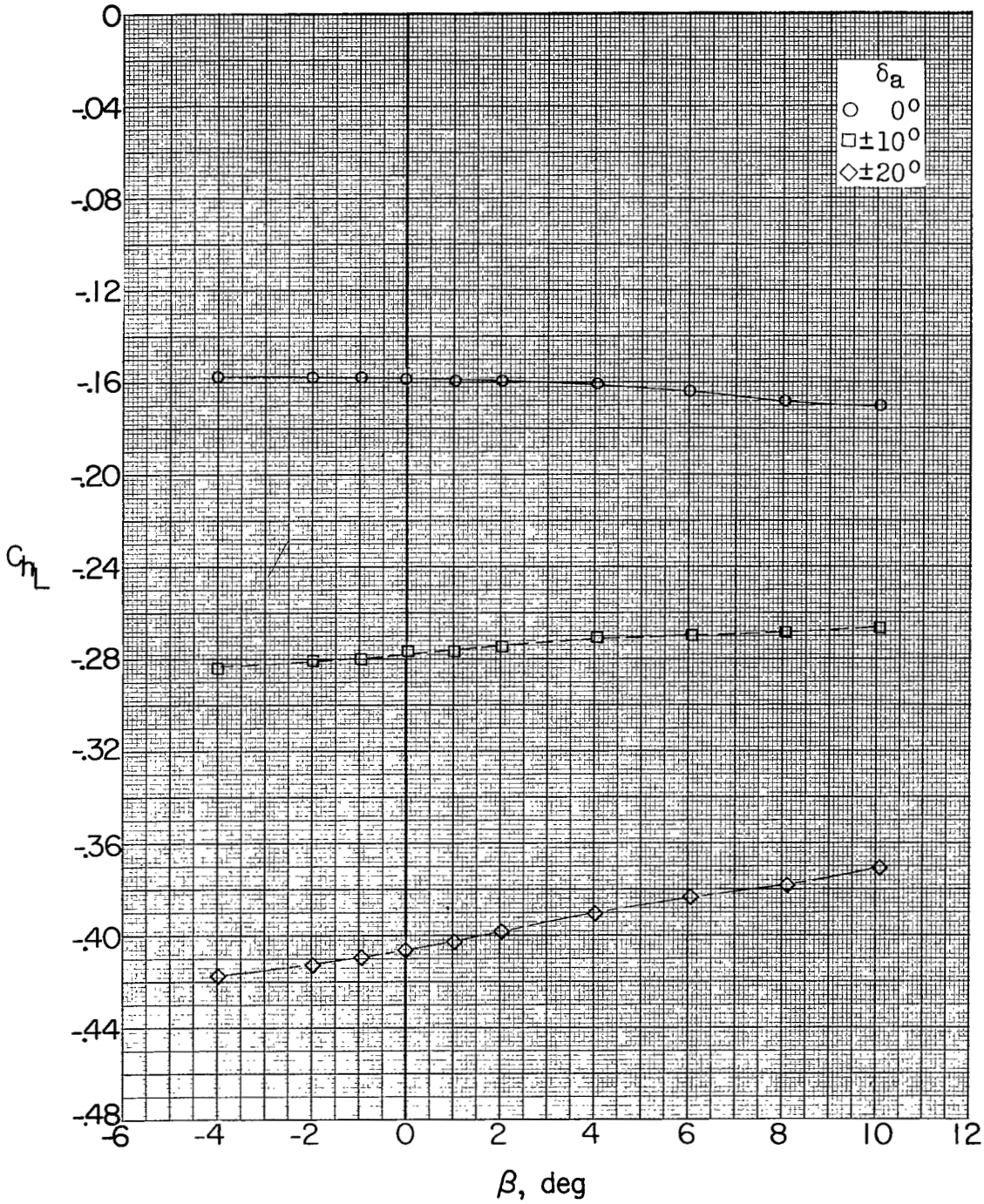

(f) M = 2.06; $\alpha \approx 9.6^\circ$.

Figure 20.- Continued.

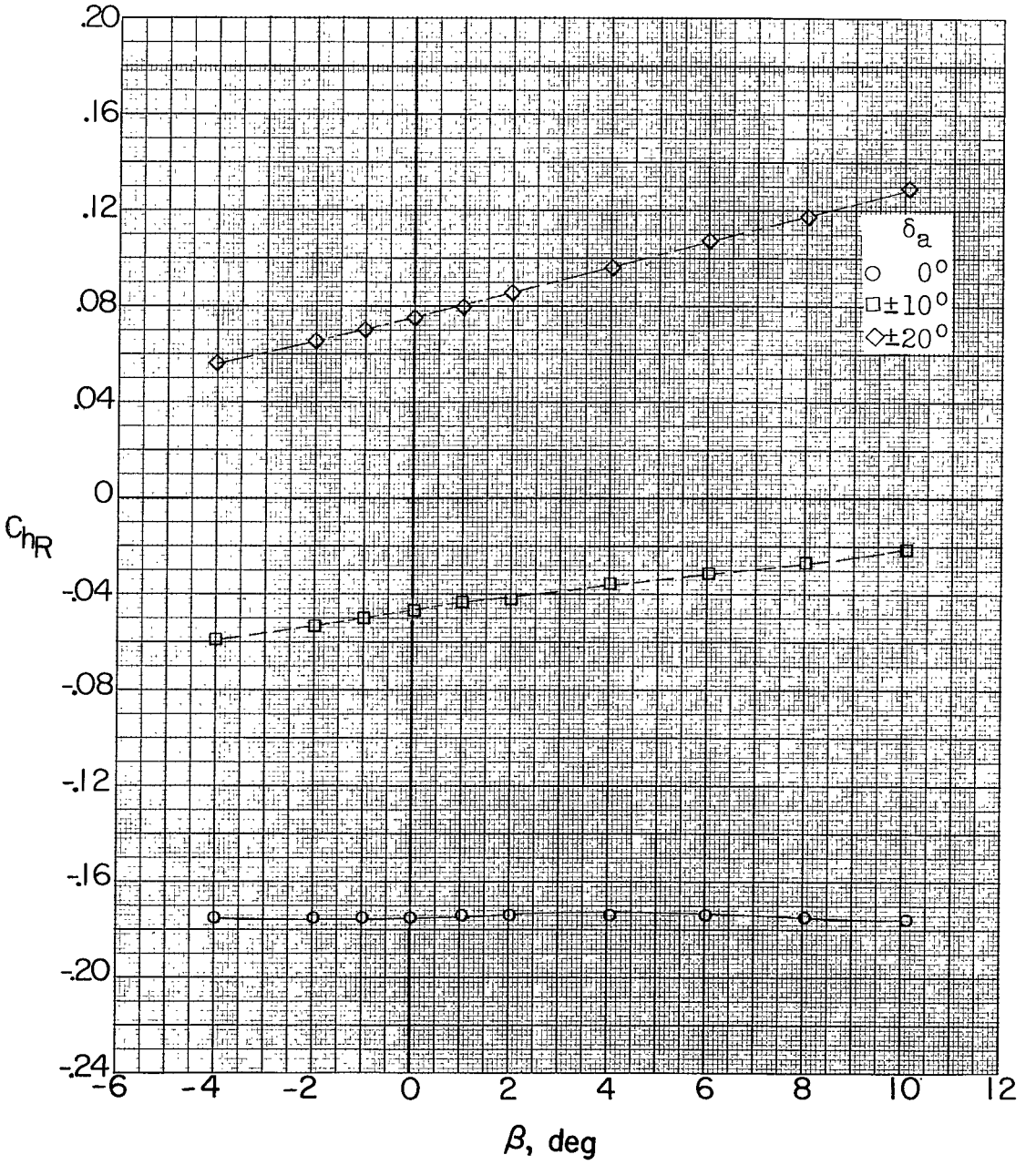

(f) Concluded.

Figure 20.- Continued.

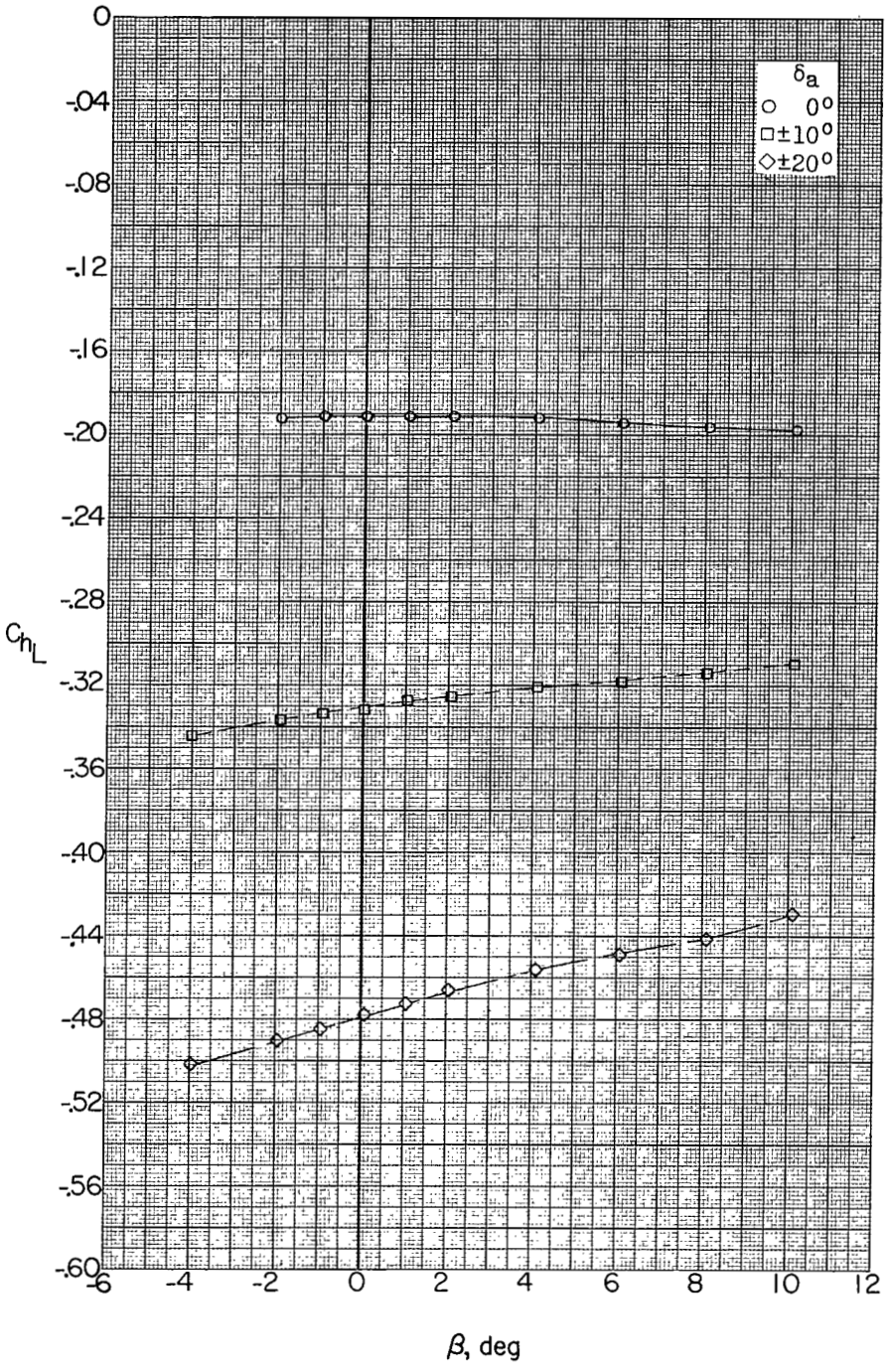

(g) M = 2.06; $\alpha \approx 12.0^\circ$.

Figure 20.- Continued.

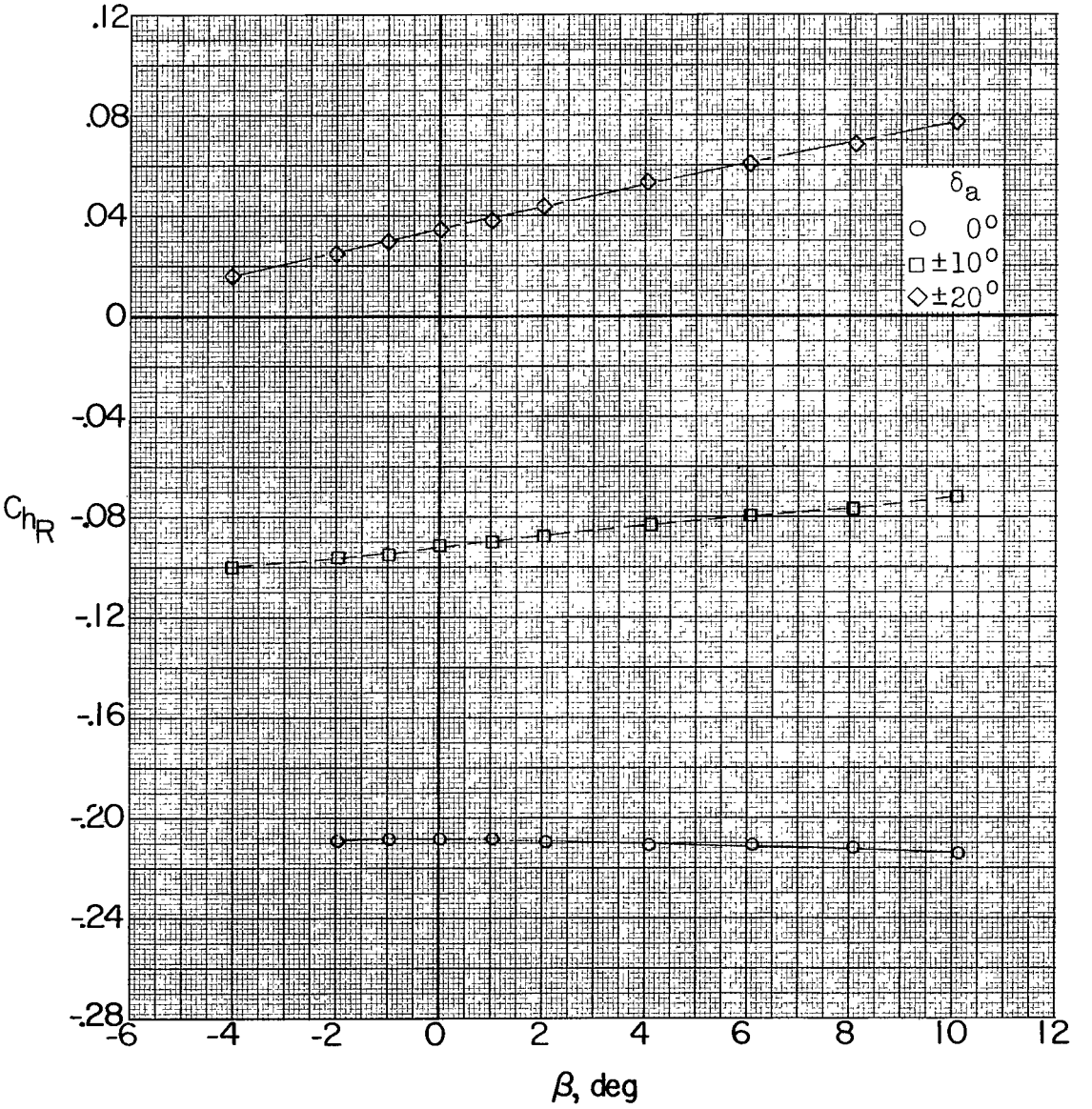

(g) Concluded.

Figure 20.- Continued.

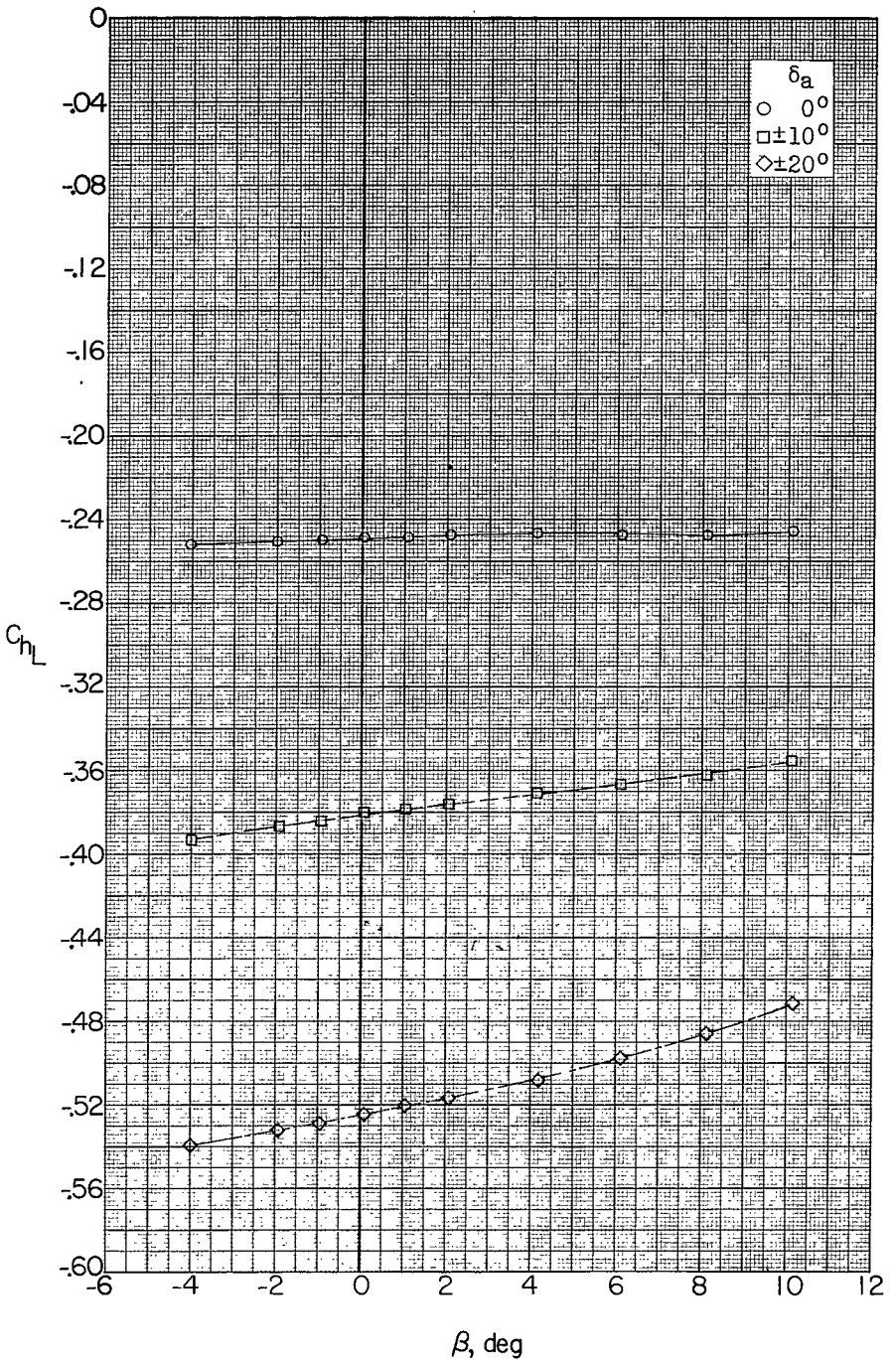

(h) M = 2.06; α = 16.1°.

Figure 20.- Continued.

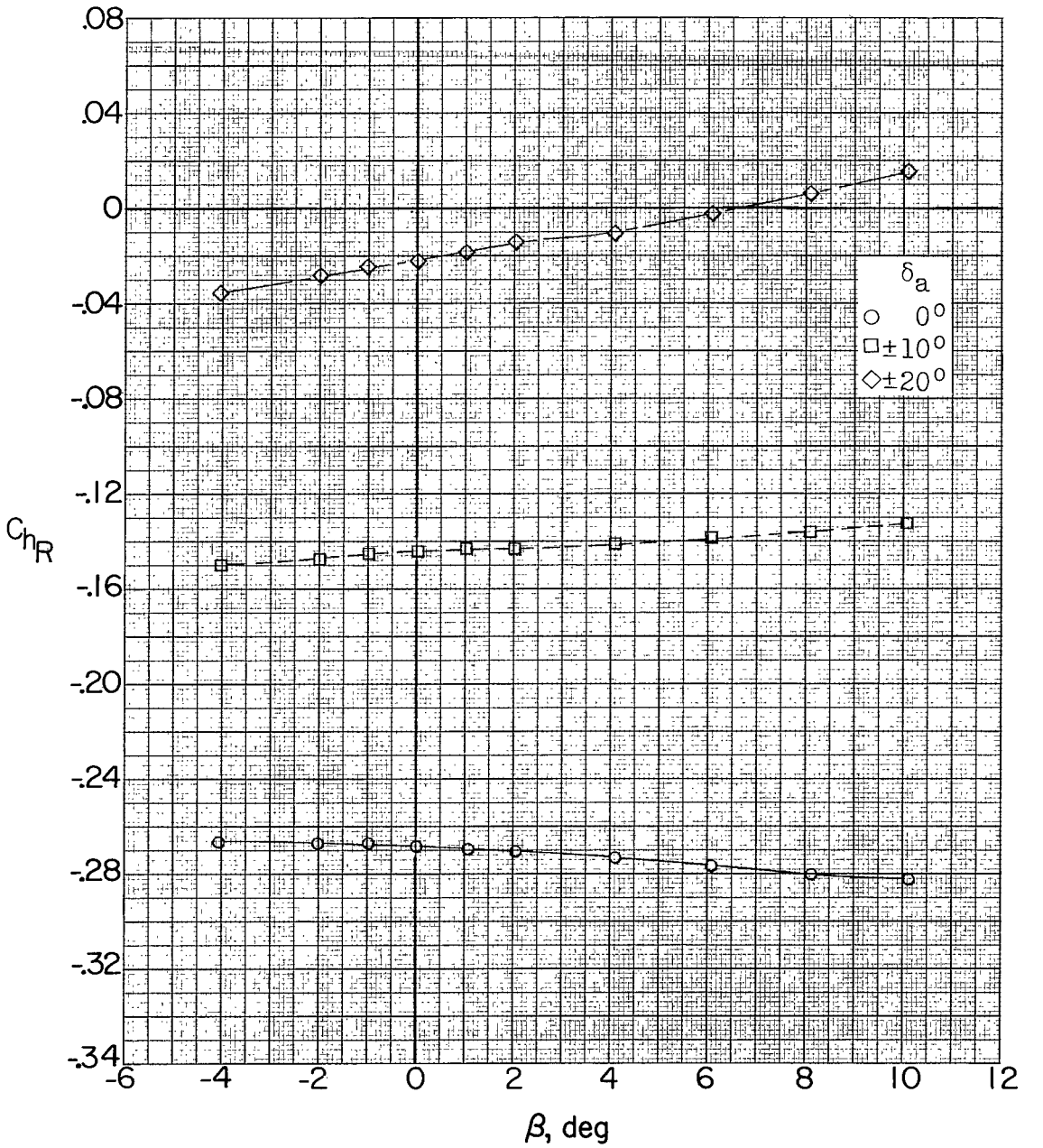

(h) Concluded.

Figure 20.- Concluded.

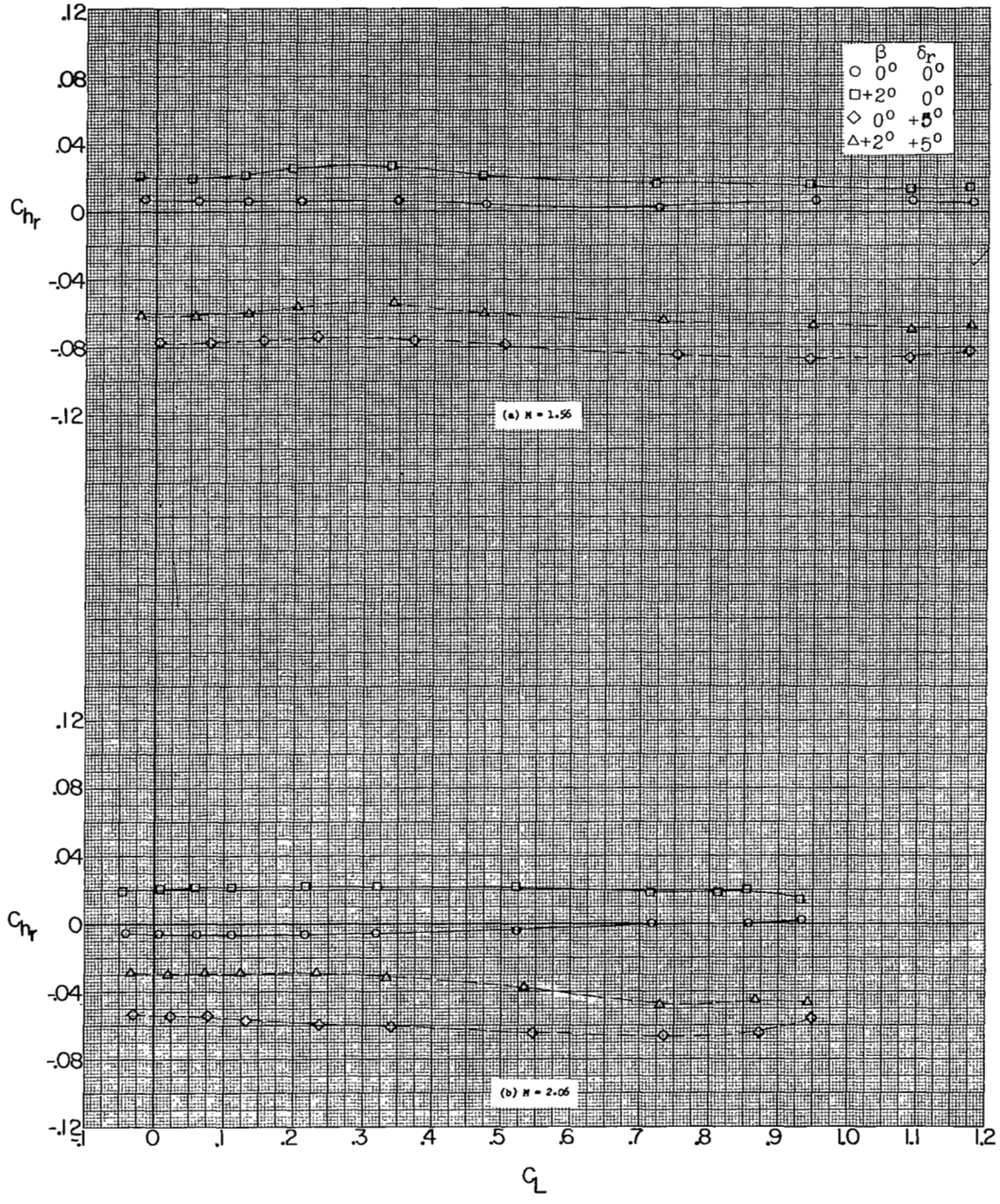

Figure 21.- Effect of rudder deflection on rudder hinge-moment coefficient.

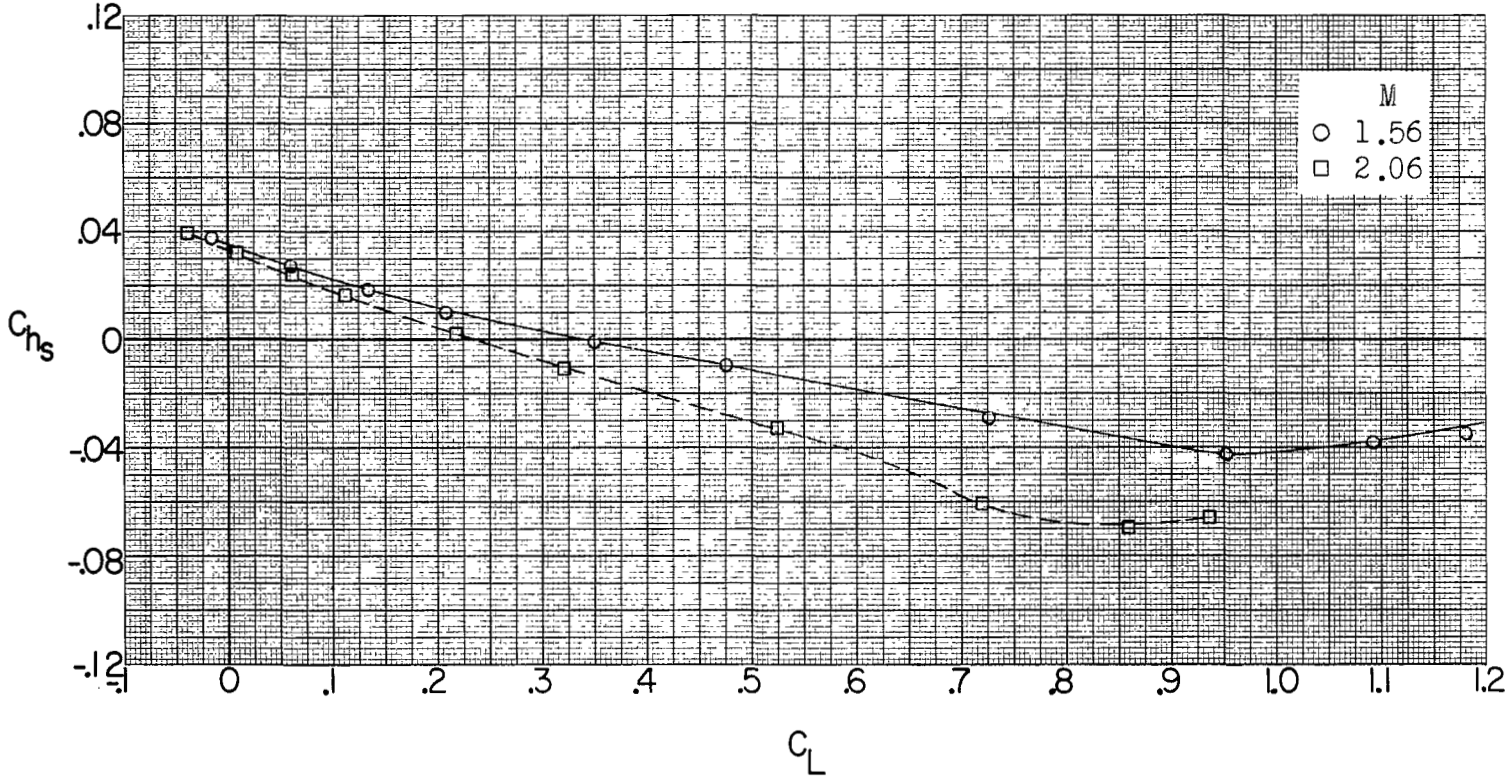

Figure 22.- Effect of lift coefficient on stabilator hinge-moment coefficient for basic-model configuration; $i_t = -4^\circ$.

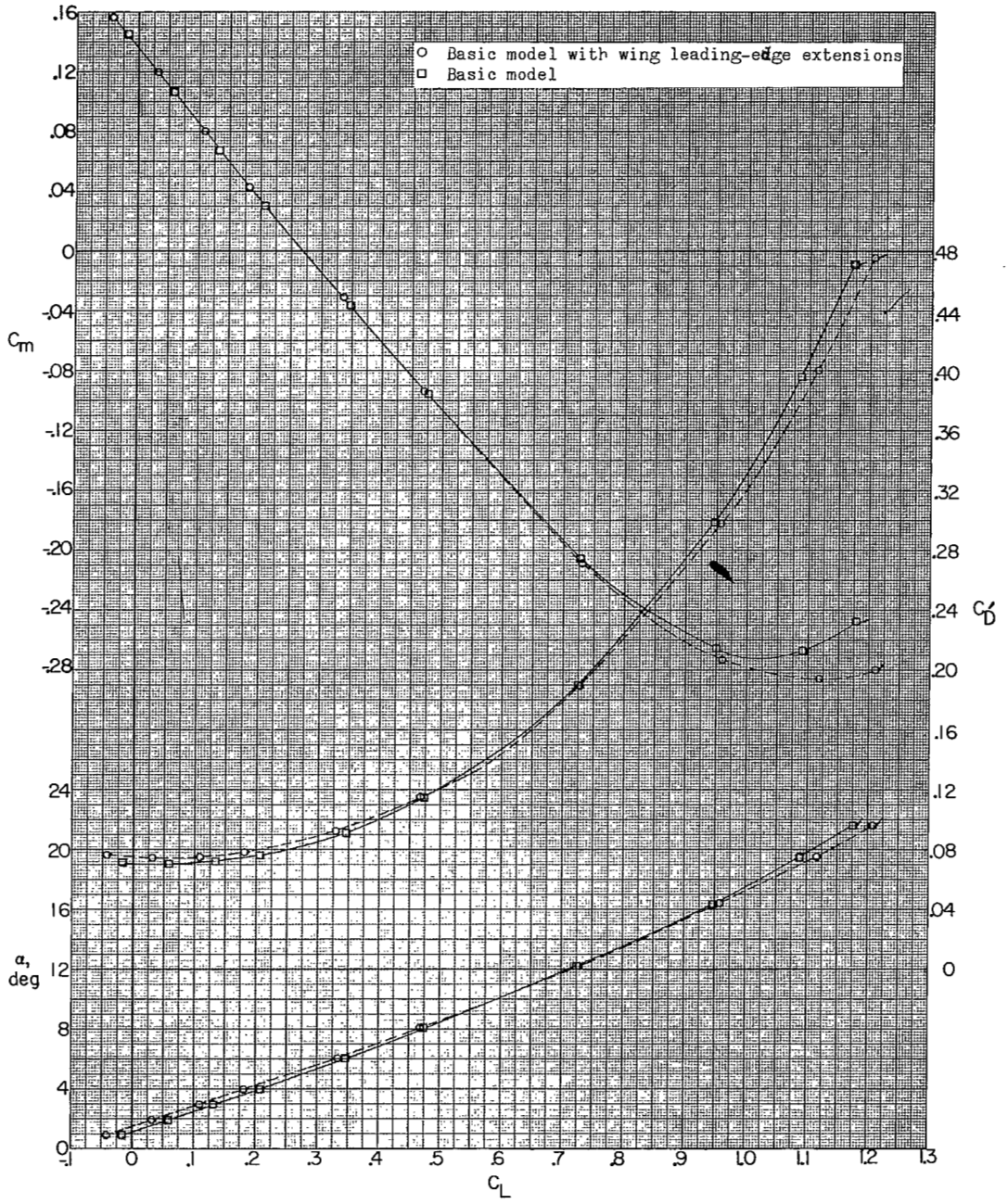

(a) M = 1.56.

Figure 23.- Effect of wing leading-edge extensions on aerodynamic characteristics in pitch; $\beta = 0^{\circ}$. Data uncorrected for base and internal duct drag. (Flagged symbols denote wall reflected shock waves striking tail.)

[redacted]

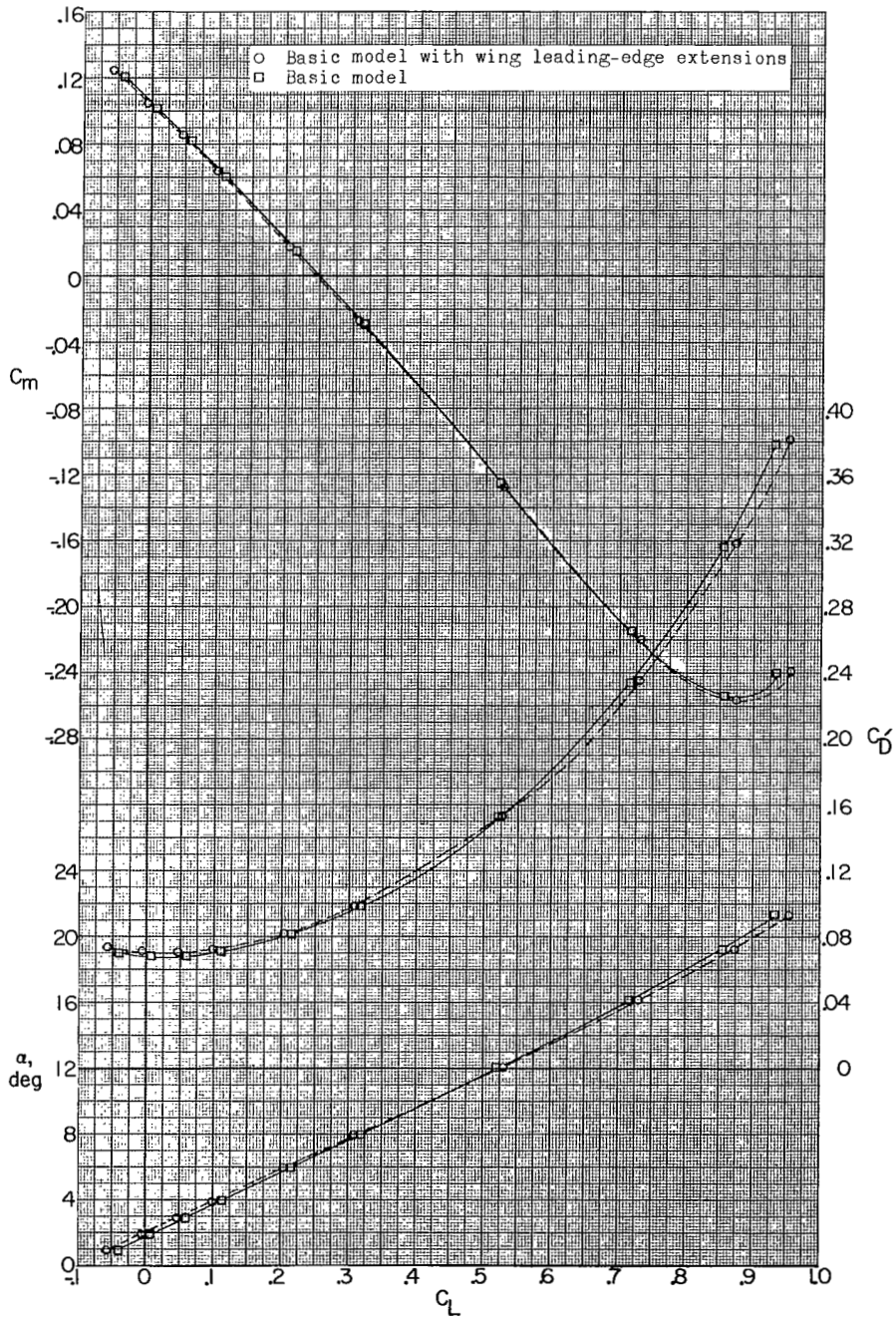

(b) M = 2.06.

Figure 23.- Concluded.

[redacted]

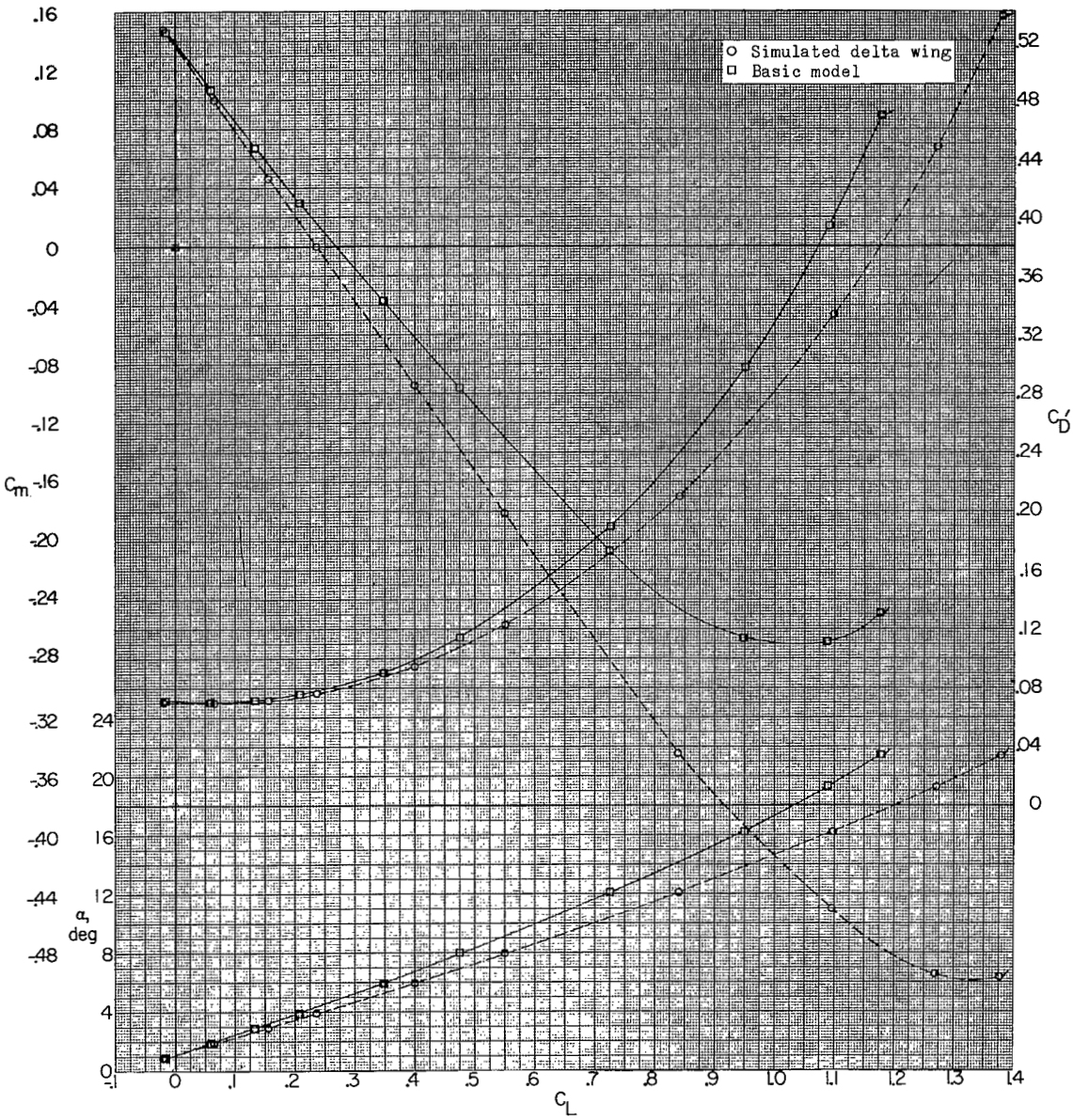

(a) M = 1.56.

Figure 24.- Effect of wing plan form on aerodynamic characteristics in pitch; $\beta = 0^\circ$. Data uncorrected for base and internal duct drag. (Flagged symbols denote wall reflected shock waves striking tail.)

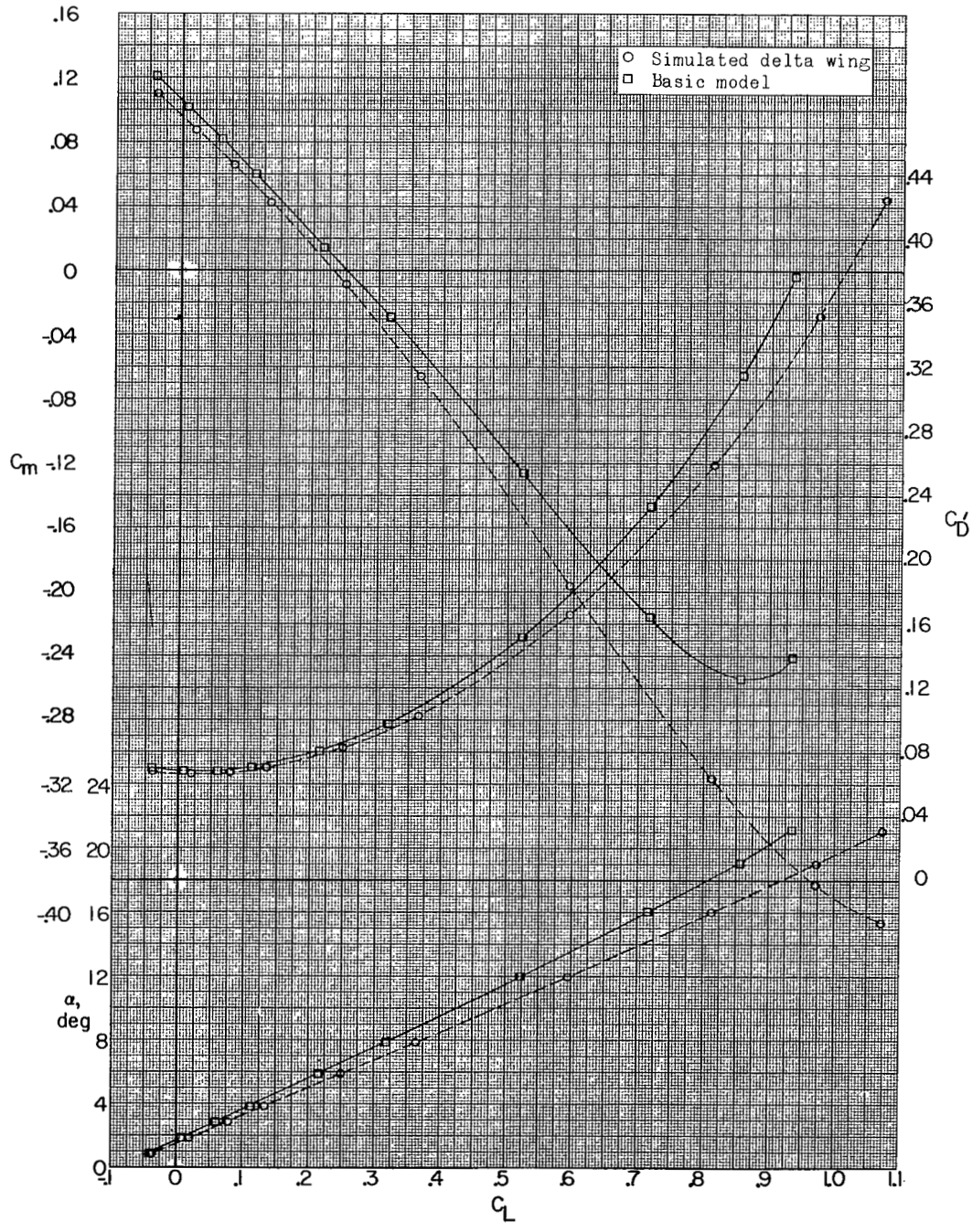

(b) M = 2.06.

Figure 24.- Concluded.

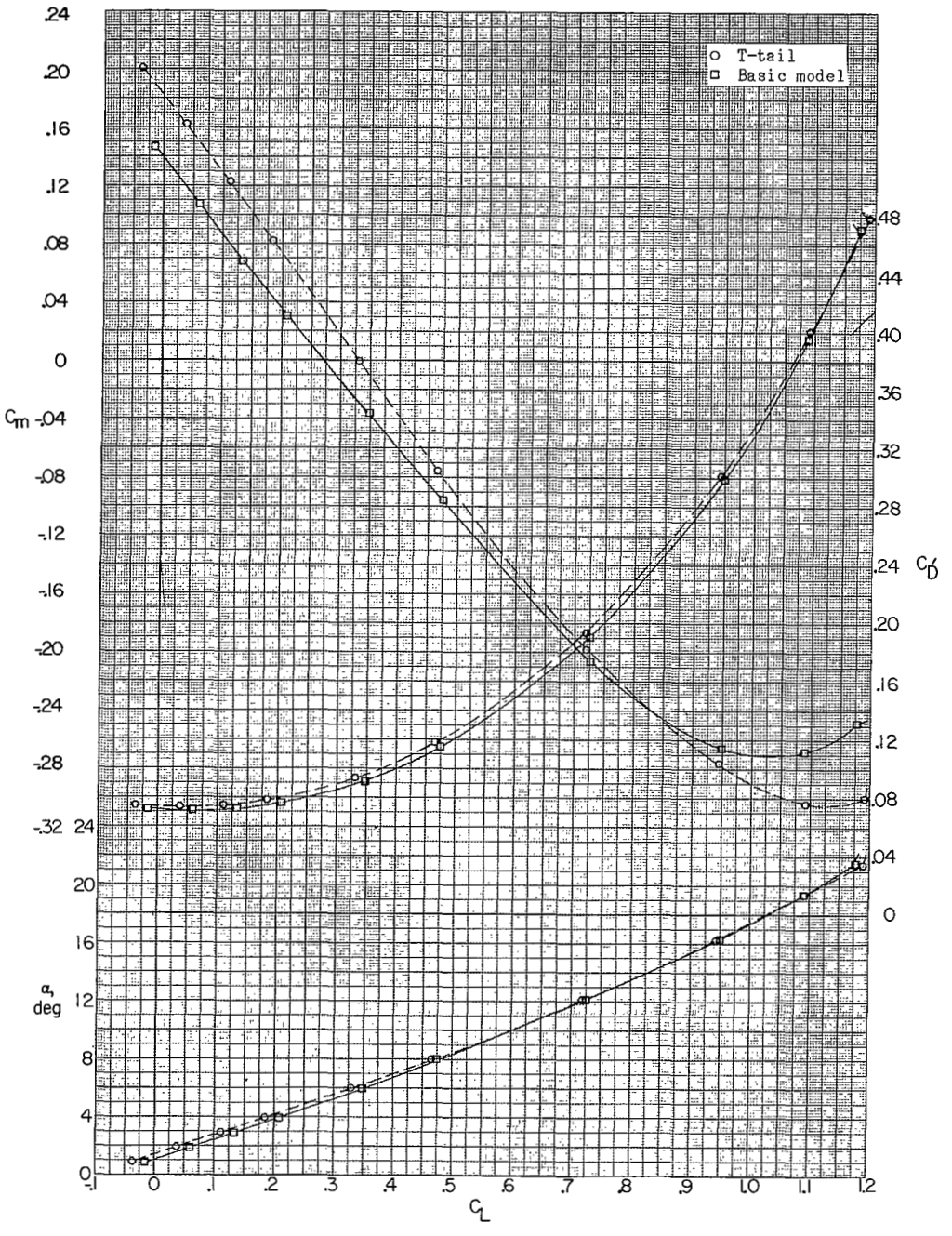

(a) M = 1.56.

Figure 25.- Effect of T-tail on aerodynamic characteristics in pitch; $\beta = 0^\circ$. Data uncorrected for base and internal duct drag. (Flagged symbols denote wall reflected shock waves striking tail.)

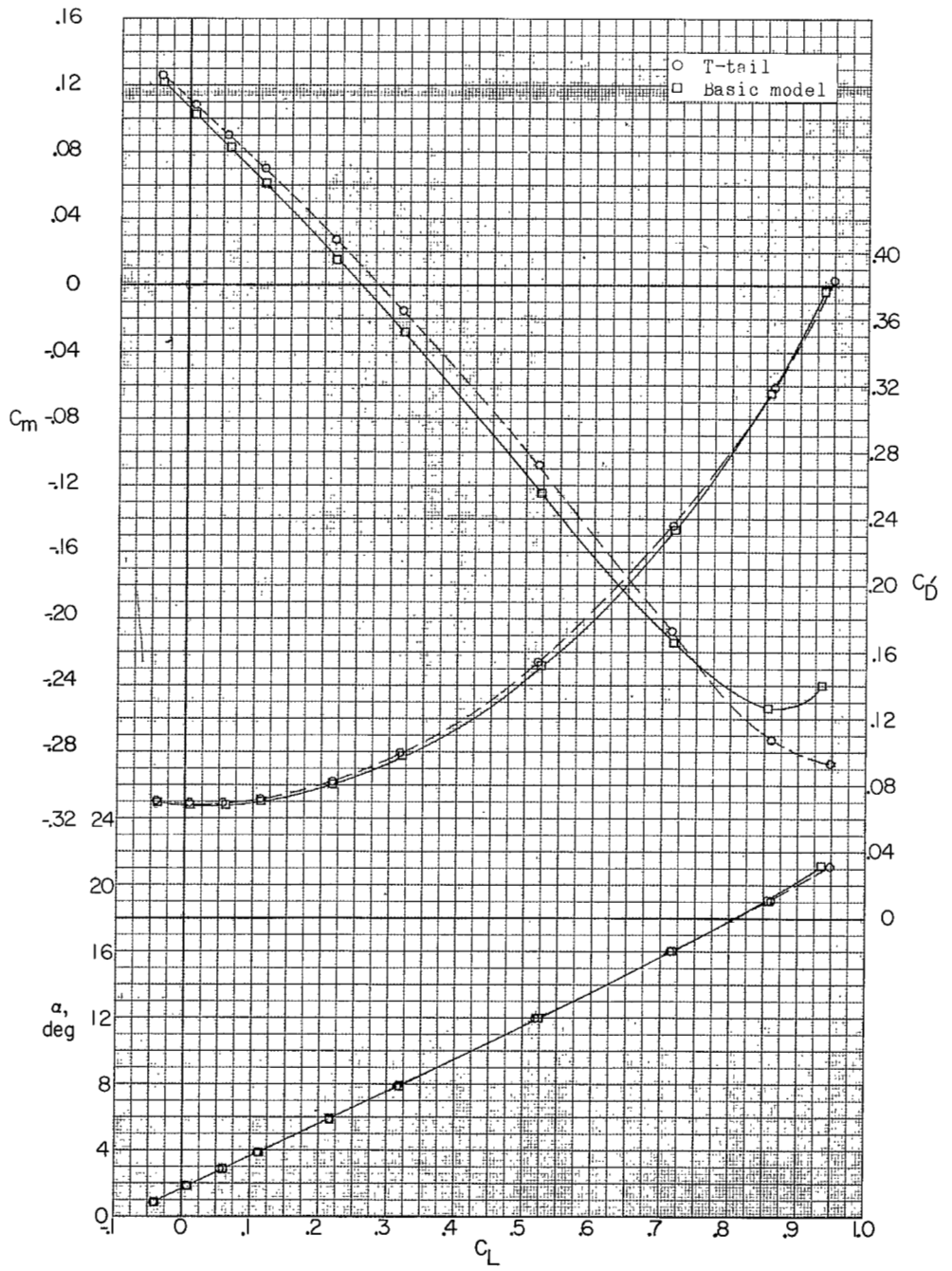

(b) M = 2.06.

Figure 25.- Concluded.

[redacted]

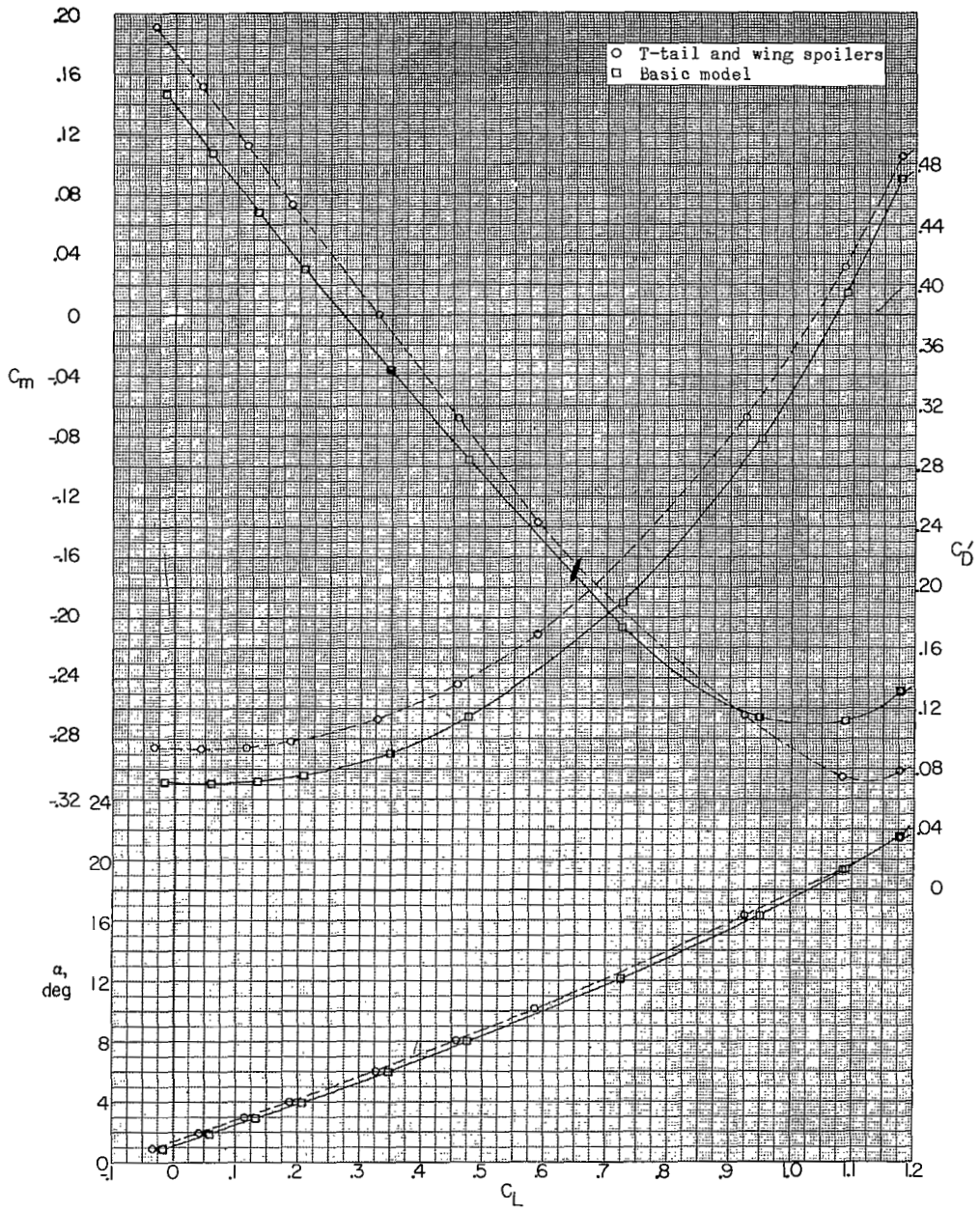

(a) M = 1.56.

Figure 26.- Effect of wing spoilers in combination with T-tail on aerodynamic characteristics in pitch; $\beta = 0^{\circ}$. Data uncorrected for base and internal duct drag. (Flagged symbols denote wall reflected shock waves striking tail.)

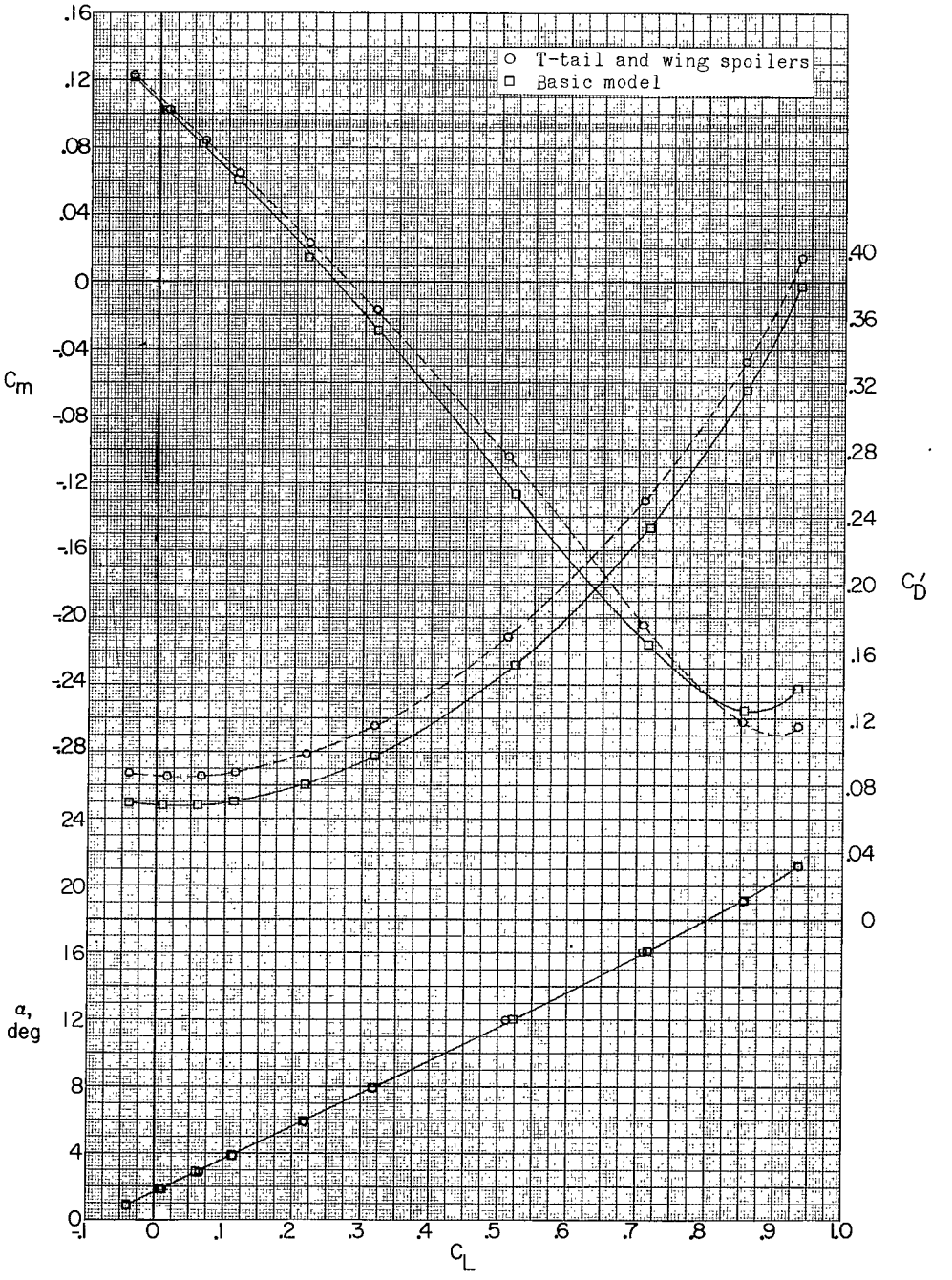

(b) M = 2.06.

Figure 26.- Concluded.

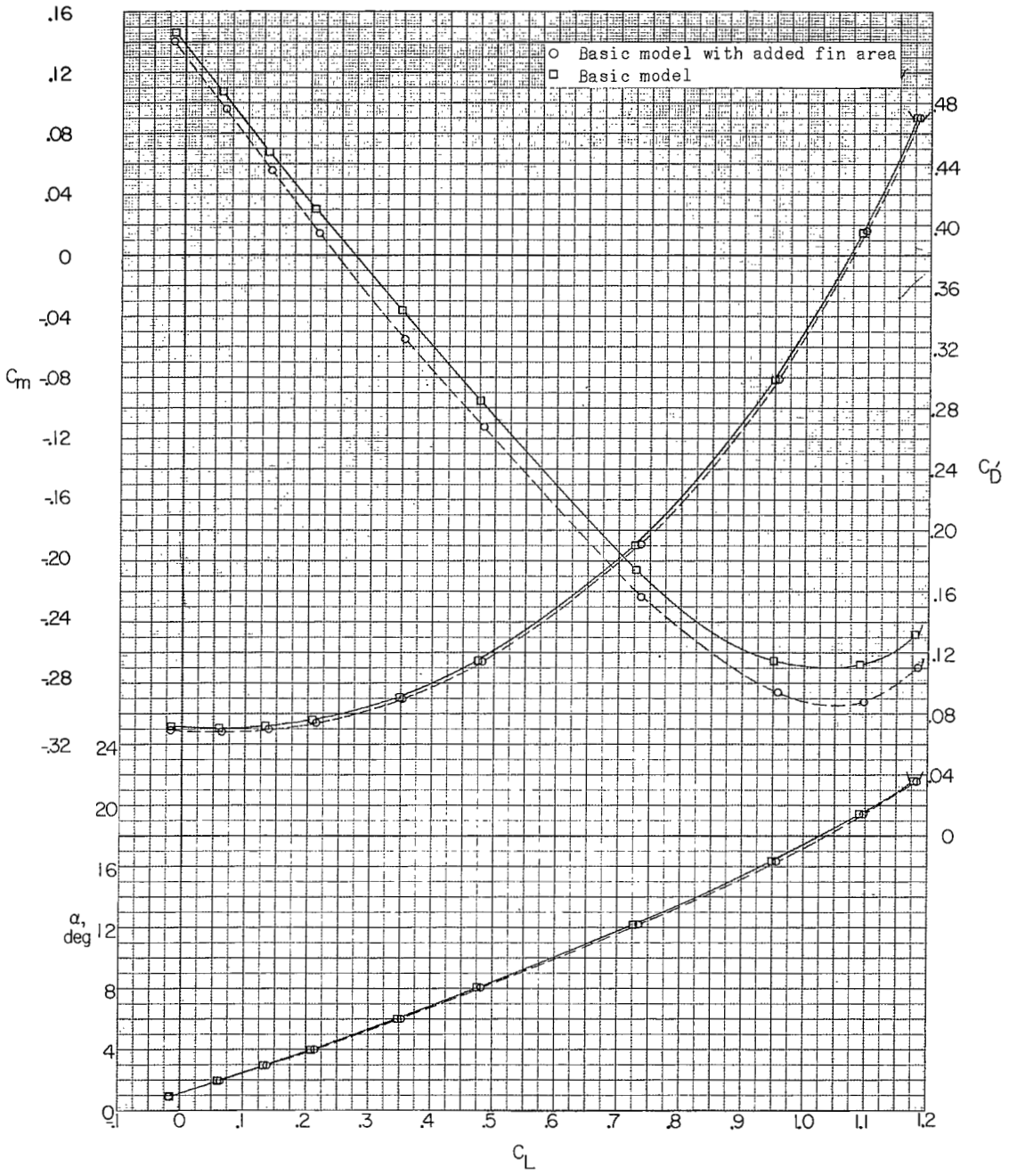

(a) M = 1.56.

Figure 27.- Effect of added fin area on aerodynamic characteristics in pitch; $\beta = 0^{\circ}$. Data uncorrected for base and internal duct drag. (Flagged symbols denote wall reflected shock waves striking tail.)

[redacted]

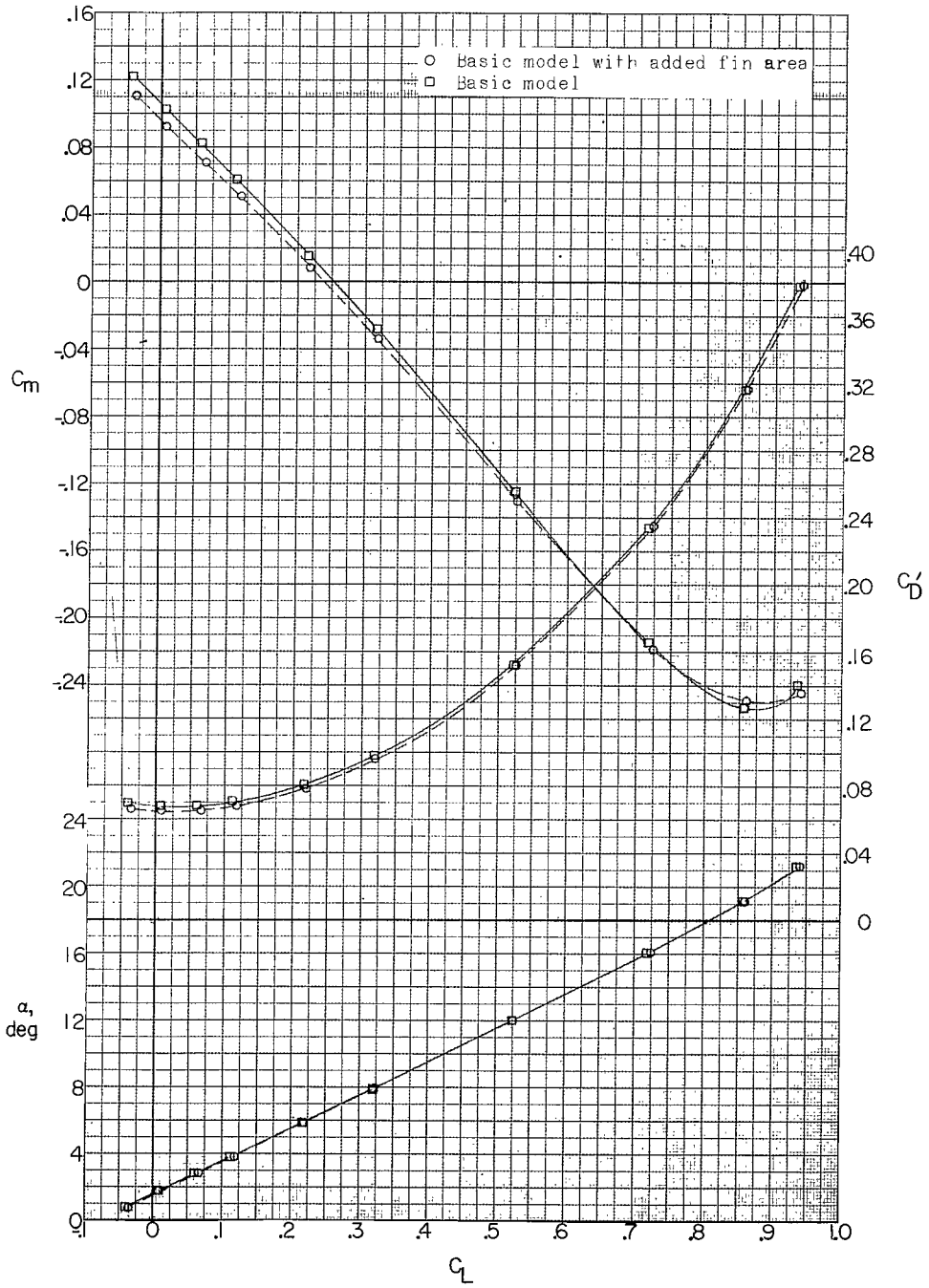

(b) M = 2.06.

Figure 27.- Concluded.

[redacted]

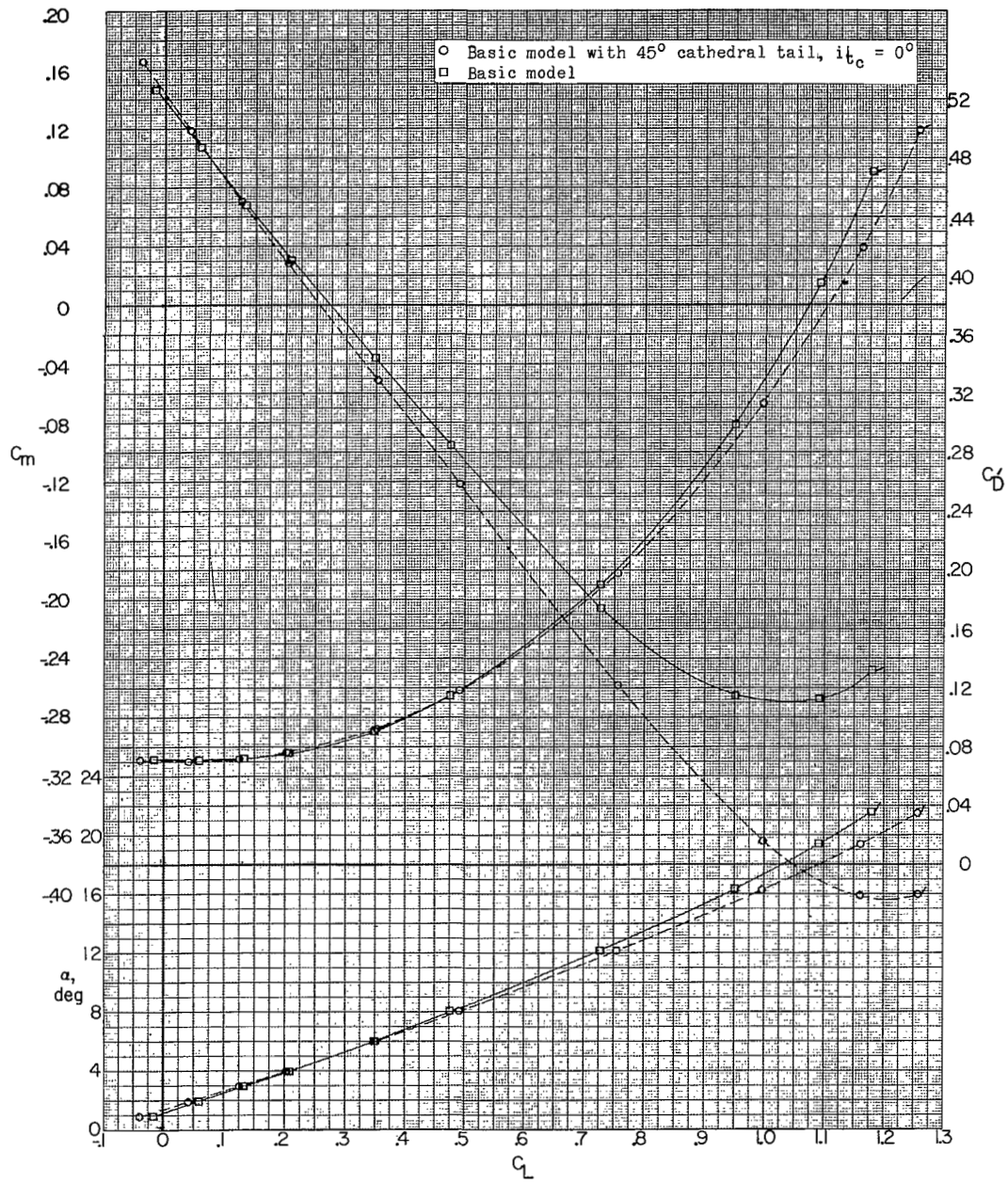

(a) M = 1.56.

Figure 28.- Effect of added tail with negative dihedral on aerodynamic characteristics in pitch; β = 0°. Data uncorrected for base and internal duct. (Flagged symbols denote wall reflected shock waves striking tail.)

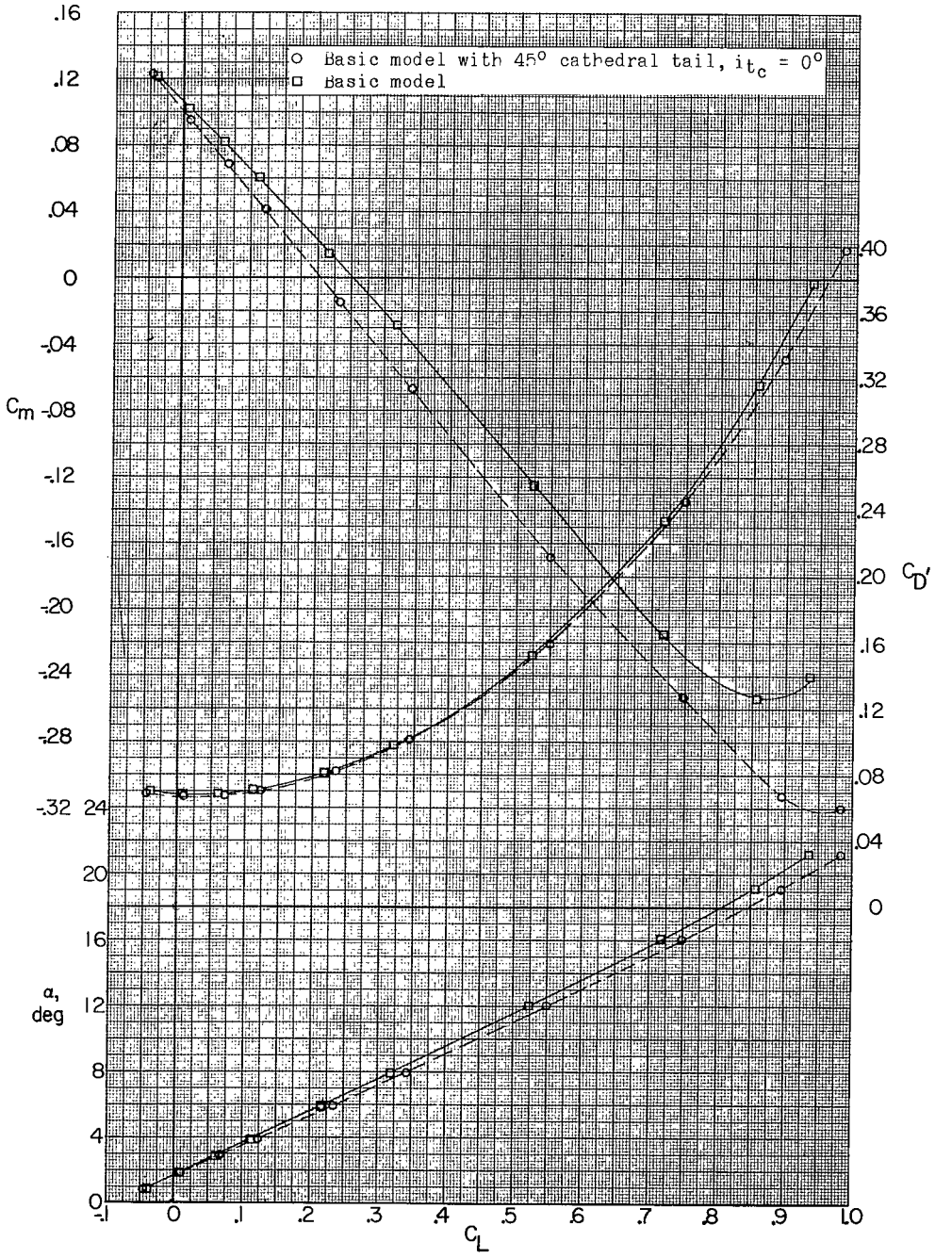

(b) M = 2.06.

Figure 28.- Concluded.